Springer Theses
Recognizing Outstanding Ph.D. Research

Yunchen Bi

Study of the Calcium Regulation Mechanism of TCR Activation Using Nanodisc and NMR Technologies

Springer

Springer Theses

Recognizing Outstanding Ph.D. Research

Aims and Scope

The series "Springer Theses" brings together a selection of the very best Ph.D. theses from around the world and across the physical sciences. Nominated and endorsed by two recognized specialists, each published volume has been selected for its scientific excellence and the high impact of its contents for the pertinent field of research. For greater accessibility to non-specialists, the published versions include an extended introduction, as well as a foreword by the student's supervisor explaining the special relevance of the work for the field. As a whole, the series will provide a valuable resource both for newcomers to the research fields described, and for other scientists seeking detailed background information on special questions. Finally, it provides an accredited documentation of the valuable contributions made by today's younger generation of scientists.

Theses are accepted into the series by invited nomination only and must fulfill all of the following criteria

- They must be written in good English.
- The topic should fall within the confines of Chemistry, Physics, Earth Sciences, Engineering and related interdisciplinary fields such as Materials, Nanoscience, Chemical Engineering, Complex Systems and Biophysics.
- The work reported in the thesis must represent a significant scientific advance.
- If the thesis includes previously published material, permission to reproduce this must be gained from the respective copyright holder.
- They must have been examined and passed during the 12 months prior to nomination.
- Each thesis should include a foreword by the supervisor outlining the significance of its content.
- The theses should have a clearly defined structure including an introduction accessible to scientists not expert in that particular field.

More information about this series at http://www.springer.com/series/8790

Yunchen Bi

Study of the Calcium Regulation Mechanism of TCR Activation Using Nanodisc and NMR Technologies

Doctoral Thesis accepted by
The Graduate School of Chinese Academy of Sciences, Beijing, China

Springer

Author
Dr. Yunchen Bi
High Magnetic Field Laboratory
Hefei Institutes of Physical Science, Chinese Academy of Sciences
Hefei, Anhui
China

Supervisor
Prof. Junfeng Wang
High Magnetic Field Laboratory
Chinese Academy of Sciences
Hefei, Anhui
China

ISSN 2190-5053 ISSN 2190-5061 (electronic)
Springer Theses
ISBN 978-3-662-54616-1 ISBN 978-3-662-54618-5 (eBook)
DOI 10.1007/978-3-662-54618-5

Library of Congress Control Number: 2017942973

© Springer-Verlag GmbH Germany 2018
This work is subject to copyright. All rights are reserved by the Publisher, whether the whole or part of the material is concerned, specifically the rights of translation, reprinting, reuse of illustrations, recitation, broadcasting, reproduction on microfilms or in any other physical way, and transmission or information storage and retrieval, electronic adaptation, computer software, or by similar or dissimilar methodology now known or hereafter developed.
The use of general descriptive names, registered names, trademarks, service marks, etc. in this publication does not imply, even in the absence of a specific statement, that such names are exempt from the relevant protective laws and regulations and therefore free for general use.
The publisher, the authors and the editors are safe to assume that the advice and information in this book are believed to be true and accurate at the date of publication. Neither the publisher nor the authors or the editors give a warranty, express or implied, with respect to the material contained herein or for any errors or omissions that may have been made. The publisher remains neutral with regard to jurisdictional claims in published maps and institutional affiliations.

Printed on acid-free paper

This Springer imprint is published by Springer Nature
The registered company is Springer-Verlag GmbH Germany
The registered company address is: Heidelberger Platz 3, 14197 Berlin, Germany

Supervisor's Foreword

Membrane protein plays a variety of important functions in biological and pathological processes; therefore, studies of membrane protein structure and function have been hot topics in biology nowadays. Combining nuclear magnetic resonance (NMR) and nanodisc, a native-like lipid membrane system, this thesis focuses on answering an important question of how organisms orchestrate the membrane proteins to response the biological signal, which ultimately result in a cascade of biochemical events along the downstream signal pathway.

(1) Membrane mimic is essential to keep the idiosyncrasies of membrane protein in vitro. Nanodisc is a newly designed membrane mimic system, which supplies a physiological membrane environment by devoid of generally used harmful detergents. This thesis optimizes the nanodisc assembling protocol, which eventually proves to be a suitable system for studying membrane proteins by solution NMR.
(2) It reveals that structural rearrangement of TCR CD3ε is necessary for immune signal transduction. The calcium ion is the discerning driver to amplify and regulate the CD3ε activation by modulating the charge property of interacting lipids.
(3) This thesis also includes a structural study of dengue virus NS2B-NS3p protein in complex with aprotinin, which is important for screening and developing new anti-dengue viral drugs by structure-based designing strategies.

Hefei, China
March 2017

Prof. Junfeng Wang

Parts of the thesis have been published in the following journal articles:

1. Xiaoming Wang, Zongjun Mu, Yan Li, **Yunchen Bi**, Yujuan Wang*. Smaller Nanodiscs are Suitable for Studying Protein Lipid Interactions by Solution NMR. ***The Protein Journal***. 2015 Jun ; 34(3):205–11 (Reproduced by permission of Springer)
2. Xiaoshan Shi[1], **Yunchen Bi**[1], Wei Yang[1], Xingdong Guo, Yan Jiang, Chanjuan Wan, Lunyi Li, Yibing Bai, Jun Guo, Yujuan Wang, Xiangjun Chen, Bo Wu, Hongbin Sun, Wanli Liu, Junfeng Wang*, Chenqi Xu*. Ca^{2+} regulates T cell receptor activation by modulating the charge property of lipids. ***Nature***. 2013 Jan 3; 493(7430):111–5. ([1]co-first author) (Reproduced by permission of Springer)
3. **Yunchen Bi**, Lei Zhu, Hua Li, Bo Wu, Jinsong Liu*, Junfeng Wang*. Backbone ^{1}H, ^{13}C and ^{15}N resonance assignments of dengue virus NS2B-NS3p in complex with aprotinin. ***Biomol. NMR Assign***. 2013 Oct; 7(2):137–9. (Reproduced by permission of Springer)

Acknowledgements

Firstly, I would like to express my wholehearted thanks and appreciation to my supervisor, Prof. Junfeng Wang. He is always enthusiastically giving me constructive suggestions about science, but also has guided me in life. His positive attitude and amiable disposition inspired me deeply and encouraged me enjoy the "slow life" in a fast-tempo society. I have grown the most in his laboratory.

I would like to thank Prof. Chenqi Xu (SIBS, CAS). His precision and excellence in science made collaboration with his laboratory very fruitful and has contributed to my lifelong learning.

Many thanks to the membrane biology group: Dr. Hongbin Sun, Dr. Bo Wu, Dr. Xinwei Zheng, Dr. Yujuan Wang, Dr. Zhiwu Yu, Hongxin Zhao, Lei Zhu, Chanjuan Wan, Jing Yang, Yan Li, Jiarong Wang, Xiaoming Wang, Wei Chen. They established rapport easily with all other colleagues, including me. Their friendly professionalism has been much appreciated.

I would like to thank Prof. Jinsong Liu and Hua Li (GIBH, CAS) and Prof. Qing Huang, Dr. Zhigang Ke, and Jinghua Liu (ITB, CAS) for their valuable advice and comments on my research work.

My special thanks go to my family and my wife Xin Chen. Their constant love accompanied and supported me throughout my Ph.D. study.

Yunchen Bi
University of Virginia
Charlottesville, USA
e-mail: yb7y@virginia.edu

Contents

Chapter 1
Introduction

Abstract A hurricane is being influenced by minor perturbations such as the flapping of the wings of a distant butterfly. The cell is the basic structural and functional unit of living systems, but how cell orchestrates its responses to stimuli from the intracellular or extracellular environment remains a fundamental question in biology. A tiny variation in these environments will elicit a series of biochemical events known as the cascade reactions inside the cell through signal transduction pathways. The consequences of such cascade reactions depend on cell type and can lead to changes in metabolism, gene or protein expression, morphology and cell cycle regulation. The interior and exterior environments of the cell are separated by the cell membrane, a lipid bilayer composed mainly of phospholipids and embedded proteins. The intracellular environment, termed the cytoplasm, is bounded by this membrane and consists of the cytosol and the cell's organelles, which house the most important biochemical functions of the cell. However, many of the signaling molecules that mediate signal transduction pathways are located at the extracellular domain of the cell membrane and are excluded from the cytoplasm by this barrier. Like intracellular signal transduction, transmembrane signal transduction plays a key role in cell living process and must rely on these external molecules. This thesis discusses the transmembrane signal transduction study, using the calcium modulated T cell receptor (TCR) activity as a model.

1.1 Cell Membrane: Structure and Function

The cell membrane is a 5–10 nm thick lipid bilayer, which forms the outermost layer of the cell. It serves as a physical barrier to protect the interior of the cell from admixture with the extracellular environment.

© Springer-Verlag GmbH Germany 2018

Y. Bi, *Study of the Calcium Regulation Mechanism of TCR Activation Using Nanodisc and NMR Technologies*, Springer Theses,
DOI 10.1007/978-3-662-54618-5_1

1.1.1 Function of the Cell Membrane

The cell membrane is selectively permeable and able to control the materials that enter and exit the cell. The cell utilizes a variety of mechanisms to move these molecules across the membrane based on these molecules' size, charge, polarity, and concentration gradient. Such mechanisms include passive transport across the membrane or through protein channels, and active transport of specific molecules or bulk materials. Small and non-polar molecules like water, oxygen, carbon dioxide and nitrogen are capable of crossing the cell membrane down their concentration gradients by osmosis or diffusion, but ions, amino acids, lipid molecules, oligosaccharides or other large molecules must utilize channels, transporters, or bulk transport (endo- or exocytosis) to move in or out the cells. Channels are mostly used for ion translocation, which allow ions to pass down their electrochemical gradient. Ions lose their hydration shells as they enter a channel, which is essential for selection of the correct substrate ion. Hence, the rate of ion transportation through the channel is extremely high, that could reach 10^6 ions per second or greater.

By contrast, the rate of transporters is relatively low (10^2 molecules per second). Typically, a transporter contains two gates that open and close in a controlled manner and are never both open simultaneously, which will limit the rate of spurious molecular movement. Endocytosis and exocytosis are less specific transportation processes that involve absorption or extrusion of the materials that contain the small molecules, ions and macromolecules.

Besides material translocation, the cell membrane is central to many other important biological processes involving multiple cells. Membrane proteins, lipoproteins and membrane-associated proteins are directly involved in cell recognition, cell immunization, cell motion, cell division, nerve conduction and metabolic regulation via signal transduction. In a tissue environment, membranes of adjacent cells may be directly connected at gap junctions or indirectly via the extracellular matrix, or biofilms in bacteria. Its pivotal role in living systems makes the cell membrane an important area of research.

1.1.2 Composition of the Cell Membrane

The cell membrane is composed of proteins and amphiphilic lipids (mainly phospholipids), carbohydrates, water molecules, mineral and metal ions. The biochemical composition of the membrane is stabilized through electrostatic forces, the hydrophobic effect and Van der Waals interactions. The electrostatic force is the attractive or repulsive interaction between different particles and materials based on their electrical charges, which exists in all hydrophilic molecules. The hydrophobic effect is the tendency of nonpolar substances to aggregate, and occurs between the hydrophobic amino acids from the membrane embedded protein and the long aliphatic chain from the phospholipid. The Van der Waals attraction are the attractive

forces between the molecules or atomic groups in the cell membrane, that are the complement of hydrophobic effect. The most important electrostatic forces in the cell membrane include the interactions between the phospholipids and membrane embedded proteins, as well as the repulsion force among the phospholipids. The phospholipid composition of the cell membrane varies in each leaflet and cell type, but notably some types of the phospholipid, such as phosphatidylserine (PS) and phosphoinositol (PI), contain a negatively charged headgroup at physiological pH. Positively charged amino acids in a membrane protein can form highly conserved motifs, such as arginine-rich motif, that drive tight association of the protein with negatively charged phospholipids like PS and PI. On the other hand, the repulsive forces among the hydrophilic headgroups of phospholipids could reduce the steric effects, enabling the tumbling of the phospholipid molecule. However, due to the hydrophobic environment inside the membrane, the permittivity of such events is relatively low and the electrostatic force is consequently high. Even though the electrostatic is comparably strong, it is countered by the abundant hydrophobic effect and Van der Waals forces occurring between the fatty acid chains of the lipids. This is essential to the overall structure of the cell membrane. The coordinate bonds formed between the membrane and ions, and between hydrogen bonds of the hydrophilic faces of the membrane bilayer and the aqueous environments of the cell interior and exterior are also significantly involved in the structure of the membrane.

1.1.3 Structure of the Cell Membrane

Since the 1930s, several hypotheses were put forward to explain the molecular structure of the cell membrane. The fluid mosaic model, which was proposed by Singer and Nicolson in 1972 [1], is widely supported by experiment evidence and generally accepted (Fig. 1.1). This model defines the cell membrane as a two-dimensional liquid that restricts the lateral diffusion of membrane components and highlights two quintessential features. First, the cell membrane is asymmetric.

The hydrophobic end of the membrane borders the lipid bilayers, in which each molecule is arranged with its hydrophobic end directed inward toward the opposite leaflet of the lipid bilayer and its hydrophilic end directed outward. Each side of the lipid bilayer is composed of different proteins and lipids, which contributes to the asymmetry of the cell membrane. The lipid asymmetry is maintained by the translocation of specific phospholipids to each leaflet which mediated by the type IV P-type ATPases, lipid transporters flippase and scramblase [2, 3]. This phospholipid asymmetry across the membrane can result in membrane domains—for example, localized membrane curvature, which is required during the membrane fusion events, can result from packing of phospholipids with bulky headgroups into one leaflet versus packing of phospholipids with small headgroups in the other leaflet.

Secondly, the cell membrane is highly fluid. The phospholipid molecules and the membrane embedded proteins are mobile in the cell membrane, which is very important for the assembly of the macromolecular complexes that mediate specific

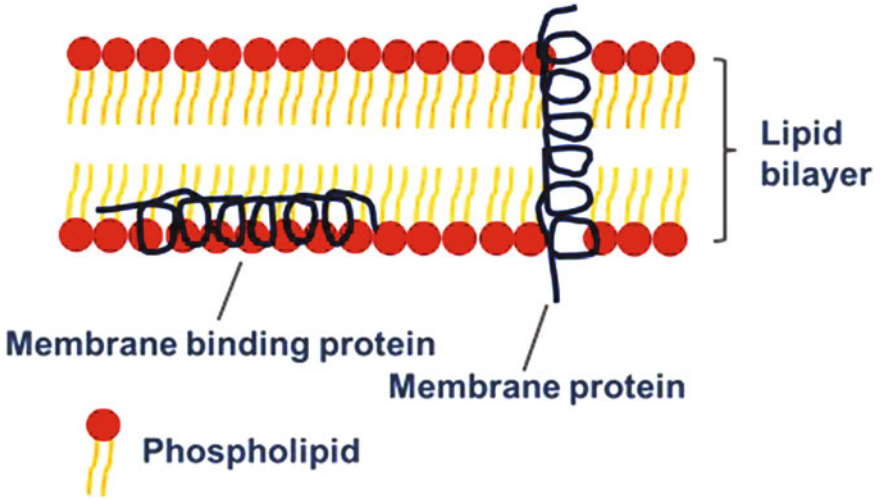

Fig. 1.1 Basic cell membrane model

functions of the membrane like signaling, bulk transport and cell-cell adhesion since the dynamics of membrane embedded proteins is influenced by the abutting phospholipid molecules. The lipid molecule can also undergo phase transitions at given temperatures, existing in either a liquid if the transition temperature is exceeded or as a solid phase if the environment temperature is below the transition temperature. The temperatures at which a lipid molecule undergoes a phase transition depend on the length and degree of unsaturation of the acyl chains of the phospholipids. The concentration of different ions and pH also affect the membrane's fluidity.

1.1.4 Phospholipid in Cell Membrane

Lipids are the foundational materials in the cell membrane and may include phospholipids, cholesterol and glycolipids, of which phospholipids are the most important and widely distributed class of lipids. All phospholipids including glycerophospholipids and sphingolipids are amphiphilic, and contain a hydrophobic fatty acid tail and a hydrophilic headgroup.

Glycerophospholipids are the major component of the cell membrane (for this reason they are the lipid of choice for in vitro lipid bilayer reconstitution). Besides acts as the dominant structural element of the cell membrane, glycerolphospholipids also play a key role in membrane embedded protein recognition and signal transduction.

These lipids are chiefly composed of two hydrophobic tails and a hydrophilic headgroup that are joined together by a glycerol molecule. The hydroxy groups from position 1 and 2 of the glycerol react with the two fatty acids to undergo

esterification and form the hydrophobic fatty acid tails. The hydrophilic headgroup is linked to the hydroxyl group from position 3 of the glycerol molecule through a phosphodiester bond.

The volume ratio of hydrophobic "tail"/hydrophilic headgroup is a significant factor that keeps the cell membrane intact. An illustration of this phenomenon can be seen with phospholipase, an active component in some venoms. Phospholipase digests one hydrophobic alkane chain of a lipid molecule, which shrinks the hydrophobic region of the molecule substantially and makes the lipid similar to a detergent molecule. These damaged lipid molecules can further disrupt the cell membrane and effect lysis of the cell.

Glycerolphospholipids are classified by their headgroups, which are a great source of molecular diversity: Dioleoyl phosphatidic acid, Phosphatidic acid, Phosphatidylcholine (lecithin), Phosphatidylserine, Phosphatidylethanolamine (cephalin), Phosphatidylinositol and Diphosphatidylglycerol (Cardiolipin). The phosphite of all phospholipid molecules has a negative charge at physiological conditions. The net charge of the phospholipid molecule varies due to the different charges that headgroups may have. For example, the headgroup of Phosphatidylcholine and phosphatidylethanolamine each contain a positive charge, resulting in an overall neutral charge for these two glycerophospholipids. The headgroups of Phosphatidylinositol and Cardiolipin are also electrically neutral. In contrast, the headgroup of Phosphatidylserine contains a positive as well as a negative charge, resulting in a net negative charge for the whole molecule. Such negatively charged phospholipids are also known as acid phospholipids.

Additional structural diversity in the glycerophospholipids come from variations in the length and saturation of the aliphatic chains. This is of important interesting in the study of biological membranes and membrane proteins because these features may be important determinants in the function of the system being studied. For the purposes of membrane studies the abbreviations PO, DM, DO and DH are frequently used to distinguish between the different types of lipid by the length and saturation of their aliphatic chains. The degree of chain saturation may require special handling—the unsaturated bonds of an aliphatic chain could be oxidized on exposure to air. Therefore, a sample of phospholipid should usually be stored under nitrogen or other inert gas to prevent oxidation. Figure 1.2 demonstrates how the aliphatic chains can contribute to the molecular diversity within of a particular class of glycerophospholipids. It is conventional to name glycerophospholipids by both their hydrophilic headgroup and their hydrophobic tails. In this nomenclature, each hydrophobic tail chain is named by "X:Y", separated by "/", with X giving the number of total carbon atoms in the tail chain and Y representing the number of the unsaturated bond in that tail chain. For example, POPC (1-palmitoyl-2-oleoyl-sn-glycero-3-phosphocholine) can be named as PC (16:0/18:1). The physicochemical properties of the glycerophospholipid, like the transition temperature, are strongly influenced by the aliphatic chains. The wide variation in the transition temperatures for the various PC lipids demonstrate this phenomenon. POPC is −2 °C; DMPC (1,2-ditetradecanoyl-sn-glycero-3-phosphocholine) is 23 °C; DOPC (1, 2-di-(9Z-octadecenoyl)-sn-glycero-3-phosphocholine) is −17 °C.

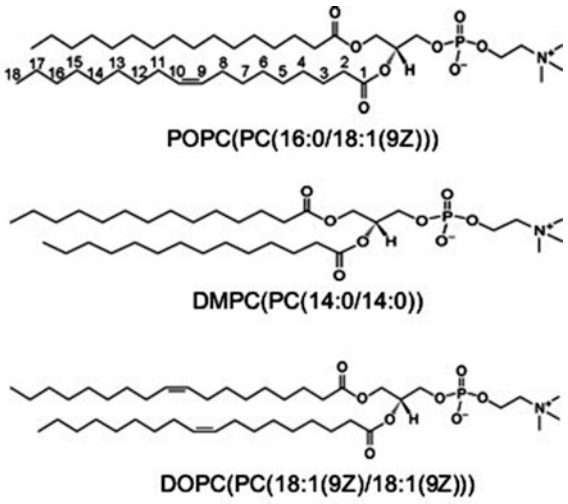

Fig. 1.2 Phosphatidylcholine with different aliphatic chains

Sphingolipids represent an unusual class of phospholipid in the cell membrane. Originally isolated in the 1870s from brain extracts, sphingolipids were first named after the mythical Sphinx because of their enigmatic nature. Sphingolipids contain a backbone of sphingoid bases that are linked to two groups. The backbone is amide-linked to a fatty acid and O-linked to a variable charged head group, designated as "X". "X" could be a hydrogen atom (ceramide), a phosphocholine group (sphingomyelin, SM), a glucose (glucosylcerebroside), or a monosaccharide or polysaccharide (globoside or ganglioside, also called glycosphingolipid). The sphingolipids play important roles in signal transmission and cell recognition, especially in neural tissue.

Some glycosphingolipids, such as globoside and ganglioside, are indispensable in the formation of lipid rafts. Lipid rafts are 10–100 nm subdomains of the cell membrane that contain high concentrations of glycosphingolipid and cholesterol [4]. The lipid rafts are more ordered and tightly packed than other liquid-ordered regions of the cell membrane, but drift freely in the lipid bilayer [5]. Lipid rafts are believed to form the sites of membrane protein complex assembly [4, 6].

The phospholipid composition of the cell membrane varies in different species. Sphingolipids are found in mammalian, yeast and plant cells but not in prokaryotic cells. Phospholipids containing the same headgroup can also vary in different species by length and saturation of aliphatic chains. Figure 1.3 shows the phosphocholine phospholipid in different species with various aliphatic chains. Additionally, the composition of the bilayers in the cell membrane also varies. In mammalian cells, the outer layer of the cell membrane mainly contains uncharged phospholipids like PC and SM. Meanwhile, the inner layer contains negatively charged phospholipids, such as PS and PI Fig. 1.4.

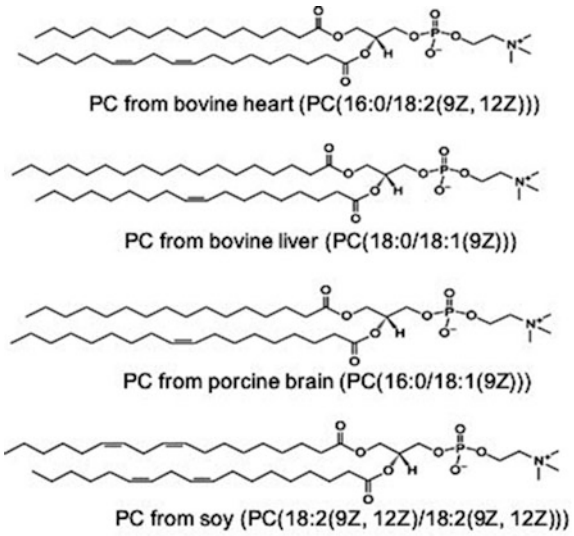

Fig. 1.3 Phosphocholine phospholipid in varied species and organs

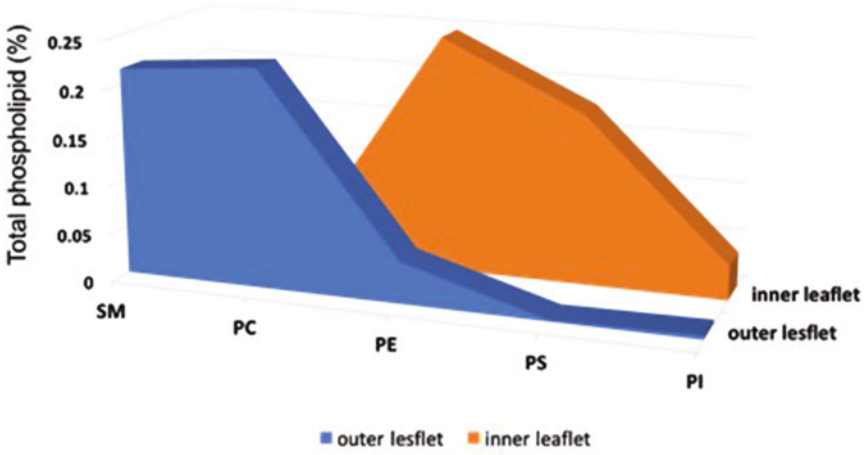

Fig. 1.4 Phospholipid distribution of mammal cell membrane

1.2 Membrane Proteins and in Vitro Reconstitution

A large proportion of genes (about 25–35%) encode membrane proteins in both prokaryotic and eukaryotic cells [6, 7]. Membrane proteins are proteins that in their native state are permanently or temporarily anchored to the membrane. Integral membrane proteins span the lipid bilayer, which makes them permanently

integrated in the membrane. These proteins can fold into two transmembrane topologies: helix bundles or beta barrels. The helix bundle proteins are the most frequently occurring integral membrane proteins and normally contain one to ten transmembrane helixes. Helix bundle proteins may form oligomers to be functional. The beta barrel transmembrane proteins are mainly found in the outer membranes of Gram-negative bacteria, as well as outer membrane of mitochondria and chloroplasts of higher organisms. Many beta barrel proteins are monomeric, but some oligomer forms also exist [8]. By contrast, membrane binding proteins are temporarily anchored to the membrane; this will be discussed later.

In order to study the membrane proteins in vitro, a suitable model membrane that mimics the cell membrane is essential. A number of well-established artificial membrane systems are available and differ in the molecular shape of lipids and detergents used and the hydrophobic-hydrophilic volume ratio. Detergent micelles, detergent/lipid bicelles, liposomes and nanodiscs are the most popular membrane formats Fig. 1.5.

Detergents have many of the same physicochemical characteristics as lipid molecules. Both are amphipathic, with a hydrophilic headgroup and a hydrophobic "tail". The distinguishing feature when comparing detergents and lipids is in the length of the hydrophobic tail, which is typically much shorter in detergents. The hydrophobic "tail" of lipid molecules is longer, which enables spontaneous formation of lipid bilayers in a physiological environment. The volume of the hydrophobic alkane chains in a detergent molecule is equivalent to or even smaller than the volume of the hydrophilic headgroup in the molecule, which limits the ability of the detergents to pack into a uniform layer in the way lipids can. Therefore, the detergents prefer to form micelles in a liquid colloid, an arrangement in which the headgroup of the detergent contacts the surrounding solvent while sequestering the hydrophobic "tail" in the micelle's hydrophobic center. Free detergent molecules spontaneously form micelles when a threshold concentration of the detergent is exceeded in solution. This concentration is known as the critical micelle concentration (CMC) and is defined as the concentration of detergent above which micelles form. At this point, increasing the concentration of the detergent in solution drives all additional detergent monomers into forming micelles.

Bicelles can be thought of as a lipid bilayer encapsulated by detergent molecules. The size of a bicelle depends on the relative amounts of detergent and lipid present in the solution. The ratio of lipid molecules to detergent molecules is called q value and is used to calculate the size of the bicelles. The larger the q value (more lipids), the larger the average size of the bicelles. Liposomes are spherical lipid vesicles having at least one lipid bilayer. Liposomes can vary by their size and number of bilayers they contain: multilamellar vesicles (MLVs) contain more than one bilayer and are of moderate size; small unilamellar vesicles (SUVs) and large unilamellar vesicles (LUVs) each contain a single bilayer.

As lipids and detergent are added into solution, the solution can exchange between micelles, bicelles and liposomes as the relative concentrations of lipid and detergent are changed; membrane proteins present in solution can likewise exchange between these different formats as they form. Liposomes are the most

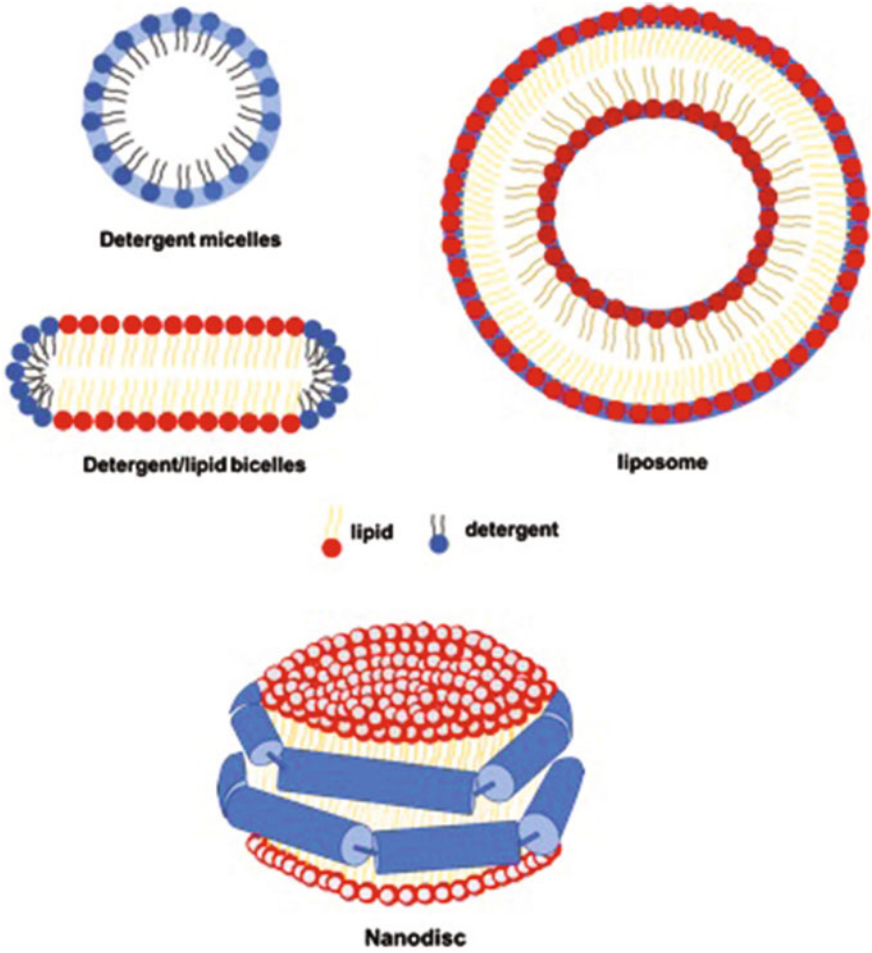

Fig. 1.5 A schematic representation of a detergent micelles, detergent/lipid bicelles, liposome and nanodisc

popular model membrane system for studying the activity of membrane proteins, while micelles are the prominent format for extracting the membrane protein from its native membrane. For preparing sample to study the membrane protein function, reconstitution of the membrane protein into a desired membrane system is often the final step. In this step, excess detergent is removed from the solubilized, purified membrane protein sample at the end of the purification procedure by dialysis or by adsorption to hydrophobic beads when mixing the membrane protein embedded micelle and bicelles. This results in the formation of liposomes embedded with membrane proteins.

Finally, nanodiscs are essentially bicelles edged with amphipathic proteins instead of the detergent molecules. The advantages of the nanodisc format will be discussed in Chap. 2 with great detail.

1.3 Membrane Binding Protein

Membrane binding proteins (MBPs) are soluble proteins that dynamically attach to the cell membrane or to integral membrane proteins. It is this ability to temporarily bind its target that enables the MBP to play an important role in cell signal transduction [9].

There are different possible interactions between membrane binding proteins and the cell membrane. Binding to the membrane can occur through non-specific hydrophobic interactions between the lipid bilayers and the hydrophobic regions of the MBPs, such as the amphiphilic alpha helix, exposed hydrophobic loop region and post-translationally modified amino acids (via acylation and esterification).

MBPs can also anchor directly to the membrane through reversible lipidation like prenylation, myristoylation and palmitoylation; in such cases these proteins are referred to as lipid-anchored proteins. Upon dissociation of MBPs from the membrane, the modified residues may be protected by the hydrophobic binding region of the membrane. Residue modifications of MBPs typically occur in the flexible regions of the protein and are not easily studied with X-ray crystallography.

Proteins may also attach to the cell membrane through binding to specific phospholipid molecules, especially at the hydrophilic headgroup. Hydrogen bonding, the hydrophobic effect, Van der Waals' forces, ion bridges between aspartic acid or glutamate residues and phosphite, add additional stability to the interaction between lipid molecules and proteins. Electrostatic forces between the protein and phospholipids also contribute to these interactions, although the ionic strength of the surrounding solvent can interfere with this interaction [9]. Table 1.1 summarizes these protein domain interactions with specific phospholipids.

Table 1.1 Summary of the domain interaction with the specific phospholipid molecule

Protein	Phospholipid
C1 domains [20]	Diacylglycerol and Phorbol esters
C2 domains [21]	Phosphatidylserine or Phosphatidylcholine
FYVE domians [22]	Ptdlns3P
ENTH domains [23]	Ptdlns(3,4)P2 or Ptdlns(4,5)P2
ANTH domains [24]	Ptdlns(4,5)P2
ERM(ezein/radixin/moesin)family [25]	
Pleckstrin homology domains [17]	Phosphoinositides
PX domains [26]	
Tubby domains [27]	

The depth that a MBP anchors into the cell membrane depends on the properties of the lipids and the protein and interactions among them. These proteins can retain their conformation on anchoring to the membrane because they remain exposed to the solution. For the protein, which contains exposed hydrophobic regions or intrinsically disordered protein, accessing the hydrophobic region of the cell membrane is mediated by the hydrophobic effect. These interactions are exothermic and can alter the transition temperature of the phospholipid. In some cases, that electrostatic force and hydrophobic effect coexist, enabling the membrane binding protein to interact with the hydrophobic core of cell membrane directly. Regardless of the mechanism, hydrophobic regions are indispensable to a protein's anchoring to the membrane.

1.4 NMR Methods to Study Membrane Protein

Studies of the cell membrane mandate structural information on the membrane and its components, especially membrane proteins. Three methods are currently widely used to determine the protein structure: X-ray Crystallography, Nuclear Magnetic Resonance (NMR) and Cryo-Electron Microscopy (cryo-EM). X-ray crystallography and NMR have been used for many years to resolve protein structures at high resolutions. Since 2013, cryo-EM has emerged as a powerful tool for the study of protein structure with high resolution because of improvements in camera technology and reconstitution methods. Unlike the other two techniques, which rely on immobilization of the protein for structure determination, NMR (solution NMR) is used to obtain the structure in the aqueous environment, which means that the protein is closer to its physiological condition. Besides structure determination, NMR is also used to study protein-protein interactions, protein-lipid interactions, protein refolding and protein dynamics.

1.4.1 Background of NMR

Nuclear Magnetic Resonance (NMR) can be explained word by word. "Nuclear" refers to a nucleus for which the spin quantum number is not zero. "Magnetic" indicates the application of an external magnetic field. "Resonance" means that when a nucleus (spin quantum number is not zero) is placed into the magnetic field, it can either align itself with (lower energy) or against (higher energy) the extra magnetic field. If this nucleus is then irradiated by radio waves, it may absorb the energy and jump to the higher energy level from the lower energy lever. Due to relaxation, they will go back to the lower energy level, and we will observe the emission of electromagnetic radiation "resonance" process.

NMR was independently discovered by the Purcell group at Harvard University and the Bloch group at Stanford University in 1946. During the next several

decades, NMR developed well and found application in biology, medical diagnosis, materials science and geologic examination. In the 1950s, the discovery of chemical shift and J-coupling linked information about the chemical structure and NMR signals, which was of great relevance in protein biology. Fourier transformation NMR could irradiate multiple-frequency nuclei at the same time by the 1960s. The progress of high magnetic field and two dimensions, three dimension spectrum solves the signal overlap problem. Combined with growing pulse sequence and computer science, Wüthrich resolved the first protein structure by NMR in 1985. After that milestone event, the boost of related pulse sequence and software made solution NMR become a very important tool to study protein structure and dynamics.

In recent decades, the software, hardware and the sample preparation of NMR underwent huge progress. Deuteration, specific labeling, alignment medium, and paramagnetic labeling were introduced into the NMR sample preparation. In addition, advances in software greatly progressed with the development of TROSY pulse [10], Four Dimension spectrum [11, 12], PRE (Paramagnetic relaxation enhancement) [13, 14] and RDC (Residual dipolar coupling) [15]. Hardware improvements included graduating, cryo-probe and high field magnetic body and were combined with the development of software and sample preparation to solve a wealth of new protein structures. By Nov 11 2016, 11669 structures were resolved by NMR and recorded in the Protein Data Bank (PDB) Fig. 1.6. The molecular weight limitation of the technique was also surpassed, and quantitative NMR-relaxation studies have been addressed for species as large as 670 kDa [16].

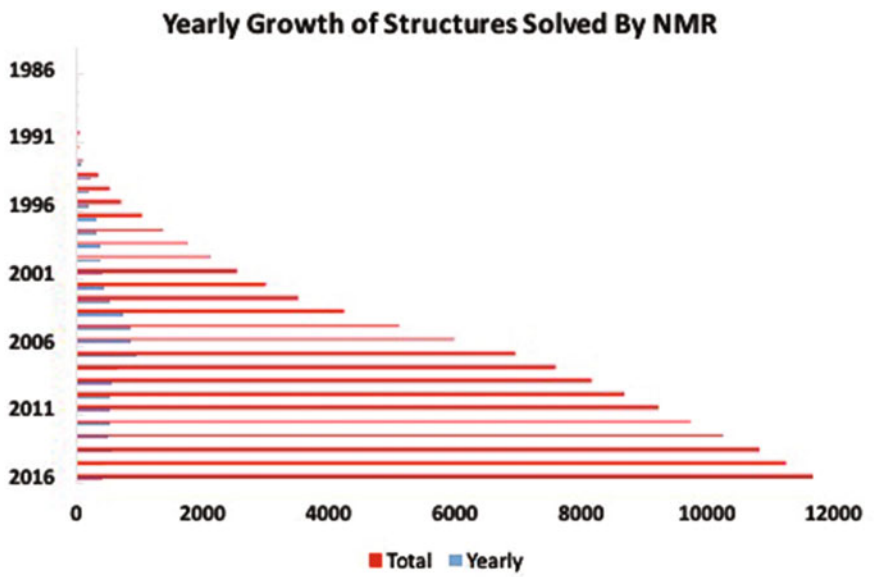

Fig. 1.6 NMR structure statistics from PDB

1.4.2 Use NMR to Study Protein Structure

To get the final protein structure by NMR, four important steps are required. First, the protein must be labelled with ^{15}N and ^{13}C, which can be excited and detected. Secondly, data is collected and assignments are made to the chemical shift. Thirdly, the constraints of the experiment must be obtained. Finally, the structure can be calculated and evaluated.

1.4.2.1 Protein Label and Sample Preparation

NMR can be performed on nuclei for which the spin quantum number is 1/2 (such as ^{1}H, ^{13}C, ^{15}N, ^{19}F and ^{31}P). The NMR signal is not amenable if the I's value of the detected nucleus is zero because of the absence of spin angular momentum. For nuclei with I values above ½, such as ^{14}N and ^{17}O, the effective shape of the nuclear charge distributes like an ellipsoid; this is caused by the nuclear electric quadrupole moment. The spectrum of the nuclear $I > 1/2$ is much broader compared with $I = 1/2$ in solution due to the decreased life time. Proteins are chiefly composed of hydrogen, carbon and nitrogen; for that reason, isotopes of these elements are relied upon by NMR: ^{1}H, ^{13}C, ^{15}N. Unfortunately, the natural abundance of ^{13}C and ^{15}N is low, which necessitates the use of the isotope labeling technique to prepare the NMR protein sample. In the prokaryotic *E.coli* express system, minimal medium is prepared for expression of the target protein. Minimal medium can contain $^{15}NH_4Cl$ or $^{15}NH_4SO_4$ as the unique nitrogen source and ^{13}C-glucose or ^{13}C-glycerol as the unique carbon source [17, 18].

The line widths increment and peak overlap are the two major problems that will make it difficult to study high molecular weight proteins by NMR. The peak overlap problem could be greatly improved by application of isotope labeling and two dimensional or three dimensional experiments. The chemical shift will be dispersed in 2D or 3D, even 4D space, which considerably attenuates the peak overlap. Larger protein molecules have longer rotational correlation times, and consequently shorter transverse relaxation times (T2). In other words, the NMR signal from larger protein molecules decays more rapidly, which result in incremental linewidths and poor resolution. For nuclei with $I = 1/2$, the relaxation is mainly contributed by the chemical shift anisotropy (CSA) and dipole-dipole (DD) coupling. To reduce the relaxation coming from the DD coupling, triple labelling is introduced during the protein sample preparation. The protein is expressed from prokaryotic *E.coli* in minimal medium, which supplies the ^{15}N and ^{13}C labeled nitrogen and carbon sources, uses D_2O instead of H_2O [19]. The gyromagnetic ratio of $^{2}H(\gamma D)$ is 1/6.5 of $1H(\gamma H)$, hence the relaxation coming from ^{2}H is 1/16, compared with $^{1}H([(I_{H+1})/I_D(I_{D+1})]\ (\gamma H/\gamma D)^2 \sim 16)$. Triple labelling will lead to about 70–80% deuteration of the side-chains, as there is certain amount of contaminating ^{1}H present from other media components. Higher levels of deuteration could be achieved by replace the ^{1}H medium component with ^{2}H component, such as using ^{13}C, ^{2}H-glucose

instead of ^{13}C glucose; unfortunately it is very expensive to do this. Additionally the backbone NH group is exchangeable, in that the NH will exchange back to ^{1}H during the protein purification with normal aqueous solutions. Hence, the triple-labelled protein sample could be used in normal NH-based experiments. Deuteration of protein can also cause a chemical shift change versus an undeuterated sample. Thus, the process of chemical shift assignment data should be performed cautiously if they come from experiments that were done with both deuterated and normal samples. In addition, spin–lattice relaxation time (T1) is also optimized after deuteration samples because it causes the longer delay time (D1) during collecting data. In order to simplify the spectrum or collect unique data, the specific labelling is also introduced and may involve partial labelling of the peptide, specific type of amino acid labelling and special group of side chain labelling.

After purifying the labelled protein, the next step is to prepare the final NMR sample with the labelled protein. The basic common requirement is that the protein is concentrated (typically about 1 mM) and stable (stable over several days). The solvent buffer should be neutral or slightly acidic. The exchange rate between NH groups and H_2O significantly increases when the pH is above 7 and thus such conditions can abrogate the signal from NH-based experiments. There are some issues that should also be considered for choosing the buffer. The pH should avoid the protein PI value in order to prevent the sample's precipitation. The buffer molecules should not interact with the protein sample and remain in the aqueous state during the variable-temperature experiments. There should also be no solvent signal in the protein signal range. The salt concentration should be less than 500 mM for conventional probes and less than 100 mM for cryogenic probes. Additives are also widely considered in the sample preparation. Glutathione (GSH), Glutathione disulfide (GSSG), Dithiothreitol (DTT) and glycerol are introduced to improve the protein folding. Sodium Azide (NaN_3) is an important antimicrobial to use for preventing the growth of bacteria. Some samples can be air-sensitive, and in such cases the NMR tube should be purged with argon gas. Finally, 5–10% D_2O and 10–50 μM calibration standard compound (such as 4,4-dimethyl-4-silapentane-1-sulfonic acid (DSS)) should be mixed with samples in the NMR tube; these will function as locking and inner references.

1.4.2.2 Collecting Data and Chemical Shift Assignment

In NMR spectroscopy, the chemical shift is the resonant frequency of the nucleus relative to the reference signal from the standard compound in a magnetic field. In physical terms, the currents of electrons in the molecular orbital induce the local magnetic field of the nucleus, which experiences the magnetic field. The electron distribution of the nucleus will eventually affect the resonance frequency. The variation of the nuclear resonance frequency of the nucleus due to variation in the electron distribution is called the chemical shift. Any factors that could affect the electron distribution of the nucleus will change the chemical shift of the nucleus. Hence, not only the local geometry (binding partners, bond lengths, angles between

Table 1.2 The experiments used for chemical shift assignment and corresponding magnetic moment transfer pathway

NMR Experiment	Magnetic moment transfer pathway
Backbone assignment	
HNCACB	$H^N(i) \rightarrow N(i) \rightarrow \underline{C^{\alpha}(i)/C^{\alpha}(i-1)}, \underline{C^{\beta}(i)/C^{\beta}(i-1)} \rightarrow \underline{N(i)} \rightarrow \underline{H^N(i)}$
CBCA(CO)NH	$H^{\alpha}(i-1), H^{\beta}(i-1) \rightarrow \underline{C^{\alpha}(i-1)}, \underline{C^{\beta}(i-1)} \rightarrow \underline{CO(i-1)} \rightarrow \underline{N(i)} \rightarrow \underline{H^N(i)}$
HN(CO)CACB	$H^N(i) \rightarrow N(i) \rightarrow CO(i-1) \rightarrow \underline{C^{\alpha}(i-1)}, \underline{C^{\beta}(i-1)} \rightarrow CO(i-1) \rightarrow \underline{N(i)} \rightarrow \underline{H^N(i)}$
HNCA	$H^N(i) \rightarrow N(i) \rightarrow \underline{C^{\alpha}(i)/C^{\alpha}(i-1)} \rightarrow \underline{N(i)} \rightarrow \underline{H^N(i)}$
HN(CO)CA	$H^N(i) \rightarrow N(i) \rightarrow CO(i-1) \rightarrow \underline{C^{\alpha}(i-1)} \rightarrow CO(i-1) \rightarrow \underline{N(i)} \rightarrow \underline{H^N(i)}$
HNCO	$H^N(i) \rightarrow N(i) \rightarrow \underline{CO(i-1)} \rightarrow \underline{N(i)} \rightarrow \underline{H^N(i)}$
HN(CA)CO	$H^N(i) \rightarrow N(i) \rightarrow C^{\alpha}(i)/C^{\alpha}(i-1) \rightarrow \underline{CO(i)/CO(i-1)} \rightarrow C^{\alpha}(i)/C^{\alpha}(i-1) \rightarrow \underline{N(i)} \rightarrow \underline{H^N(i)}$
HBHA(CO)NH	$\underline{H^{\alpha}(i-1)}, \underline{H^{\beta}(i-1)} \rightarrow C^{\alpha}(i-1), C^{\beta}(i-1) \rightarrow CO(i-1) \rightarrow \underline{N(i)} \rightarrow \underline{H^N(i)}$
Side-chain assignment	
^{15}N-TOCSY-HSQC	$\underline{H^{aliph}(i)} \Rightarrow H^N(i) \rightarrow \underline{N(i)} \rightarrow \underline{H^N(i)}$
(H)CC(CO)NH-TOCSY	$\underline{H^{aliph}(i-1)} \rightarrow \underline{C^{aliph}(i-1)} \Rightarrow C^{\alpha}(i-1) \rightarrow CO(i-1) \rightarrow \underline{N(i)} \rightarrow \underline{H^N(i)}$
H(CC)(CO)NH-TOCSY	$\underline{H^{aliph}(i-1)} \rightarrow \underline{C^{aliph}(i-1)} \Rightarrow C^{\alpha}(i-1) \rightarrow CO(i-1) \rightarrow \underline{N(i)} \rightarrow \underline{H^N(i)}$
H(C)CH-TOCSY	$\underline{H^{aliph}(i)} \rightarrow C^{aliph}(i) \Rightarrow \underline{C^x(i)} \rightarrow \underline{H^x(i)}$
(H)CCH-TOCSY	$\underline{H^{aliph}(i)} \rightarrow \underline{C^{aliph}(i)} \Rightarrow \underline{C^x(i)} \rightarrow \underline{H^x(i)}$
H(C)CH-COSY	$\underline{H^x(i)} \rightarrow C^x(i) \rightarrow \underline{C^y(i)} \rightarrow \underline{H^y(i)}$
(H)CCH-COSY	$\underline{H^x(i)} \rightarrow \underline{C^x(i)} \rightarrow \underline{C^y(i)} \rightarrow \underline{H^y(i)}$

→ Represent the magnetic moment transfer pathway, ⇒ represents the magnetic moment transfer pathway through the Total Correlation Spectroscopy (TOCSY). The last atom which is underlined is the directly detected atom. The other atoms, that are underlined, are indirectly detected atoms H^{aliph}, C^{aliph} represent the proton and carbon atoms from side chain; $H^x(C^x)$ and $H^y(C^y)$ represent the linked CH group from side chain

bonds, and so on), but also the neighbors (electron density, electronegativity of the neighboring groups and anisotropic induced magnetic field effects) of the nucleus could affect the chemical shift. In other words, the chemical shift reflects the nucleus itself and its microenvironment. Hence, the first step in elucidating the protein structure by NMR is chemical shift assignment.

The chemical shift assignment can be obtained by Nuclear Overhauser Effect (NOE) information or experiments based on the J-coupling (spin-spin splitting), which is the primary approach. Protein chemical shift assignments can be performed on backbone and side chains separately, distinguishing between them. The general approach for assigning the backbone and side chain resonances listed in Table 1.2 was based on the use of the ^{1}H,^{15}N HSQC spectrum as a fingerprint of the observable amides. The several experiments, HNCACB, CBCA(CO)NH (or HN(CO)CACB), HNCA, HN(CO)CA, HN(CA)CO and HBHA(CO)NH, are designed to assign the chemical shift of backbone atoms (^{15}N,^{1}HN,^{13}CO, ^{13}Ca and ^{1}H). Notably, the chemical shift of ^{13}CO atoms disperse better than other backbone atoms if the protein is unfolded. Hence, HNCO and HN(CA)CO are commonly recruited for backbone assignment of unfolded protein. The 3D experiments, ^{15}N-TOCSY-HSQC, (H)CC(CO)NH-TOCSY, H(CC)(CO)NH-TOCSY, H(C)

CH-TOCSY, (H)CCH-TOCSY, H(C)CH-COSY and (H)CCH-COSY are carried out for side chain assignment.

The interpretation and assignment of NMR data of a protein usually starts with assignment of the backbone atoms and linking with their sequential neighbors. Here is how the backbone is assigned based on HNCACB and CBCA(CO)NH experiments. For the HNCACB spectrum, there are four peaks, the $C_{\alpha,}$ $C_{\alpha-1}$, C_{β} and $C_{\beta-1}$, which represent the carbon atoms of previous residue as well as those of itself. For the CBCA(CO)NH, there are only two peaks, the $C_{\alpha-1}$ and $C_{\beta-1}$, which represent the carbon atoms of the previous residue. After collecting the data from these two experiments, it is possible to identify which peaks belong to the previous residue or to itself. And from the specific chemical shifts region of the specific amino acid's backbone, there is a chance to guess which amino acids that are present. Then the chemical shift of whole backbone could be accomplished with the same strategy. After assigning the chemical shift of the backbone, the side chain assignment could be achieved by experiments that connect the atoms between the backbone and side chain through J-coupling.

To assign the chemical shift of large protein molecules, the transverse relaxation-optimized spectroscopy (TROSY) technique is utilized [10]. For spectra in which decoupling has not been applied, peaks appear as multiplets due to J-coupling. The line width of different multiplets are varied due to constructive or destructive interactions between different relaxation mechanisms. Typically, the relaxation of the large protein molecule is mainly dominated by the chemical shift anisotropy (CSA) and dipole-dipole (DD) coupling. The TROSY-based experiment is designed to isolate the component that the CSA and DD have almost cancelled. The CSA is induced by magnetic field; thus the strength of the CSA is field-dependent, while DD is field-independent. Accordingly, the TROSY approach requires high magnetic fields to obtain the necessary balance between the CSA and DD relaxation mechanism, as well as the deuteration of the samples for attenuating the DD relaxation.

Of note, for deuterated samples, the backbone NH group is exchangeable, while deuterium atoms that linked to the carbon atom are not exchangeable. Thus, some experiments, especially the experiments accomplished in the side chain assignment (such H(C)CH-COSY), for which the start or the end atom during the magnetic moment transfer pathway is Hc, could not be compatible with deuterated samples. $^{15}N/^{13}C$ labelled samples is the best choice for such experiments.

1.4.2.3 Obtaining the Constraints for Structure Calculation

Distance constraints, hydrogen bond constraints, and dihedral constraints are the leading constraints that are recruited in the protein structure calculation by NMR. Among them, the distance constraints from Nuclear Overhauser Effects (NOEs) are very important.

The NOE, an important consequence of dipole-dipole (DD) relaxation, is the transfer of nuclear spin polarization from one spin bath to another nearby spin bath.

Hence the NOE effect can be used to determine atomic distances. NOESY [20] (the abbreviation of NOE SpectroscopY) is a type of NMR experiment exploiting the NOE. This technique is capable of determining which signals, or cross peaks, arise from protons that are close to each other in space even if they are not chemical-bonded. The cross peak occurs if the distance between two proton atoms is less than 5 Å, indicating a strong NOE. The intensity of the cross peak is the scale of the NOE effect, which is approximately proportional to $1/r^6$ due to the $1/r^6$ distance dependence of DD relaxation, where r is the distance between the protons. The exact distance can be calculated by comparing the intensity difference between the cross peak of the protons of interest and that of the two protons from a methylene group, for which the distance is 1.75 Å.

However, in calculating the correct distance constraint, one must account for spin diffusion. Spin diffusion occurs when the nuclear spin polarization transfers from nucleus A to B and then from B to C, but appears as a direct transfer from A to C. Spin diffusion occurs primarily for long mixing times outside the "linear approximation", and this will cause the misleading cross peaks and give an incorrect distance (nuclear A to C). For some peptides, the rotational correlation time falls in a range where the NOE effect is too weak to be detected. In these cases the ROESY (Rotating Frame Nuclear Overhauser Effect Spectroscopy) is used instead of NOESY to achieve the same readout [21, 22].

A hydrogen bond, a special case of dipole forces, is the electrostatic attraction between two polar groups that occurs when a hydrogen (H) atom covalently bound to an electronegative atom of one polar group undergoes a dipole-dipole interaction with another highly electronegative atom, such as nitrogen (N), oxygen (O), from another polar group. The hydrogen bond plays an important role in stabilizing protein structure and is especially important in mediating the formation of secondary structures. NMR is a powerful tool for determining the hydrogen bonding arrangements in proteins, especially the hydrogen bonds that form between the backbone oxygens and amide hydrogens. Sample preparation is straightforward—after lyophilization, the ^{15}N labelled protein is dissolved in D_2O. Then, the hydrogen-deuterium (HD) exchange experiment [23], a series of ^{1}H–^{15}N HSQC experiments that are carried out at different time points, is introduced to study the hydrogen bond. In this case the observable signal comes only from the residues that are involved in hydrogen bonding; other signals from protons are negligible compared with the regular sample because the backbone amide protons (involved in the H–bonds) has exchanged to deuterium.

The dihedral angle is another important constraint in studying protein structure by NMR. Two torsion angles that describe the rotations of the protein backbone around the bonds between N–Ca(Phi, ϕ) and Ca–C(Psi, ψ) are the preferentially used dihedral angle constraints. The ϕ and ψ values vary if the residues are located at different types of secondary structure regions and result in a change of the chemical shift. For example, for an α helix the chemical shift of Hα and C_β shifts to the high field while the Cα and CO group shifts to the low field with respect to the shifts for the same atom from a β sheet. It should be noted that for this reason the software TALOS [24] and Chemical Shift Index (CSI) [25] are very useful for

predicting the protein secondary structure based on the backbone chemical shift. The specific NOE signal could also be used to study the protein secondary structure. The strong NOE signal appears between the I_{HN} and $I+2_{HN}$, as well as the $I_H\alpha$ and $I+3_{HN}$ or $I+3_{H\beta}$ for an α helix region. While the NOE signal of I_{HN} and $I+1_H\alpha$ is much stronger than I_{HN} and $I_H\alpha$ for β sheet region. The dihedral angle constraints could also be acquired by applying the Kaplus equation [26], which describes the correlation between dihedral torsion angles and measurable 3 J-coupling constants in NMR.

Although the NOE, hydrogen bond and dihedral angle are important constraints, another constraint is needed: long-range distance constraints. To get the long-range distance constraints that are important for calculating the structure of multi-domain proteins, RDC (residual dipolar coupling) and PRE (paramagnetic relaxation enhancement) must be experimentally determined. Dipolar coupling is anisotropic and sensitive to the orientation of the chemical bond vector. Unfortunately, the dipolar coupling for diamagnetic molecules at moderate field strengths averages to zero in the solution because proteins in solution tumble rapidly and give a nearly isotropic distribution. The residual dipolar coupling between two spins in a molecule occurs if partial molecular alignment is exerted, which leads to an incomplete averaging of the dipolar coupling in the solution. Furthermore, the orientation information between the chemical bond and the applied magnetic field could be achieved by analyzing the residual dipolar coupling. Thus, the RDC experiment is widely applied in the structural study of multidomain proteins and can supply the orientation information between different domains. There are numerous methods designed for measuring residual dipolar coupling [27], but these are generally classified into two groups: frequency based methods and intensity based methods, but that is beyond the scope of this discussion.

PRE (paramagnetic resonance enhancement) is another method to provide the long-range distance (15–24 Å) information in the protein structure study that can complement NOE restraints. In PRE experiments, a paramagnetic probe is introduced into the protein sample; this causes enhanced relaxation and decreased signal of the spins in proximity to the paramagnetic spin label via dipole-dipole interactions. As with the NOE, the PRE effect is approximately proportional to $1/r^6$ due to the $1/r^6$ distance dependence of DD relaxation, where r is the distance between the paramagnetic probe and the observed spin. A variety of methods are available for introduction of the paramagnetic spin label at a specific site [28]. This can be done by chemical modification or genetic engineering, or simply by dissolving the paramagnetic probe directly into the sample solution. The use of paramagnetic spin labels is very important in the study of membrane proteins. In this case the paramagnetic spin labels can be attached to lipids, which allows them to intercalate into the space of the phospholipid bilayer by hydrophobic interactions between the label and the hydrophobic core of the bilayer. By studying the spectra of different paramagnetic probes introduced into the sample, information about the amino acid location with respect to the phospholipid bilayer can be acquired.

1.4.2.4 Structure Calculation and Refinement

Structure calculation is the process of determining the self-consistent system of the protein structure from all of the information collected in the experiments. This can be separated into initial structure model determination, structure calculation and structure refinement.

The initial structure model can be achieved by homology modeling or a preliminary structure calculation. The latter one is the typical method, which combines chemical shift assignment and a number of reasonable constraints, such as the NOE constraints and dihedral constraints to determine an initial structure. Newly developed software, like the CANDID module from the CYANA program [29, 30], is capable of automatically assigning the NOE signals and converting them to distance constraints, and then finally calculating the initial structure model. The initial structure can then be used to analyze and correct the NOE constraints and chemical shift assignments. Then the new set of chemical shift assignments and distance constraints is used to recalculate the initial structure until there are no violations. The predicted topology of the protein is achieved from the initial structure.

In the next structure calculation step, the iterative refinement calculations must be performed. This requires repeating the structure calculations based on NOE and chemical shift assignments. During this step, which is also the most important and time-consuming step, a few of the ambiguous NOE constraints are added to the calculation process. After a number of calculation cycles, the ambiguous NOE constraints become a clearly assigned NOE signal. In this process, the system errors agree to occur for proteins with high molecular weight. Errors for proton, carbon and nitrogen chemical shifts are 0.02, 0.3 and 0.3 ppm respectively. There are numerous programs, such as CYANA [29, 30], Xplor-NIH [31] and CNS [32], that are designed for calculating the protein structure. These rely on two types of modeling: geometric distance model and simulated annealing. The last step of the structure calculation process is structure refinement, which is the simulated annealing process based on the optimized force field. Some programs, like AMBER [33], Xplor-NIH [31] and CNS [32], are widely employed in this step.

1.4.3 Using NMR to Study Protein Function

NMR can be exploited to study the function and structure relationships of proteins under near-physiological conditions. Elucidating a protein's function with respect to its structure is one of the distinguishing advantages of NMR. In this section, the NMR applications will be discussed from the perspective of protein dynamics and the interaction between proteins and their ligands.

1.4.3.1 Protein Dynamics Study by NMR

Proteins are generally considered to adopt unique structures. However, dynamics are essential for proteins to function both in vivo and in vitro. It is important to recognize that proteins are not static objects; rather, they are highly dynamic molecules capable of adopting multiple conformations. Transitions between different conformations can be described with various length scales and time scales. In a time scale, atomic vibrations occur at a picosecond (ps) scale, backbone and side chain motions occur at picosecond-nanosecond (ns) scale, allosteric interactions occur at a millisecond (ms) scale, and slow-breathing modes occur at the second (s) scale. The corresponding length scales are in the range of 10^{-2}–10^{2} Å [34]. In the last thirty years, research in this field clearly shows that protein dynamics has a high correlation with the protein's function. Thus, protein function research relying heavily on the study of dynamics has become more and more popular.

NMR has unique advantages in the study of protein dynamics. NMR experiments can probe protein dynamics with wide time scales, as large as 10^{-12}–10^{5} s (Fig. 1.7). In that range, almost all of the protein's motions can be studied. Additionally, when combined with the specific labelling technique, NMR can use most of the atoms from the native protein individually as a probe to study the protein's dynamics without introducing an artificial probe that may interrupt the

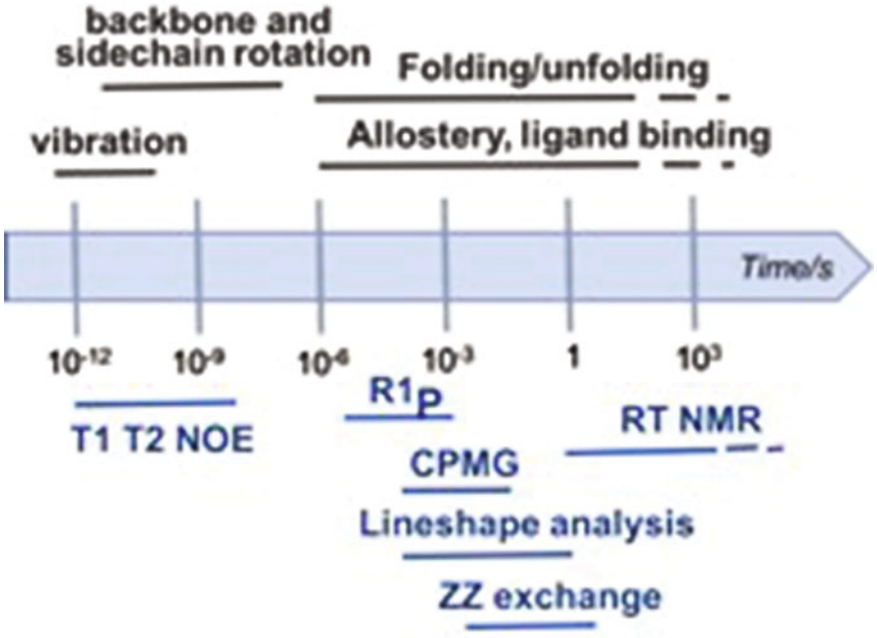

Fig. 1.7 NMR time scale of studing protein dynamics

protein motion and function. Importantly, multiple probes can be detected simultaneously. In other words, NMR could study the dynamics of a protein under near-physiological conditions at multiple regions of the protein simultaneously.

TROESY-based experiments can also be effectively used to study protein dynamics. In one notable example, scientists have successfully studied the dynamics of the ClpP, a 300 kDa protein [35]. In addition, when TROESY is combined with fluorescence techniques, in-cell NMR can be used in studying protein dynamics in vivo [36, 37].

There are numerous parameters that contain information about a protein's motions—relaxation, residual dipolar coupling, scalar coupling and H–D exchange. Of these parameters, relaxation is frequently used because it covers various time ranges. In NMR, relaxation describes how quickly spins convert from the non-equilibrium and over-population of an excited state (higher energy level) to a normal population (lower energy level). In optical bands, the mechanism of relaxation is stimulated emission and spontaneous emission. Actually, the rate of spontaneous emission is very low. Thus, the major effect is the interaction between the nuclear spin and lattice. There are several factors that could affect the spin-lattice coupling strength, such as dipole-dipole coupling, chemical shift anisotropy, scalar coupling, spin rotation, isotropic chemical shift and the quadrupolar effect [38]. In solution, due to the random motion of biomacromolecules, the spin-lattice interaction is a stochastic fluctuation variable. This time-dependent variable could separate into two directions: be parallel or be perpendicular to the external magnetic field. The parallel component is spin-spin relaxation and the perpendicular component is spin-lattice relaxation.

Relaxation can be understood in another uncomplicated way. In solution NMR, dipole-dipole coupling and chemical shift anisotropy could result in a micromagnetic field or electric field around the nucleus. The orientation of these micromagnetic fields and electric fields will stochastically fluctuate due to the random motion of the protein. The net magnetic field of spin will also vary with the motion of the protein. The random change of the micromagnetic field or electric field leads to the spin relaxation. Thus, the relaxation parameter contains the protein motion information, which can be used to probe the protein's dynamics. Moreover, the motion at various time scales can cause different relaxations. For example, the motion at ps-ns range affects dipole-dipole coupling, chemical shift anisotropy and the quadrupolar effect, while the motion on the microsecond-millisecond (us-ms) range mainly affects isotropic chemical shift [38].

Protein NMR focuses on the ^{1}H, ^{13}C and ^{15}N nuclei. For NMR protein dynamics studies, the backbone NH groups are commonly selected because the amino acid resolution spectrum is superior and the relaxation mechanism is uncomplicated. Typically, the relaxation of nuclei with a spin quantum number of ½ is mainly dominated by the dipole-dipole coupling and chemical shift anisotropy, which are influenced by ps-ns timescale motions. Thus, the relaxation parameters, which are sensitive to ps-ns time range motions, are employed for analysis. These include spin-lattice relaxation rate R1, spin-spin relaxation rate R2 and heteronuclear steady-state NOE. In addition, the spectral density mapping could link the

macroscopic dynamics parameters and microscopic protein motion. The goal in protein dynamics is to understand the spectral density mapping. After simplifying and approximating the spectral density mapping, valuable information about the protein's motion can be achieved [39].

Besides the ps-ns fast time scale protein motions, there also exists slow protein motions that occur at the us-ms timescale. These motions include chemical exchange and conformation exchange, which can be described as an atom transiting between multiple states. The atom being studied could remain within the same molecule with various states, or it could move into different molecules. In other words, chemical exchange is relevant both in situations where a protein undergoes internal motions and where it interacts with another molecule. For an exchange between state A and state B, the exchange process could be described as follows:

$$\mathrm{A} \underset{\mathrm{K}_{-1}}{\overset{\mathrm{K}_1}{\rightleftharpoons}} \mathrm{B}$$

The single NMR-active nucleus with different chemical shifts, ω_A and ω_B, in the two states. The chemical shift deviation of the two states is $\mathrm{V}\omega = |\omega_A - \omega_B|$ and the lifetime of the nuclear at state A and B is τ_A and τ_B. The rate that the nucleus switches from state A to B is $\mathrm{K}_1 = 1/\tau_A$. Correspondingly, the rate that the nucleus switches from state B to A is $\mathrm{K}_{-1} = 1/\tau_B$. The chemical shift exchange rate k_{ex} and exchange time τ_{ex} is defined as:

$$k_{ex} = 1/\tau_{ex} = (1/\tau_A + 1/\tau_B)/2$$

The population of states A and B under the equilibrium state are $\mathrm{P_A}$ and $\mathrm{P_B}$, and are defined as:

$$P_B = \frac{\frac{1}{\tau_A}}{\frac{1}{\tau_A} + \frac{1}{\tau_B}} = \frac{\tau_B}{\tau_A + \tau_B} \qquad P_A = \frac{\frac{1}{\tau_B}}{\frac{1}{\tau_A} + \frac{1}{\tau_B}} = \frac{\tau_A}{\tau_A + \tau_B}$$

The chemical exchange can be classified into three types by their NMR time scale. If the chemical exchange rate is far more than chemical shift deviation, that is $k_{\mathrm{ex}} \gg \mathrm{V}\omega$, there is only one set of the NMR signal, which is termed "fast exchange". The signal position depends on the chemical shift and population of two states. When the chemical exchange rate goes slower, that is close to the chemical shift deviation ($k_{\mathrm{ex}} \sim \mathrm{V}\omega$), the signal becomes broad or may even disappear; this is called "intermediate exchange". If the chemical exchange rate goes slower again, which is far less than chemical exchange rate ($k_{\mathrm{ex}} \ll \mathrm{V}\omega$), two sets of the NMR signals could be recorded; this is known as "slow exchange".

The slow motions at us-ms time scales correspond to important biological processes like protein folding, allostery and ligand binding. A plethora of research is focused on the associated protein dynamics, like GPMG relaxation dispersion, $\mathrm{R_{1p}}$ and ZZ exchange. Among them, CPMG is the most popular method [40]. The Carr-Purcell-Meiboom-Gill sequence (CPMG) experiment employs a series of 180

degree pulses with varied delay times. When no conformational exchange occurs, the effective spin-spin relaxation rate (R_2^{eff}) has a linear relationship with the reciprocal of the delay time ($1/\tau_{cp}$), devoid of the conformation exchange. The existing conformation exchanges at us-ms time scale could additionally contribute to the spin-spin relaxation, which is named as R_{ex}. When the value of τ_{cp} is limited, the R_{ex} is inhibited. R_{ex} becomes large when τ_{cp} is increased, and the relation between R_{ex} and $1/\tau_{cp}$ becomes nonlinear. By analyzing this dispersion curve one can obtain the kinetic, thermodynamic and structural information for the exchange process [41].

Understanding the structural bases of the protein dynamics processes is indispensable for elucidating the molecular mechanisms of biomacromolecular functions. In enzyme molecules, the amino acids that occupy the space around the ligand binding region often show slow motions at us-ms time scale in the *apo* (unbound) state, which indicates that these residues are structurally flexible. After binding the ligand (*holo* state), the slow motion disappears and these residues become structurally rigid [42]. These observations support the "conformation selection" hypothesis, which is employed in determining the ligand binding sites.

1.4.3.2 NMR Studies of Protein-Ligand Interactions

The binding of a protein with ligands (peptides, nucleic acids, chemicals, ions and so on) is very specific and is a molecular recognition that is a defining feature of protein function. NMR is a powerful approach to studying the protein-ligand interaction through not only the aforementioned complex structure and dynamics of molecular recognition, but also the binding interface.

To use NMR to study the interface of the protein-ligand binding, the chemical exchange regime compared to the NMR frequency should be confirmed first. The method for this analysis is similar to the chemical exchange analysis in dynamics studies by NMR. The common kinetic scheme of protein (P) binding to the ligand (L) can be described by the second order reaction as

$$\mathrm{P} + \mathrm{L} \underset{\mathrm{k_r}}{\overset{\mathrm{k_f}}{\rightleftarrows}} \mathrm{PL}$$

in which k_f is the forward reaction rate or association rate, the k_r is the backward reaction rate or dissociation rate, the lifetime of chemical exchange is $\tau_{ex} = 1/k_{ex}$, and the frequency of the chemical shift exchange is $k_{ex} = k_{f[L]} + k_r$. The chemical shift regime is classified into three types based on the NMR time scale:

slow exchange: $k_{ex} \ll |\omega_P - \omega_{PL}|$
intermediate exchange: $k_{ex} \sim |\omega_P - \omega_{PL}|$
fast exchange: $k_{ex} \gg |\omega_P - \omega_{PL}|$

ω_P and ω_{PL} are the chemical shift of the nucleus with different states (apo- or holo-form). 1D ^{1}H or 2D ^{1}H–^{15}N HSQC is employed to confirm the chemical

exchange regime as ligand is titrated into the protein sample. The spectrum has various properties under different chemical exchange regimes:

Slow exchange: The newly appeared holo-form peak increases with titrated ligands. In the meantime, the apo-form peak becomes weak. The chemical shift and linewidth do not change during titration process.

Intermediate exchange: The linewidth broadens with increased ligand concentration, even disappearing at one point. If the ligand is still added at this point, the new peak will appear with a different chemical shift. There is only one set of peaks during the titration process.

Fast exchange: As with intermediate exchange, only one set of peaks is observed during the titration process. The chemical shift undergoes a linear change as ligand is added. The exact signal position depends on the chemical shift and population of two states. The linewidth increases a little due to the chemical exchange process.

Normally, the chemical exchange regime could also supply the protein-ligand binding affinity information. The fast exchange corresponds to weak binding (equilibrium dissociation constant $K_d > 10^{-6}$ M), while the slow exchange coincides with strong binding ($K_d < 10^{-4}$ M). If 10^{-6} M > $K_d > 10^{-5}$ M, it indicates intermediate exchange.

If the chemical shift regime has been confirmed, the NMR method will be chosen to study the interface of the protein-ligand binding. As part of this process it is important to adjust the experiment temperature or external magnetic field strength in order to change the sample from intermediate exchange (which shows no signal) to the slow or fast exchange.

For the fast exchange process, which relates to weak binding, the chemical shift mapping method is a powerful approach, which normally selects the ^{1}H–^{15}N HSQC as the experiment spectrum. The chemical shift deviation of each amino acid is calculated during the ligand titration process and the residues that show the relative larger chemical shift perturbation are assigned to the binding sites. The value of the chemical shift deviation $\Delta\delta$ is calculated through the following function, in which $\Delta\delta_{HN}$ and $\Delta\delta_N$ are the chemical shifts changes of the $^{1}H^{N}$ and ^{15}N respectively. The factor of proportionality 0.1 is obtained by comparing the gyromagnetic ratio of the nucleus ($\gamma_N/\gamma_H = 0.1$) [43].

$$\Delta\delta = [\Delta\delta_{HN}^2 + (0.1\Delta\delta_N)^2]^{1/2}$$

The equilibrium dissociation constant K_d could also be achieved if calculating with the following function, in which the Δ is the chemical shift deviation compared with initial apo-form state under the specific ligand concentration $[L]_T$. The $[P]_T$ is defined as the protein concentration and the Δmax is the chemical shift deviation under the saturated ligand concentration.

$$\Delta = \Delta\max([L]_T + [P]_T + K_d - \{([L]_T + [P]_T + K_d)^2 - 4[L]_T[P]_T\}^{1/2})/(2[P]_T)$$

Many weak interactions occur between a protein and its ligand(s) in vivo. These complexes often defy crystallization, which makes their study difficult in X-ray crystallography. The chemical shift mapping method is suitable for such systems.

The backbone H–D exchange rate is selected to study the slow exchange process. The residues that populate the binding sites of the complex will show a slower H–D exchange rate compared with the amino acids of non-interface regions. Because slow exchanges often result from strong interactions that could change the protein conformation, they can lead to different assignments of the residues. Thus, the peak should be assigned twice, for the apo- and holo-form respectively.

The specially designed approaches for studying the protein-ligand interaction by NMR are growing. For large proteins, the saturated transfer experiment combined with varied labeling of the protein and ligand is employed, while the linewidth analysis is used to study the small molecular-weight protein systems.

1.4.3.3 Studies of the Membrane Binding Protein (MBP) by ^{31}P NMR

The ^{31}P atom is a very useful tool for NMR. The ^{31}P nuclear spin quantum number is 1/2, and the gyromagnetic ratio is high (42.5% of ^{1}H). The natural abundance is 100%, which means that the sample does not need to be labelled. Meanwhile, important biomacromolecules contain ^{31}P: nucleic acids, phosphorylated proteins and phospholipid molecules. Thus, it is worth studying these biomacromolecules by ^{31}P NMR, especially ^{31}P solution NMR.

^{31}P NMR also plays an important role in the study of membrane biology and membrane binding proteins and is a source of valuable information, such as phospholipid bilayer packing, phase transitions of the phospholipid molecules, and of course the orientation and dynamic properties of the phosphorus of the hydrophilic headgroup of the phospholipid molecules and the protein-anchored site on the lipid bilayers. H–N…(O)–P INEPT polarization transfer experiment can be used to identify hydrogen bonding between the phosphorus from the phospholipid molecule and the backbone NH groups of the protein, through J coupling (JH–P $\sim$ 5 Hz) (Roy Hoffman, 2007, 31Phosphorus NMR, Hebrew University). The reference of ^{31}P NMR is 85% phosphoric acid, which dissolved in the H_2O. The corresponding signal is assigned to the 0 ppm (Roy Hoffman, 2007, 31Phosphorus NMR, Hebrew University).

References

1. Singer SJ, Nicolson GL (1972) The fluid mosaic model of the structure of cell membranes. Science 175(4023):720–731
2. Daleke DL (2003) Regulation of transbilayer plasma membrane phospholipid asymmetry. J Lipid Res 44(2):233–242
3. Baldridge RD, Graham TR (2013) Two-gate mechanism for phospholipid selection and transport by type IV P-type ATPases. Proc Natl Acad Sci U S A 110(5), p. E358–67

4. Thomas S et al (2004) Analysis of lipid rafts in T cells. Mol Immunol 41(4):399–409
5. Korade Z, Kenworthy AK (2008) Lipid rafts, cholesterol, and the brain. Neuropharmacol 55 (8):1265–1273
6. Wallin E, von Heijne G (1998) Genome-wide analysis of integral membrane proteins from eubacterial, archaean, and eukaryotic organisms. Protein Sci 7(4):1029–1038
7. Tamm LK, Hong H, Liang B (2004) Folding and assembly of beta-barrel membrane proteins. Biochim Biophys Acta 1666(1–2):250–263
8. Czerski L, Sanders CR (2000) Functionality of a membrane protein in bicelles. Anal Biochem 284(2):327–333
9. Tamm LK (2005) Protein-lipid interactions: from membrane domains to cellular networks. Wiley-VCH, Weinheim, p 444 (xxvi)
10. Pervushin K et al (1997) Attenuated T2 relaxation by mutual cancellation of dipole-dipole coupling and chemical shift anisotropy indicates an avenue to NMR structures of very large biological macromolecules in solution. Proc Natl Acad Sci U S A 94(23):12366–12371
11. Tugarinov V et al (2005) Solution NMR-derived global fold of a monomeric 82-kDa enzyme. Proc Natl Acad Sci U S A 102(3):622–627
12. Konrat R, Yang D, Kay LE (1999) A 4D TROSY-based pulse scheme for correlating 1HNi, 15Ni, 13Calphai, 13C'i-1 chemical shifts in high molecular weight, 15N, 13C, 2H labeled proteins. J Biomol NMR 15(4):309–313
13. Clore GM, Tang C, Iwahara J (2007) Elucidating transient macromolecular interactions using paramagnetic relaxation enhancement. Curr Opin Struct Biol 17(5):603–616
14. Hilty C et al (2004) Membrane protein-lipid interactions in mixed micelles studied by NMR spectroscopy with the use of paramagnetic reagents. ChemBioChem 5(4):467–473
15. Bax A (2003) Weak alignment offers new NMR opportunities to study protein structure and dynamics. Protein Sci 12(1):1–16
16. Luy B (2007) Approaching the megadalton: NMR spectroscopy of protein complexes. Angew Chem Int Ed Engl 46(23):4214–4216
17. Hibler DW et al (1989) Isotopic labeling with hydrogen-2 and carbon-13 to compare conformations of proteins and mutants generated by site-directed mutagenesis. I Methods Enzymol 177:74–86
18. Muchmore DC et al (1989) Expression and nitrogen-15 labeling of proteins for proton and nitrogen-15 nuclear magnetic resonance. Methods Enzymol 177:44–73
19. Goto NK, Kay LE (2000) New developments in isotope labeling strategies for protein solution NMR spectroscopy. Curr Opin Struct Biol 10(5):585–592
20. Cavanagh J (2007) Protein NMR spectroscopy: principles and practice, vol xxv, 2nd edn. Elsevier Academic Press, Amsterdam, Boston, p 885
21. Keeler J (2010) NMR Understanding spectroscopy, vol xiii, 2nd edn. John Wiley and Sons, Chichester, U.K., p 511
22. Nakanishi KJ (1990) One-dimensional and two-dimensional NMR spectra by modern pulse techniques. Kodansha University Science Books, Tokyo Sausalito, California, vol xii p 234
23. Veglia G et al (2002) Deuterium/hydrogen exchange factors measured by solution nuclear magnetic resonance spectroscopy as indicators of the structure and topology of membrane proteins. Biophys J 82(4):2176–2183
24. Cornilescu G, Delaglio F, Bax A (1999) Protein backbone angle restraints from searching a database for chemical shift and sequence homology. J Biomol NMR 13(3):289–302
25. Wishart DS, Sykes BD (1994) The 13C chemical-shift index: a simple method for the identification of protein secondary structure using 13C chemical-shift data. J Biomol NMR 4 (2):171–180
26. Cung MT, Marraud M, Neel J (1974) Experimental calibration of a Karplus relationship in order to study the conformations of peptides by nuclear magnetic resonance. Macromol 7 (5):606–613
27. Prestegard JH, Al-Hashimi HM, Tolman JR (2000) NMR structures of biomolecules using field oriented media and residual dipolar couplings. Q Rev Biophys 33(4):371–424

28. Clore GM, Iwahara J (2009) Theory, practice, and applications of paramagnetic relaxation enhancement for the characterization of transient low-population states of biological macromolecules and their complexes. Chem Rev 109(9):4108–4139
29. Guntert P, Mumenthaler C, Wuthrich K (1997) Torsion angle dynamics for NMR structure calculation with the new program DYANA. J Mol Biol 273(1):283–298
30. Herrmann T, Guntert P, Wuthrich K (2002) Protein NMR structure determination with automated NOE-identification in the NOESY spectra using the new software ATNOS. J Biomol NMR 24(3):171–189
31. Schwieters CD et al (2003) The Xplor-NIH NMR molecular structure determination package. J Magn Reson 160(1):65–73
32. Brunger AT et al (1998) Crystallography & NMR system: a new software suite for macromolecular structure determination. Acta Crystallogr D Biol Crystallogr 54(Pt 5):905–921
33. Case DA et al (2005) The Amber biomolecular simulation programs. J Comput Chem 26 (16):1668–1688
34. Boehr DD, Dyson HJ, Wright PE (2006) An NMR perspective on enzyme dynamics. Chem Rev 106(8):3055–3079
35. Sprangers R et al (2005) Quantitative NMR spectroscopy of supramolecular complexes: dynamic side pores in ClpP are important for product release. Proc Natl Acad Sci U S A 102 (46):16678–16683
36. Bryant JE et al (2005) Protein dynamics in living cells. Biochem 44(26):9275–9279
37. Reckel S, Lohr F, Dotsch V (2005) In-cell NMR spectroscopy. ChemBioChem 6(9):1601–1606
38. Palmer AG 3rd (2004) NMR characterization of the dynamics of biomacromolecules. Chem Rev 104(8):3623–3640
39. Jarymowycz VA, Stone MJ (2006) Fast time scale dynamics of protein backbones: NMR relaxation methods, applications, and functional consequences. Chem Rev 106(5):1624–1671
40. Mittermaier A, Kay LE (2006) New tools provide new insights in NMR studies of protein dynamics. Science 312(5771):224–228
41. Kleckner IR, Foster MP (2011) An introduction to NMR-based approaches for measuring protein dynamics. Biochim Biophys Acta 1814(8):942–968
42. Hu Y et al (2006) Solution structures and backbone dynamics of a flavodoxin MioC from Escherichia coli in both Apo- and Holo-forms: implications for cofactor binding and electron transfer. J Biol Chem 281(46):35454–35466
43. Farmer BT 2nd et al (1996) Localizing the NADP+ binding site on the MurB enzyme by NMR. Nat Struct Biol 3(12):995–997

Chapter 2
Lipid Molecular-Ion Interaction Study Based on Nanodisc

Abstract Reconstituting the membrane protein into a suitable model membrane is the first and essential step in studying the membrane protein in vitro. Commonly used membrane mimics include detergent micelles, detergent/lipid bicelles, and lipo somes (reviewed in the previous chapter). A newer model system is the "nanodisc," originally designed by Dr. Sligar [1]. The nanodisc's properties as a model membrane are discussed at length in this chapter, but in general its defining qualities are that it is a stable membrane mimic with a precisely controlled size and stoichiometry, making it a suitable system to study membrane proteins in their native environments.

2.1 What Is a Nanodisc?

A nanodisc is a soluble, nanoscale patch of phospholipid bilayer that is composed of phospholipids ringed by two monomers of the amphipathic protein apolipoprotein A-1 (Apo A-1). Apo A-1 is the major component of high-density lipoprotein (HDL), which combines with the phospholipids to form discoidal HDL. Apo A-1 is a cofactor of the lecithin-cholesterol acyltransferase, which converts the free cholesterol that binds to the surface of the HDL into cholesteryl ester. The cholesteryl ester will then sequestered into the core of the HDL, leading to the spherically mature HDL [2, 3].

Essentially, nanodiscs are structural mimics of discoidal HDL. A variety of models have been proposed for explaining the exact structure of the nanodisc: the "belt" model, "picket fence" model and "Helix hairpin" model [4–7]. However, recent studies using a variety of methods, such as polarized internal reflection infrared spectroscopy [8], cross-linking/mass spectrometry [9–12], mutation [13], Electron paramagnetic resonance (EPR) [14], Fluorescence Spectroscopy [15], fluorescence resonance energy transfer (FRET) [16] and solid NMR [17], verify the nanoscale phospholipid bilayer structure and point unambiguously to the "belt" model. The "belt" model states that the amphipathic helices of Apo A-1 girdle the outside of the phospholipid bilayer and are perpendicularly aligned to the acyl

© Springer-Verlag GmbH Germany 2018

Y. Bi, *Study of the Calcium Regulation Mechanism of TCR Activation Using Nanodisc and NMR Technologies*, Springer Theses,
DOI 10.1007/978-3-662-54618-5_2

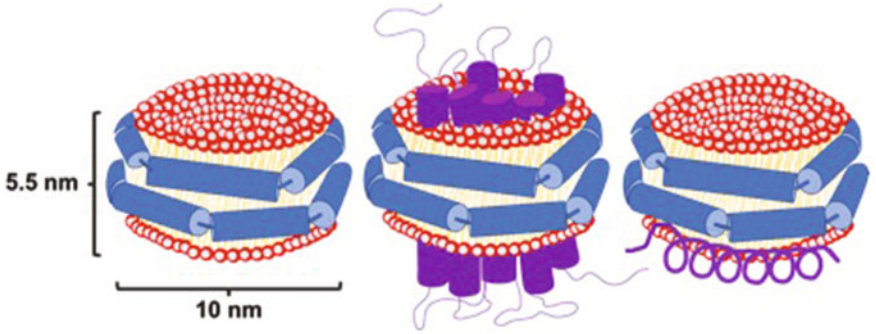

Fig. 2.1 A schematic representation of nanodisc structure. From *left* to *right* empty nanodisc, nanodisc with embedded membrane protein, and membrane binding protein-anchored nanodisc. The diameter of nanodiscs is 10 nm and the height is 5.5 nm

chains of the phospholipid bilayer. As described above, the hydrophobic residues form the inside face of the helices, which interact with the acyl chains of the phospholipid molecule through hydrophobic interactions. The hydrophilic amino acids are located at the outside surfaces of the helices and allow the nanodisc to be soluble in the solution [8, 18, 19]. On average, nanodiscs have a diameter of 10 nm and a height of 5.5 nm, which is consistent with the native discoidal HDL [20] Fig. 2.1.

The crystal structure of ApoA-1Δ(1–43) in a non-phospholipid-binding state shows that it is composed of ten amphipathic helices, in which the hydrophilic residues face outward (exposed to the solvent) and the hydrophobic residues face the inner side of the helix (packed against the hydrophobic core of the phospholipid bilayer) [21]. The simulation and small-angel X-ray scattering research from Shih indicates that the N-terminal domain and C-terminal domain of Apo A-1 do not bind to phospholipids during HDL maturation [22, 23]. The ApoA-1 used in generating nanodisc was designed by Sligar, who removed the amino acids from N-terminal domain to produce a homogeneous size. The newly designed Apo A-1 was named membrane scaffold protein (MSP) and contains two hundred amino acids with structural flexibility [24]. The most popular MSP proteins used in the assembly of nanodiscs are MSP1D1 and MSP1E3D1. In MSP1D1 the first eleven amino acids have been deleted from the original MSP protein; as mentioned before, the first eleven amino acids locate to the non-phospholipid binding region, which means that deleting them does not change the conformation of the first helix. In the MSP1E3D1, additional helix sequences are introduced to lengthen the MSP amino acid sequence while maintaining the same conformation and folding as the traditional MSP. MSP1E3D1 is typically employed to make larger nanodiscs [24].

During nanodisc assembly, the MSP protein and the target membrane protein are transiently mixed with detergent-solubilized phospholipid. After incubating at the phospholipid transition temperature, the detergent is removed by dialysis or adsorption to hydrophobic beads, like Bio-Beads SM-2 (Bio-Rad, Hercules, CA).

As the detergent concentration drops, the phospholipids spontaneously assemble with the MSP to form the nanoscale lipid bilayer with a homogeneous disc size controlled by the length of the MSP used. Simultaneously, the target membrane protein also inserts itself into the lipid bilayers and the entire entity is rendered soluble via the encircling MSP belt. The assembled nanobody can then be further purified through fast protein liquid chromatography (FPLC) [24–29]. To prepare the nanodisc sample with membrane binding protein, the empty nanodisc is produced first and then mixed with the target membrane binding protein.

Nanodiscs also play important roles in membrane protein expression and purification. Natural production of membrane protein generates yields that are too low to purify directly. On the other hand, recombinant expression of membrane proteins is also usually toxic to the cell and can result in the membrane aggregation or misfolding of the protein, resulting in low yield. Cell-free biosystems can avoid both of these problems, and is simply a mixture of numerous purified enzymes and coenzymes. Thus, it is easily controlled to synthesize proteins [30–32].

To express membrane proteins by cell-free biosystems, the membrane mimics must be supplied as the protein is expressed; nanodiscs have proven to be the optimal choice of membrane mimic in this context. There are two approaches to introduce nanodiscs into cell-free biosystem—either by introducing the empty nanodiscs into the cell-free biosystem or by coexpressing the MSP protein and target membrane protein while adding additional phospholipid molecules. The former method has low efficiency due to the lack of appropriate transcription factor [33–35]. A number of membrane proteins have been successfully expressed into nanodiscs in cell-free systems [33, 36–38].

2.2 Optimizing Nanodisc Assembly for NMR Studies

2.2.1 Experiment Methodology and Materials

(1) Phospholipid molecule

All phospholipid molecules are purchased from Avanti Polar Lipids. Inc.

(2) Cloning, expression and purification of MSP protein

The PUC57-MSP gene was synthesized by GenScript. In order to design smaller nanodisc, the primers were designed to delete helix 7–10 from the MSP protein. The MSP gene was then subcloned into pET28a (Novagen). To express the recombinant MSP protein, the plasmid pET28a-MSP was transformed into *E.coli* BL21(DE3)(Novagen). The *E.coli* cells were inoculated into LB media and grown at 37 °C until the OD_{600} value reached between 0.7 and 0.8 and then induced to express protein by addition of 0.5 mM IPTG (Isopropyl-β-D-thiogalactoside) into

the media. Cells were grown under these conditions for 4 more hours with the temperature lowered to 25 °C.

The cells were harvested by centrifugation of the liquid culture (8000 *g* for 10 min at 4,°) and the cell pellets were resuspended in lysis buffer (20 mM Tris-HCL pH 8.0, 50 mM NaCl, 1 mM PMSF (phenylmethyl sulfonyl fluoride)). The cells were disrupted by sonication and then centrifuged again (14,000 *g* for 20 min at 4,°). The supernatant was loaded onto the Ni sepharose™ resin (GE Healthcare). MSP protein was eluted with buffer A (20 mM Tris-HCL, pH 8.0, 500 mM NaCl, 200 mM imidazole). The purity of the protein was assessed by sodium dodecyl sulfate polyacrylamide gel electrophoresis (SDS-PAGE) in 12% acrylamide slab gels under reducing conditions. The purification method for truncated MSP is the same as that for the wildtype MSP protein.

(3) Nanodisc assembly

Nanodiscs were assembled as described previously [7]. In brief, the solution of purified MSP at 0.15–0.3 mM concentration was mixed with detergent (or urea) and lipids at optical molar ratios (1:65:130 for the classic Nanodisc). After incubating at the optimal temperature (often at phase transition temperature) for 15 h, bio-beads were added to initiate the self-assembly process. The nanodiscs were purified by FPLC with the Superdex 200 (GE Healthcare) column. The elution fractions were pooled for downstream analysis.

(4) Nanodisc size measurements by Dynamic Light Scattering

Dynamic light scattering experiments were carried out at 25 °C with DNYAPRO-MS800 (ATC). Fresh nanodisc samples from size exclusion chromatography fractions were used with buffer B (20 mM Tris-HCL pH 7.2, 100 mM NaCl, 0.5 mM EDTA).

(5) Transmission electron microscopy

Nanodiscs were diluted to a final concentration of 0.5 uM in 20 mM Tris–HCl, pH 8, 50 mM NaCl and adsorbed to glow-discharged, carbon-coated EM grids. Samples were prepared by conventional negative staining with 2% (w/v) phosphotungstic acid. EM images were collected with a JEM-2100 electron microscope (JEOL).

2.2.2 Results

The ratio of different components is the most important parameter in successfully assembling nanodisc. Specifically, the optimal ratio between phospholipid and MSP protein varies with different phospholipid surface area. The concentration of detergent—normally cholate is used—is twice the concentration of phospholipid and must be higher than 14 mM (the CMC of cholate is about 14 mM). When assembling the nanodisc with embedded membrane protein, the optimal ratio of

these components will need to be empirically determined because insertion of the membrane protein displaces some of the phospholipid into solution, and the extent to which this happens depends on the particular membrane protein. The nanodisc could still form, even in low yield, if the ratio deviate the best one less than 30%. Otherwise, nanodisc will be missed. The incubation temperature is another important factor to consider. When making single phospholipid component nanodisc, the chosen temperature should be at transition temperature of the phospholipids used in the nanodisc [24]. When assembling mixed-phospholipid nanodiscs to mimic the native phospholipid environment, the highest transition temperature of the phospholipids present should be choosed as the incubation temperature.

To prepare the nanodiscs with the membrane protein embedded, the nanodisc size should be as close as possible to the embedded membrane protein's native size in order to prevent multiple proteins from packing into the same nanodisc (additionally, NMR signals decay due to the large molecule weight in a sample so this should be avoided whenever possible). The diameter of the classic nanodisc is 10 nm (Figs. 2.1, 2.2 and 2.3), which is not suitable for small membrane proteins. Thus, we assemble smaller nanodiscs using shorter MSP protein [39] that still retain the shape of the classic nanodisc. The first six helices are used as the shorter MSP protein. The purification of shorter MSP protein and assembly of nanodisc with it is the same procedure as used for the classic nanodisc, with the exception that less phospholipid is used for the smaller nanodisc size (Fig. 2.4).

Additionally, two detergents can co-exist in the nanodisc assembly process: the detergent used to purify the target membrane protein, and cholate, which is included

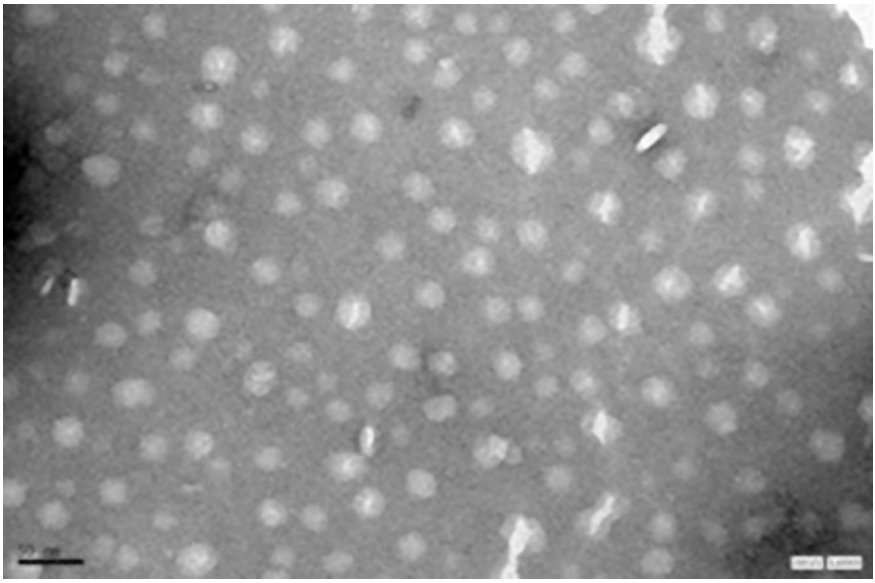

Fig. 2.2 Transmission electron microscopy (TEM) of DMPC nanodiscs. A uniform monodisperse Nanodisc shows that the diameter is 10 nm

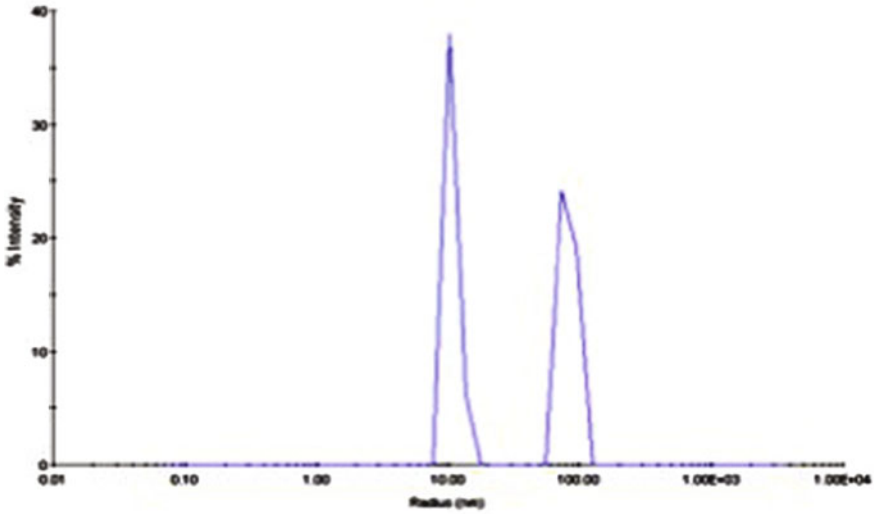

Fig. 2.3 Nanodisc particle size distribution analysis by dynamic light scattering (DLS). The nanodisc sample contains uniform particles with a radius of 10 nm, which is consistent with the TEM experiment result

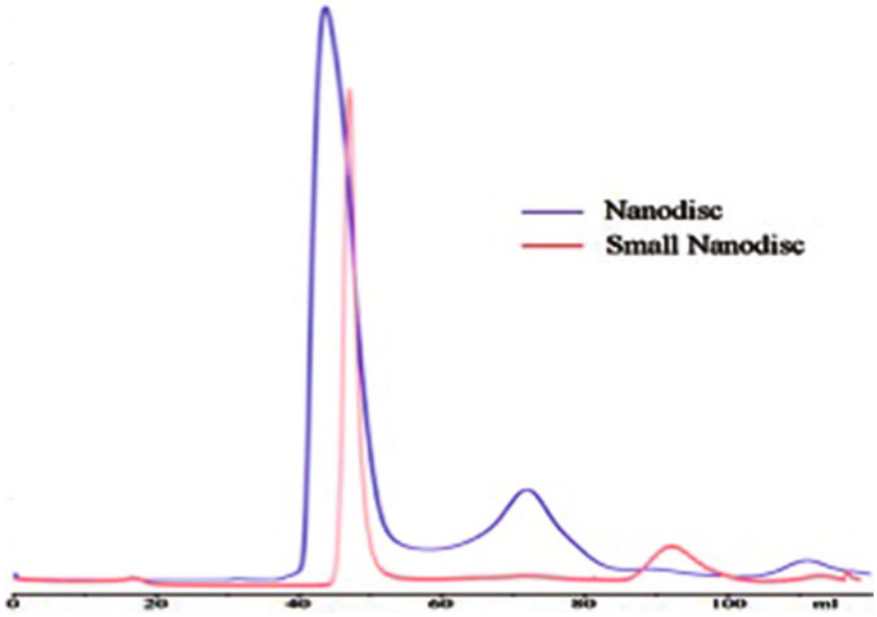

Fig. 2.4 The FPLC purification of (conventional) nanodisc and small nanodisc. Both nanodisc and small nanodisc are monodisperse and elute at 72 and 92 mL respectively. As expected, the small nanodiscs elute later compared with the classic nanodisc

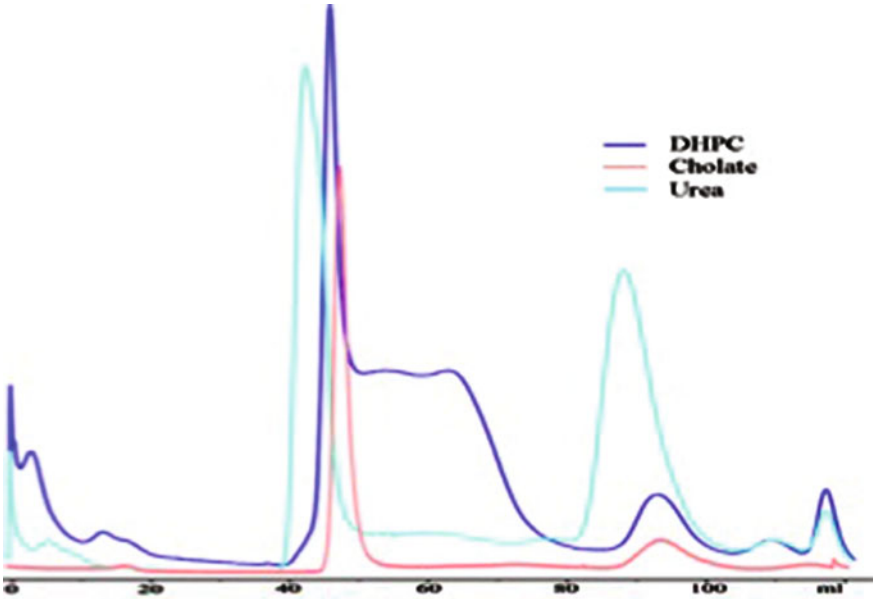

Fig. 2.5 FPLC purification of nanodiscs assembled with various detergents and urea

standard nanodisc assembly. Because cholate is a type of ionic detergent and can affect the membrane protein conformation, it is desirable to use just one detergent in the whole nanodisc assembly process. Urea is a good choice because it is suitable in the denaturing/refolding process that is commonly used in membrane protein purification. DHPC is usually the detergent of choice due to its low CMC value. Figure 2.4 shows the FPLC purification of small nanodiscs that were assembled with DHPC or urea, as well as cholate, which is a positive control. The elution position and yield of small nanodiscs made by DHPC or cholate are similar, which indicates that the DHPC could be included in the nanodisc assembly because it tends to produce a monodisperse sample. However, nanodisc assembled in urea elute earlier, which may be attributed to excess urea that was not fully removed from the sample during adsorption/self assembly. In this case dialysis may be used instead of the biobeads adsorption method to fully eliminate the urea in the optimization step (Fig. 2.5).

2.3 Lipid Molecular-Ion Interaction

Ions contribute to the composition of the cell membrane and play an important role in its function. Ion channels and ion transporters are membrane proteins that control the flow of ions across the cell membrane. Accurately regulated ions could interact with the lipid molecule through various mechanisms.

2.3.1 Experiment Methods

(1) 1D ^{31}P-NMR Analysis

Nanodisc samples were prepared in a pH 7.0 Tris–HCl buffer, containing 100 mM NaCl and a final POPG concentration of 4 mM. Ions were titrated into the POPG nanodisc sample at a molar ratio of [Ion]:[POPG] from 0 to 100. ^{31}P NMR spectra were recorded on a Bruker Avance 850 MHz spectrometer in a 5-mm broad band probe at 298 K. The zg pulse program was applied with a P1 pulse of 29.4us for ^{31}P and a ^{1}H decoupling power of 19.54 db. The recycle delay was set at 1.5 s. 256 scans were accumulated. The free induction decay data was processed in nmrPipe using a line broadening of 25 Hz to improve the signal-to-noise ratio.

(2) Fourier transform infrared spectroscopy (FTIR)

Fourier Transform Infrared (FTIR) spectroscopy was used to confirm Ca^{2+}-lipid phosphate binding. POPG nanodisc samples with various $CaCl_2$ concentrations were overspread on the BaF_2 substrates and air dried at room temperature. FTIR measurements were performed at room temperature on an FTIR spectrometer (BRUKER ALPHA-T) and the software OPUS 6.5 (Bruker Optics GmbH, Ettlingen, Germany) was used to process the data. The sample buffer was 20 mM Tris-HCl, pH 7.0, 100 mM NaCl.

(3) Chemical shift perturbation experiment

A series of ^{1}H,^{13}C-HSQC spectra were recorded to detect the chemical shift perturbed by calcium or CD3ε_{CD}. Nanodisc samples were prepared in a pH 7.0 Tris–HCl buffer, containing 100 mM NaCl with a final POPG concentration of 9 mM. The calcium (3.6 mM) or CD3ε_{CD} (0.06 mM) was titrated into the sample. The spectra were recorded on a Bruker Avance 850 MHz spectrometer at 300 K, with 256 scans.

(4) Differential scanning calorimetry (DSC)

Nanodisc samples were prepared in a pH 7.0 Tris–HCl buffer, containing 100 mM NaCl and a final DMPG concentration of 2.5 mM was reached. The calcium was added to the sample with indicated, which the concentration is 2.5 mM. The experiment was recorded on the VP-DSC (Microcal), which operated by the increase-decrease-increase temperature model. The temperature change region is 5–60 °C. The rate of increase or decrease is 60 °C/h.

2.3.2 Results

2.3.2.1 Ions Interact with the Phosphate Radical of the Lipid Molecule

High resolution ^{31}P NMR spectroscopy has proven to be a convenient and precise analytical tool for phospholipids in biological samples. In this study we characterized the phospholipids by 1D ^{31}P NMR spectroscopy, in which the chemical shift information provides a good indication of the chemical environment changes around the phosphorus atom (Fig. 2.6). Monovalent ions like Na^+ and K^+ could cause the

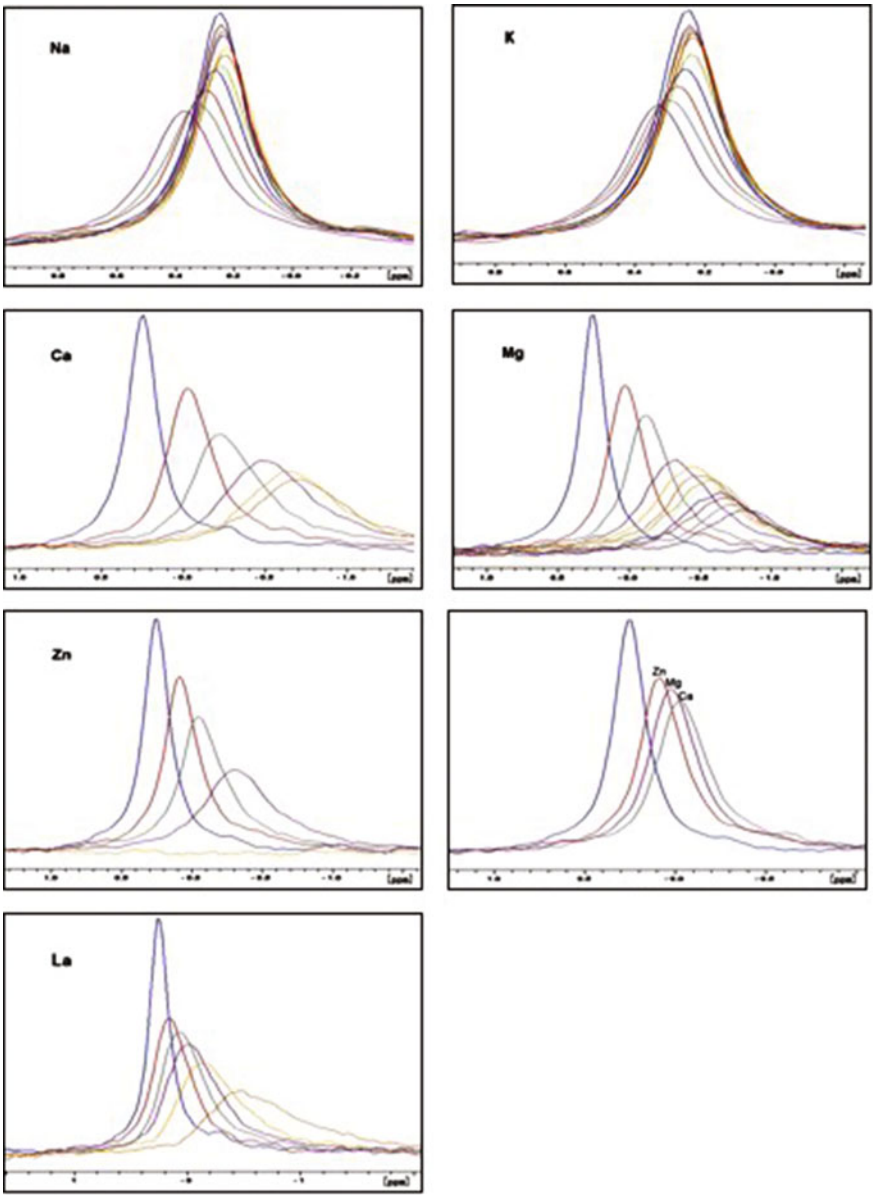

Fig. 2.6 One-dimensional ^{31}P NMR experiments were performed to probe the change in the local chemical environment of the phospholipid phosphate group induced by the binding of varied ions. A POPG nanodisc system was used to provide a membrane bilayer environment without the interference of detergent molecules. The sample buffer was 20 mM Tris-HCl, pH 7.0, containing 100 mM NaCl. The signals of varied [Ca^{2+}]:[POPG] molar ratios are shown with different colors: blue(0), red(0.2), green(0.4), purple(0.8), yellow(1.5), orange(3), cyan(5). At higher molar ratios, some colors are reused: blue(10), red(25), green(50), purple(100)

chemical shift of phosphorus from the phospholipid molecule to have a high-field shift and then low-field shift, which happens when the ratio of ion to phospholipid is 0.8–1.5. The monovalent ion addition does not cause drastic changes in the chemical shift and linewidth. The change of chemical shift does not exceed 0.2 ppm, even after 100-fold increases in monovalent ion concentration. This also does not cause precipitation of the sample. By contrast, divalent ions like Ca^{2+}, Mg^{2+}, and Zn^{2+} can cause substantial changes in the chemical shift, broaden the linewidth and cause the sample to precipitate. Ca^{2+} causes the maximum chemical shift changes followed by Mg^{2+}, and Zn^{2+} causes the minimum chemical shift changes. Trivalent ions like La^{3+} can also cause the high-field shift of the chemical shift of phosphorus, broad linewidth, and sample precipitation. These data indicated that the ions, which included monovalent ions, divalent ions and trivalent ions, could interact with the phospholipid through varied patterns. If only electrostatic forces contributed to the change, the chemical shift changes should take place in one direction, but the observed chemical shift changes exist in two directions. Therefore, besides the electrostatic force, there exist other interaction (s), such as coordinate bonds.

FTIR was used to further study the interaction between ions and phospholipids. The asymmetric stretching of PO_2^- is around 1222 cm^{-1}. When calcium addition at a molar ratio of [Ca^{2+}]:[phospholipid] is 0.4, the peak starts to have a shift to the higher wavenumber, probably due to the dehydration of the hydrophilic headgroup of the phospholipid by calcium (Fig. 2.7). Next, chemical shift perturbations of

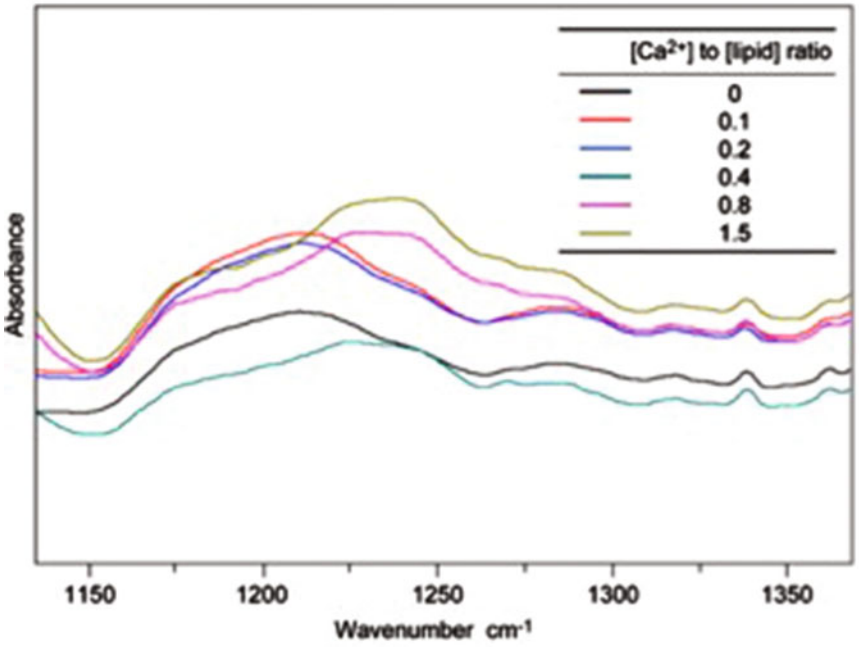

Fig. 2.7 With the Ca^{2+}/POPG ratio above 0.4, the PO2 asymmetric vibration band of POPG, which was centered around 1222 cm^{-1}, shifted towards higher wavenumbers. This shift was caused by a dehydration effect from Ca^{2+} and indicated an ionic interaction between Ca^{2+} and the phosphate group

NMR were recorded to detect the chemical shift change of CH group caused by calcium (Fig. 2.8). Taking the PO_2–group as a border, calcium could cause the chemical shift changes at the hydrophilic headgroup. In the control experiment, the signals both from hydrophilic headgroup and hydrophobic acyl chains can be perturbed by CD3ε_{CD}, which is consistent with the earlier result showing that CD3ε_{CD} could insert into the hydrophobic region of the lipid bilayer and interact with the acyl chain through hydrophobic forces [40]. These data show that calcium could interact with the headgroup of the negatively charged phospholipid, but not with the acyl chains.

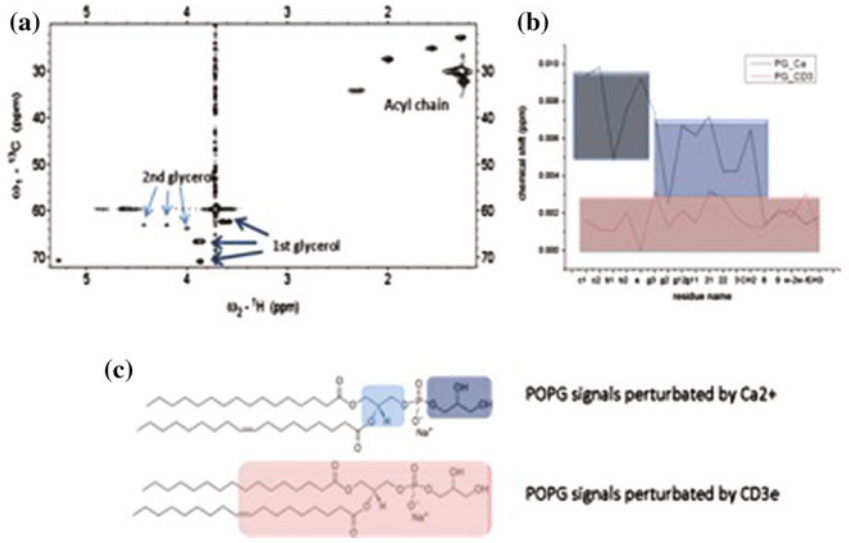

Fig. 2.8 **a** ^{1}H-^{13}C HSQC spectra of POPG nanodisc were recorded to detect the calcium ion and CD3ε_{CD} binding regions to the phospholipids. The assignment was performed by analyzing the ^{1}H-^{13}C HSQC of glycerol and headgroup of PA lipid as in the previous study. **b** The chemical shift changes after calcium or CD3ε_{CD} addition. The function to calculate the chemical shift changes is $\Delta\delta = [\Delta\delta_{HC}^2 + (0.25\Delta\delta_C)^2]^{1/2}$ where $\Delta\delta_{HC}$ and $\Delta\delta_C$ represent the chemical shift changes of $^{1}H^{C}$ and ^{13}C. The ratio of 2.5 is calculated by the gyromagnetic ratio ($\gamma_C/\gamma_H = 0.25$). **c** The chemical shift change regions shown on the POPG lipid. The chemical shift perturbation region by calcium locates at the hydrophilic headgroup region (dark grey). The light blue part represents the tiny chemical shift change region also caused by calcium. The chemical shift perturbation region by CD3ε_{CD} is labelled red, and covers both the hydrophilic headgroup and hydrophobic acyl chain regions

2.3.2.2 Ions Affect the Phase Behavior of the Phospholipid

The fluid mosaic model suggests that fluidity is the structural basis of the cell membrane. The types and concentrations of ions present can affect the phase behavior of the lipid molecule and thus modulate the fluidity of the cell membrane. Differential scanning calorimetry (DSC) was recorded to detect the phase behavior changes of the phospholipid with/without calcium addition (Fig. 2.9). Calcium can increase the transition temperature of DMPG and sharpen the peak, indicating a more ordered arrangement and lower fluidity of the DMPG, which may further influence the conformation and function of the embedded membrane protein.

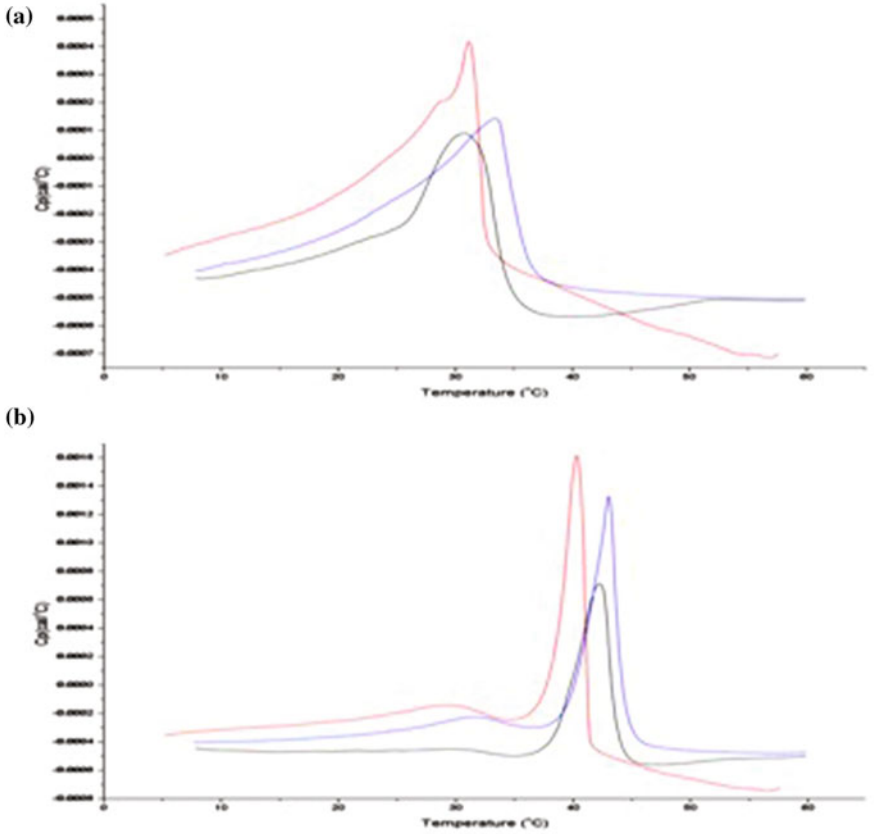

Fig. 2.9 Differential scanning calorimetry (DSC) spectra of DMPG nanodisc. **a** and **b** show the DSC spectra of DMPG nanodisc with and without calcium addition. The first temperature increase, temperature reduction and second temperature increase are traced in *red*, *black*, and *blue* respectively

The DSC experiment result is comfirmed by NMR experiments. In ^{31}P NMR experiments, the linewidth becomes broad after ion addition. It indicates that the spin-spin relaxation T2 becomes shorter and the correlation time τ_c becomes longer, which leads to the slower dynamics and lower fluidity of the phospholipid molecule.

These studies demonstrate that ions could interact with the phosphorus of the hydrophilic headgroup from the phospholipid molecule through at least two mechanisms. In the first, electrostatic forces could bring the ion and lipids into proximity, pushing away associated water molecules (ion dehydration effect). Coordinate bonds may comprise the second interaction. In either case, the interaction pattern and binding affinity changes with different ions and phospholipid molecules.

References

1. Bayburt TH, Carlson JW, Sligar SG (1998) Reconstitution and imaging of a membrane protein in a nanometer-size phospholipid bilayer. J Struct Biol 123(1):37–44
2. Phillips JC et al (1997) Predicting the structure of apolipoprotein A-I in reconstituted high-density lipoprotein disks. Biophys J 73(5):2337–2346
3. Shih AY, Sligar SG, Schulten K (2009) Maturation of high-density lipoproteins. J R Soc Interface 6(39):863–871
4. Brouillette CG et al (1984) Structural studies of apolipoprotein A-I/phosphatidylcholine recombinants by high-field proton NMR, nondenaturing gradient gel electrophoresis, and electron microscopy. Biochem 23(2):359–367
5. Segrest JP (1977) Amphipathic helixes and plasma lipoproteins: thermodynamic and geometric considerations. Chem Phys Lipids 18(1):7–22
6. Brouillette CG et al (2001) Structural models of human apolipoprotein A-I: a critical analysis and review. Biochim Biophys Acta 1531(1–2):4–46
7. Nath A, Atkins WM, Sligar SG (2007) Applications of phospholipid bilayer nanodiscs in the study of membranes and membrane proteins. Biochem 46(8):2059–2069
8. Koppaka V et al (1999) The structure of human lipoprotein A-I. Evidence for the "belt" model. J Biol Chem 274(21):14541–14544
9. Davidson WS, Hilliard GM (2003) The spatial organization of apolipoprotein A-I on the edge of discoidal high density lipoprotein particles: a mass specrometry study. J Biol Chem 278 (29):27199–27207
10. Silva RA et al (2005) A mass spectrometric determination of the conformation of dimeric apolipoprotein A-I in discoidal high density lipoproteins. Biochem 44(24):8600–8607
11. Thomas MJ, Bhat S, Sorci-Thomas MG (2006) The use of chemical cross-linking and mass spectrometry to elucidate the tertiary conformation of lipid-bound apolipoprotein A-I. Curr Opin Lipidol 17(3):214–220
12. Bhat S et al (2005) Intermolecular contact between globular N-terminal fold and C-terminal domain of ApoA-I stabilizes its lipid-bound conformation: studies employing chemical cross-linking and mass spectrometry. J Biol Chem 280(38):33015–33025
13. Gorshkova IN et al (2006) Structure and stability of apolipoprotein a-I in solution and in discoidal high-density lipoprotein probed by double charge ablation and deletion mutation. Biochem 45(4):1242–1254

14. Martin DD et al (2006) Apolipoprotein A-I assumes a “looped belt” conformation on reconstituted high density lipoprotein. J Biol Chem 281(29):20418–20426
15. Panagotopulos SE et al (2001) Apolipoprotein A-I adopts a belt-like orientation in reconstituted high density lipoproteins. J Biol Chem 276(46):42965–42970
16. Li H et al (2000) Structural determination of lipid-bound ApoA-I using fluorescence resonance energy transfer. J Biol Chem 275(47):37048–37054
17. Li Y et al (2006) Structural analysis of nanoscale self-assembled discoidal lipid bilayers by solid-state NMR spectroscopy. Biophys J 91(10):3819–3828
18. Klon AE et al (2000) Molecular belt models for the apolipoprotein A-I Paris and Milano mutations. Biophys J 79(3):1679–1685
19. Segrest JP et al (1999) A detailed molecular belt model for apolipoprotein A-I in discoidal high density lipoprotein. J Biol Chem 274(45):31755–31758
20. Cheung MC et al (1987) Characterization of high density lipoprotein subspecies: structural studies by single vertical spin ultracentrifugation and immunoaffinity chromatography. J Lipid Res 28(8):913–929
21. Borhani DW et al (1997) Crystal structure of truncated human apolipoprotein A-I suggests a lipid-bound conformation. Proc Natl Acad Sci U S A 94(23):12291–12296
22. Shih AY et al (2005) Molecular dynamics simulations of discoidal bilayers assembled from truncated human lipoproteins. Biophys J 88(1):548–556
23. Shih AY et al (2007) Assembly of lipoprotein particles revealed by coarse-grained molecular dynamics simulations. J Struct Biol 157(3):579–592
24. Denisov IG et al (2004) Directed self-assembly of monodisperse phospholipid bilayer Nanodiscs with controlled size. J Am Chem Soc 126(11):3477–3487
25. Baas BJ, Denisov IG, Sligar SG (2004) Homotropic cooperativity of monomeric cytochrome P450 3A4 in a nanoscale native bilayer environment. Arch Biochem Biophys 430(2):218–228
26. Bayburt TH, Sligar SG (2003) Self-assembly of single integral membrane proteins into soluble nanoscale phospholipid bilayers. Protein Sci 12(11):2476–2481
27. Bayburt TH, Sligar SG (2010) Membrane protein assembly into Nanodiscs. FEBS Lett 584 (9):1721–1727
28. Civjan NR, et al (2003) Direct solubilization of heterologously expressed membrane proteins by incorporation into nanoscale lipid bilayers. Biotech 35(3):p 556–60, 562–3
29. Duan H et al (2004) Co-incorporation of heterologously expressed Arabidopsis cytochrome P450 and P450 reductase into soluble nanoscale lipid bilayers. Arch Biochem Biophys 424 (2):141–153
30. Shimizu Y et al (2006) Cell-free translation systems for protein engineering. FEBS J 273 (18):4133–4140
31. Katzen F, Chang G, Kudlicki W (2005) The past, present and future of cell-free protein synthesis. Trends Biotechnol 23(3):150–156
32. Farrokhi N et al (2009) Heterologous and cell free protein expression systems. Methods Mol Biol 513:175–198
33. Katzen F, Peterson TC, Kudlicki W (2009) Membrane protein expression: no cells required. Trends Biotechnol 27(8):455–460
34. Luirink J et al (2005) Biogenesis of inner membrane proteins in Escherichia coli. Annu Rev Microbiol 59:329–355
35. Andersson H, von Heijne G (1994) Membrane protein topology: effects of delta mu H + on the translocation of charged residues explain the ‘positive inside’ rule. EMBO J 13(10): 2267–2272
36. Alami M et al (2007) Nanodiscs unravel the interaction between the SecYEG channel and its cytosolic partner SecA. EMBO J 26(8):1995–2004
37. Cappuccio JA et al (2008) Cell-free co-expression of functional membrane proteins and apolipoprotein, forming soluble nanolipoprotein particles. Mol Cell Proteomics 7(11): 2246–2253

38. Katzen F et al (2008) Insertion of membrane proteins into discoidal membranes using a cell-free protein expression approach. J Proteome Res 7(8):3535–3542
39. Wang X et al (2015) Smaller Nanodiscs are Suitable for Studying Protein Lipid Interactions by Solution NMR. Protein J 34(3):205–211
40. Xu C et al (2008) Regulation of T cell receptor activation by dynamic membrane binding of the CD3epsilon cytoplasmic tyrosine-based motif. Cell 135(4):702–713

Chapter 3
Calcium Regulates T Cell Receptor Activation by Modulating Phospholipid Electrostatic Property

Abstract Ionic protein-lipid interactions are critical for the structure and function of membrane receptors, ion channels, adhesion molecules, Ras superfamily small GTPases and other proteins.

Ionic protein-lipid interactions are critical for the structure and function of membrane receptors, ion channels, adhesion molecules, Ras superfamily small GTPases and other proteins [1–8]. However, the mechanism by which this type of interactions is regulated in cells is largely unknown. Here we show that Ca^{2+} modulates the ionic interaction between the T cell receptor-CD3 complex (TCR) and anionic phospholipids and thus facilitates TCR phosphorylation. Upon antigen stimulation, the tyrosine phosphorylation of CD3 chains is the first signalling event in T cell, which triggers downstream signalling events such as Ca^{2+} influx [9]. TCR tyrosine phosphorylation is regulated by ionic interactions between positively-charged CD3ε/ζ cytoplasmic domains ($CD3_{CD}$) and negatively-charged phospholipids in the plasma membrane [1, 10–12]. Crucial tyrosine residues are buried in the membrane and are largely protected from phosphorylation in resting T cells. It is not clear how $CD3_{CD}$ dissociates from the membrane in antigen-stimulated T cells. Our biochemical, live cell FRET and NMR experiments showed that local Ca^{2+} concentration raise induced the dissociation of $CD3\varepsilon_{CD}$ from the membrane, resulting in the solvent exposure of the tyrosine residues. Ca^{2+} influx in stimulated T cells significantly enhanced CD3 tyrosine phosphorylation. Moreover, when compared with wild-type cells, Ca^{2+} channel-deficient T cells had substantially lower levels of CD3 phosphorylation after T cell activation. The positive feedback effect of Ca^{2+} on facilitating TCR phosphorylation is due primarily to this ion's charge, as demonstrated by the fact that replacing Ca^{2+} with the nonphysiological ion Sr^{2+} resulted in the same feedback effect. Finally, ^{31}P NMR spectroscopy showed that Ca^{2+} bound to the phosphate group in the anionic phospholipid headgroup at a physiological concentration, which explains the mechanism responsible for the effect of Ca^{2+} on TCR activation. Rather than initiating CD3 phosphorylation, this regulatory pathway of Ca^{2+} has a positive feedback effect on amplifying and sustaining CD3 phosphorylation and should enhance T-cell sensitivity to foreign

© Springer-Verlag GmbH Germany 2018

Y. Bi, *Study of the Calcium Regulation Mechanism of TCR Activation Using Nanodisc and NMR Technologies*, Springer Theses,
DOI 10.1007/978-3-662-54618-5_3

antigens. Our study thus provides a novel regulatory mechanism of ionic protein-lipid interactions and reveals a novel Ca^{2+} signalling mechanism involving direct lipid manipulation.

3.1 Introduction

TCR is one of the most complicated cell surface receptors and is composed of a ligand-sensing TCRαβ subunit and three signalling subunits-CD3εδ, εζ and ζζ. TCR recognition of the peptide-Major Histocompatibility Complex (MHC) complex is an essential step in initiating the host adaptive immune response against invading pathogen [9]. Antigen binding first triggers the tyrosine phosphorylation in the Immunoreceptor Tyrosine-based Activation Motifs (ITAMs) of CD3 chains, which is primarily mediated by Lck [13], and consequently elicits a comprehensive signalling network hallmarked by Ca^{2+} influx. The activated ITAMs could recruit the Zap-70 protein tyrosine kinase, which further promote recruitment and phosphorylation of downstream adaptor LAT and PLC-r. Inositol trisphosphate (IP3), which is the hydrolysis product of phosphatidylinositol 4,5-bisphosphate (PIP2) caused by Phosphorylation of phospholipase C γ1 (PLCγ1), can triggers the release of Ca^{2+} from the ER. Upon calcium ions release from the EF-hand and SAM (EF-SAM) domain of the calcium sensor protein Stromal Interaction Molecule 1 (STIM1), the transmembrane domains of STIM1 will rearrange to adapt the aggregate of EF-SAM domain, that will ultimately make poly-basic amine acids region of STIM1 target to the anionic phospholipid of the inner-leaflet of the plasma membrane, and then STIM1 further interacts with the Ca^{2+}-release-activated Ca^{2+} channel (CRAC), that make Ca^{2+} influx [14–16]. The regulatory mechanism of ITAM phosphorylation is a longstanding puzzle [17]. Another central question that remains is why T cells can be activated by minute quantities of foreign antigen [18, 19]. Recent works show that ITAM phosphorylation is regulated by the ionic interaction between the positively-charged ITAM and the negatively-charged inner-leaflet of the plasma membrane, which is enriched in anionic phospholipids [1, 10–12, 20, 21]. In resting T cells, CD3ε and ζ cytoplasmic domains bind to the plasma membrane, and ITAM tyrosines are inserted into the hydrophobic core of the plasma membrane [1, 10–12]. This prevents spontaneous ITAM phosphorylation in unstimulated T cells even when active Lcks are constitutively available [22]. In antigen-stimulated T cells, ITAMs need to be dislodged from the plasma membrane and become accessible for Lck. After initial TCR triggering, the local Ca^{2+} concentration increases quickly in a few seconds [23]. We therefore hypothesised that this divalent cation could directly change the local electrostatic environment and interfere with the ionic $CD3\varepsilon_{CD}$-membrane interaction, thus facilitating ITAM phosphorylation. This regulatory pathway should have positive feedback effect on amplifying the initial antigen-stimulated TCR signalling and should greatly enhance T cell sensitivity to foreign antigens.

3.2 Experiment Methods

3.2.1 Methods Summary

Mouse primary $CD4^+$ T cells were sorted from C57/B6 mice splenocytes using $CD4^+$ T cell Microbeads from Miltenyi Biotec. A CRAC deficient Jurkat cell line CJ-1 was generously provide by Dr. Richard Lewis, Stanford University. Jurkat and mouse $CD4^+$ primary T cells were stimulated by α-CD3 crosslinking (for Jurkat cells: 0.2 μg/ml UCHT1 plus 0.2 μg/ml α-mouse IgG; for primary T cells, 0.5 μg/ml 145-2C11 plus 1 μg/ml α-hamster IgG) for the indicated time in Mg^{2+}-free Ringer's buffer with or without 1 mM Ca^{2+}. To chelate intracellular Ca^{2+}, T cells were pretreated with 10 μM BAPTA-AM (Invitrogen) for 30 min at 37 °C prior to antibody stimulation. CD3ε was immunoprecipitated with UCHT1 or 145-2C11 and analysed to determine its tyrosine phosphorylation status by α-pY100 immunoblotting (Cell Signaling Technology). The tyrosine phosphorylation of CD3ζ was detected by α-pCD3ζ (Santa Cruz Biotechnology) immunoblotting of cell lysate samples.

All NMR spectra were acquired at 27 °C on Bruker Avance 600 and 850 MHz spectrometers. The acquired data were further processed using the software package NMRPipe and analysed with the program Sparky (Goddard and Kneller, 2006, SPARKY3, University of California, San Francisco, CA). Due to the low concentration of protein/lipid/Ca^{2+} mixture samples, 2D proton NOESY experiments were conducted instead of 3D ^{13}C-separated NOESY experiments to observe the NOEs from $CD3\varepsilon_{CD}$ aromatic protons to lipid methyl protons. The binding of Ca^{2+} to the phosphate group of the phospholipid was probed by a one-dimensional ^{31}P NMR measurement on the 850 MHz spectrometer equipped with a ^{31}P direct-detection channel. Nanodiscs composed of different phospholipids (POPG, POPS or POPC) were used for the ^{31}P experiment to eliminate the interference of the phosphorus signal from the detergent molecule that is commonly used in other lipid bilayer systems [24]. ^{31}P spectra were measured with 256 accumulated transients.

3.2.2 Cells and Reagents

Mouse primary $CD4^+$ T cells were sorted from C57/B6 mouse splenocytes using $CD4^+$ T cell negative selection microbeads (Miltenyi Biotec). A CRAC deficient Jurkat cell line, CJ-1, was generously provided by Dr. Richard Lewis, Stanford University. Lipids and detergent (POPG (1-palmitoyl-2-oleoyl-phosphatidylglycerol), POPC (1-palmitoyl-2-oleoyl-phosphatidylcholine), POPS (1-palmitoyl-2-oleoyl-phosphatidylserine), DHPC (dihexanoyl-phosphatidylcholine)) were from Avanti polar lipids. CD3ε (M20), phospho-CD3ζ, CD3ζ (6B10.2) and GST (Z-5) antibodies were from Santa Cruz Biotechnology. Phospho-Y100 antibody was from

Cell Signaling Technology. UCHT1 was from eBioscience. 145-2C11 was from Biolegend. Isotopes for NMR experiments were from Cambridge Isotope Laboratories.

3.2.3 $CD3\varepsilon_{CD}$ Peptide Expression and Labelling

$CD3\varepsilon_{CD}$ was expressed as a GST fusion protein in *E. coli*, separated from GST by TEV cleavage and purified by reverse-phase HPLC. For microdialysis and fluorescence polarisation experiments, $CD3\varepsilon_{CD}$ was expressed with an additional N-terminal cysteine and then labelled by an Alexa488-maleimide derivative (Invitrogen). For the in vitro phosphorylation experiment, the GST-$CD3\varepsilon_{CD}$ fusion protein was directly used for the unbiased detection of phosphorylated and unphosphorylated $CD3\varepsilon_{CD}$ by anti-GST immunoblotting.

3.2.4 Tyrosine Fluorescence Polarisation (FP) Assay

To measure the binding kinetics of $CD3\varepsilon_{CD}$ to phospholipid and the inhibition of this binding by Ca^{2+}, Alexa488-labelled $CD3\varepsilon_{CD}$, POPG/DHPC bicelles (q = 0.8) and Ca^{2+} were incubated in a 384-well plate for 15 min at 27 °C. The sample buffer was 20 mM HEPES, pH 7.0, containing 150 mM NaCl. The FP values were measured using a Tecan Infinite M1000Pro Microplate Reader.

3.2.5 FRET Measurement

One million cells were resuspended in 1 ml of Mg^{2+}-free Ringer's buffer (155 mM NaCl, 4.5 mM KCl, 10 mM D-glucose, 5 mM HEPES, pH 7.4, 2 mM $CaCl_2$). A 200 µl aliquot was pipetted onto the centre of 35 mm glass-bottom dish (Shengyou Biotechnology, Zhejiang, China) and cells were allowed to adhere for 5 min at room temperature. To induce Ca^{2+} influx, 5 µM ionomycin (Sigma) or α-CD3 antibody (2 µg/ml UCHT1 and 2 µg/ml α-mouse IgG) was added into the dish, which was then incubated at room temperature for additional 5 min. To label the plasma membrane, 2 µl of 250 µg/ml octadecyl rhodamine B (R18) (Invitrogen) was added into the dish. The dish was then mounted onto a Leica TCS SP5 microscope for imaging. The FRET efficiency between mTFP1 (donor) and R18 (acceptor) was measured by the dequenching method. TFP was excited with the Argon 458 nm laser line and visualised using detection at 470–560 nm. R18 was

excited with the Helium/Neon 561 nm laser line, visualised using detection at 590–650 nm. FRET measurements and calculations were performed as previously described [1].

3.2.6 T Cell Activation and Immunoblotting

Jurkat cells and mouse $CD4^+$ primary T cells were stimulated at 37 °C by TCR crosslinking (for Jurkat: 0.2 μg/ml α-CD3 (UCHT1) plus 0.2 μg/ml α-mouse IgG; for primary T cells, 0.5 μg/ml α-CD3 (145-2C11) plus 1 μg/ml α-hamster IgG) for the indicated time in Mg^{2+}-free Ringer's buffer with or without 1 mM Ca^{2+}. To chelate intracellular Ca^{2+}, the cells were pretreated with 10 μM BAPTA-AM (Invitrogen) for 30 min at 37 °C. Stimulation reactions were terminated by adding ice-cold Mg^{2+}-free Ringer's buffer. For the detection of CD3ε phosphorylation, cells were lysed in an immunoprecipitation buffer (1% NP40, 50 mM Tris-HCl, pH 7.4, 155 mM NaCl, 2 mM EDTA, 2 mM Na_3VO_4, 20 mM NaF, 10 mM iodoacetamide, 1 mM PMSF and complete protease inhibitor cocktail (Sigma)) and then subjected to CD3ε immunoprecipitation by UCHT1 or 145-2C11. For the detection of CD3ζ phosphorylation, stimulated cells were directly lysed in SDS-PAGE sample buffer. Immunoprecipitated samples and cell lysate samples were separated by SDS-PAGE, transferred onto PVDF membranes (Millipore) and subjected to immunoblotting. CD3ε phosphorylation and CD3ζ phosphorylation were detected by α-pY100 and α-pCD3ζ immunoblotting, respectively. Membranes were then stripped off and re-blotted with α-CD3ε or α-CD3ζ for the detection of total CD3ε and CD3ζ, respectively.

3.2.7 Preparation of Nanodisc, Bicelles and Large Unilamellar Vesicles (LUVs)

To assemble nanodisc, the MSP1D1/lipid/sodium cholate reaction mixture was incubated for 15 h at the appropriate temperature (POPC 4 °C, POPG/POPS 14 °C) in buffer containing 20 mM Tris-HCl, pH 7.2, 100 mM NaCl and 0.5 mM EDTA [24]. The molar ratio of MSP1D1/lipid/sodium cholate was used as 1:65:130. The nanodisc self-assembly process was initiated upon the removal of the sodium cholate by incubating the mixture with Bio-Beads SM-2 (0.8 g per ml reaction mixture, Bio-Rad) on a shaker for 8 h at room temperature After filtering off Bio-Beads with syringe filters, the nanodisc samples were purified on a Superdex 200 gel-filtration column (GE Healthcare) equilibrated in buffer containing 20 mM Tris-HCl, pH 7.0 and 100 mM NaCl. The peak fractions were collected and concentrated using an ultracentrifugation column with a 30,000 MW cutoff (Millipore). Large unilamellar vesicle (LUV) and bicelle samples were prepared as previously described [1].

3.2.8 NMR Experiments

All NMR spectra were acquired at 27 °C on Bruker Avance 600 and 850 MHz spectrometers. The acquired data were further processed using the software package NMRPipe [25] and analysed with Sparky (Goddard and Kneller 2006, SPARKY3, UCSF).

3.2.9 Aromatic NOESY

Because of the low concentration of the protein/lipid/Ca^{2+} mixture samples, 2D proton NOESY experiments were conducted to observe NOEs from CD3ε_{CD} aromatic protons to lipid methyl protons. For the indirect dimension, background signals from CD3ε_{CD} were suppressed by double ^{13}C filtering, and only lipid methyl protons evolved. For the direct dimension, the aromatic protons Hδ and Hε from tyrosines were selected by aromatic ^{13}C edition. The samples were diluted in D_2O to achieve better water suppression and reduce the spin diffusion effect. Experiments were conducted on the Bruker 600 MHz spectrometer at 27 °C with a NOE mixing time of 300 ms, 128 points in the indirect dimension, 2048 points in the direct dimension and 1024 accumulated transients.

3.2.10 ^{31}P Spectrum

The binding of Ca^{2+} to the phosphate group of the phospholipid was measured by ^{31}P spectrum on an 850 MHz spectrometer equipped with a ^{31}P direct-detection channel. Lipid nanodisc samples were prepared in buffer containing 20 mM Tris-HCl, pH 7.0, 100–150 mM NaCl. Ca^{2+} was titrated in with a molar ratio of Ca^{2+}/lipid from 0 to 1.5. One-dimensional ^{31}P spectra were measured with 256 accumulated transients and processed with 25 Hz of line broadening.

3.3 Experiment Result

We first performed a microdialysis assay to study whether Ca^{2+} could directly interfere with the CD3ε_{CD}-membrane interaction. CD3ε_{CD} showed specific binding to a membrane bilayer composed of anionic phospholipids. The addition of Ca^{2+} significantly impaired this ionic interaction (Fig. 3.1a, b) as well as the ionic interaction between CD3ζ_{CD} and anionic lipids (Fig. 3.2). Our fluorescence polarisation experiment also confirmed this observation (Fig. 3.3). We then performed a FRET-based experiment to measure the effect of Ca^{2+} in live T cells. As described previously [1], the cytopasmic domain of a monomeric membrane

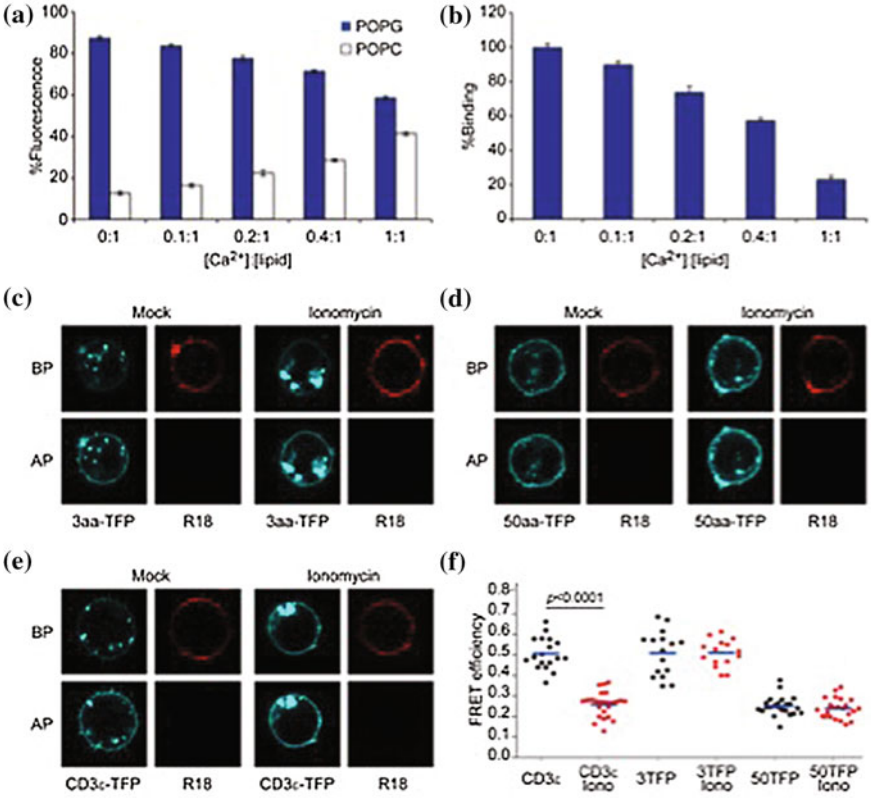

protein, KIR2DL3, was replaced by $CD3\varepsilon_{CD}$ with a C-terminal Teal Fluorescence Protein (mTFP1). The distance between $CD3\varepsilon_{CD}$ and the plasma membrane was determined by measuring the FRET efficiency between mTFP1 and a membrane dye, octadecyl rhodamine B (R18). To help translate the FRET efficiency into spatial distance, two control constructs with flexible linkers of different lengths (3aa and 50aa) between KIR2DL3 transmembrane domain and mTFP1 were used. The FRET efficiencies of these two constructs represent the states in which $CD3\varepsilon_{CD}$ is fully membrane bound (3aa) or unbound (50aa). In resting cells, $CD3\varepsilon_{CD}$-mTFP1 showed substantial FRET efficiency, similar to that of 3aa-mTFP1, indicating that $CD3\varepsilon_{CD}$ bound to the plasma membrane. After Ca^{2+} influx induced by ionomycin treatment or TCR crosslinking, the FRET efficiency of $CD3\varepsilon_{CD}$-mTPF1 declined significantly to the level similar to that of 50aa-mTFP1 (Figs. 3.1e, f and 3.4). In contrast, the FRET efficiencies of both 3aa-mTFP1 and 50aa-mTFP1 were not sensitive to ionomycin treatment (Fig. 3.1c, d, f). These data support a notion that Ca^{2+} influx can disrupt the ionic $CD3\varepsilon_{CD}$-lipid interaction and result in the dissociation of $CD3\varepsilon_{CD}$ from the plasma membrane.

◄ **Fig. 3.1** Ca^{2+} induced the dissociation of $CD3\varepsilon_{CD}$ from the membrane bilayer. The effect of Ca^{2+} on the $CD3\varepsilon_{CD}$-membrane interaction was measured by an equilibrium-based microdialysis assay (**a**, **b**) and a live-cell FRET imaging experiment (**c**–**f**). **a** The microdialysis system was composed of two equal-size chambers, an experimental chamber and a control chamber [1]. The experimental chamber was loaded with 10 nM Alexa488-labelled $CD3\varepsilon_{CD}$ and large unilamellar vesicles (LUVs) composed of 5 mM POPG (an anionic phospholipid) in buffer containing 20 mM HEPES, pH 7.0, and 100 mM KCl, whereas the control chamber was loaded with 10 nM Alexa488-labelled $CD3\varepsilon_{CD}$ and LUVs composed of 5 mM POPC (a zwitterionic phospholipid) in the same buffer. Ca^{2+} was added into the two chambers at a molar ratio relative to the phospholipid from 0 to 1. The two chambers were separated by a 300 kDa dialysis membrane, which allowed the free movement of $CD3\varepsilon_{CD}$ but not the LUVs. After reaching equilibrium at 16 h, the binding of $CD3\varepsilon_{CD}$ to the anionic phospholipid was calculated based on the fluorescence intensity difference between the two chambers. In the absence of Ca^{2+}, $CD3\varepsilon_{CD}$ bound strongly to POPG LUVs. The increase of the Ca^{2+} concentration significantly impaired the $CD3\varepsilon_{CD}$-POPG interaction. Triplicate measurements were made for each condition and the results (mean ± SD) were plotted as the percentage of the Alexa488 fluorescence intensity in the experimental (POPG) and control (POPC) chambers. **b** The binding efficiency of $CD3\varepsilon_{CD}$ to POPG was calculated by the following equation: Binding % = (FLExp − FLCon)/(FLExp + FLCon), where FLExp is the fluorescence intensity in the experimental chamber and FLCon is the fluorescence intensity in the control chamber. The binding efficiencies under different Ca^{2+} concentrations were then normalised to the value measured in the absence of Ca^{2+}. **c**–**f** The FRET efficiency was measured between mTFP1 and the membrane dye R18 by the dequenching approach in live Jurkat T cells. Ionomycin (5 μM) was used to induce Ca^{2+} influx. The FRET efficiencies of the 3TFP (3aa-mTFP1) and 50TFP (50aa-mTFP1) control constructs were not sensitive to Ca^{2+} influx whereas the FRET efficiency of $CD3\varepsilon_{CD}$-mTFP1 was reduced significantly in response to Ca^{2+} influx. BP represents Before Photobleaching and AP After Photobleaching. The FRET efficiencies were measured for more than 15 cells per condition. Each dot represents the FRET value from one individual cell

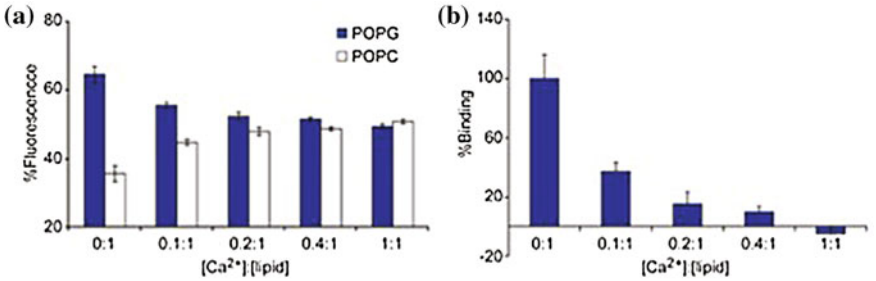

Fig. 3.2 A microdialysis experiment measuring the effect of Ca^{2+} on disrupting the $CD3\zeta_{CD}$-membrane interaction. In the absence of Ca^{2+}, $CD3\zeta_{CD}$ had substantial binding to anionic POPG LUVs, but not to POPC LUVs. The increase of the Ca^{2+} concentration in the dialysis system significantly impaired the $CD3\zeta_{CD}$-membrane interaction. The binding efficiency of $CD3\zeta_{CD}$–POPG was calculated and normalised using the same method as for Fig. 3.1. $CD3\zeta_{CD}$ was used at 10 nM, POPG or POPC bicelles was used at 5 mM and the sample buffer was 20 mM HEPES with 100 mM KCl, pH 7.0

We further utilized solution-state multi-dimensional Nuclear Magnetic Resonance (NMR) spectroscopy to trace the dynamics of the $CD3\varepsilon_{CD}$-membrane interaction in response to $[Ca^{2+}]$ increase. As measured by a ^{15}N–^{1}H Heteronuclear Single-Quantum Coherence (HSQC) experiment, titrating in Ca^{2+} caused

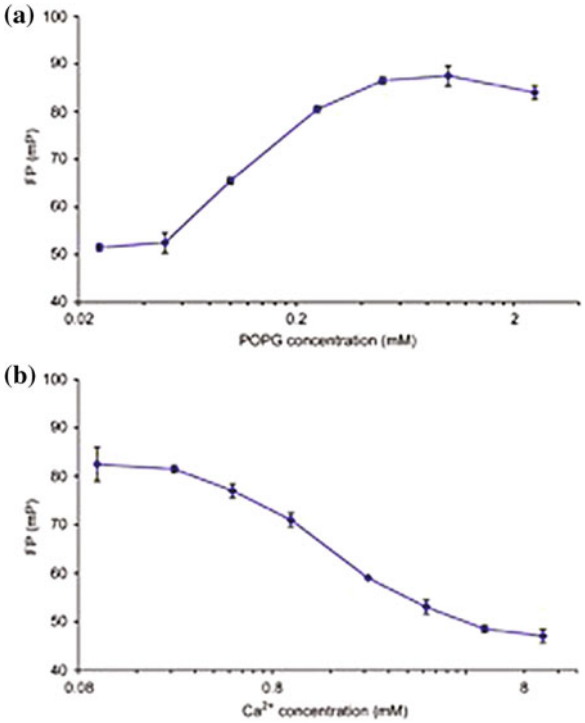

Fig. 3.3 A Fluorescence Polarisation experiment measuring the effect of Ca^{2+} on disrupting the $CD3\varepsilon_{CD}$-membrane interaction. The Fluorescence Polarisation (FP) technique was used to study the association of $CD3\varepsilon_{CD}$ to the membrane bilayer and the dissociation of $CD3\varepsilon_{CD}$ from the membrane upon Ca^{2+} treatment. This experiment was based on the principle that the rotation rate of the free $CD3\varepsilon_{CD}$ peptide is much higher than that of the membrane-bound peptide. A physiological salt concentration (150 mM NaCl) was used in the reaction to ensure the measurement of the specific $CD3\varepsilon_{CD}$-membrane association as well as the dissociation triggered by Ca^{2+}. **a** An alexa488-labeled $CD3\varepsilon_{CD}$ peptide (100 nM) was incubated with POPG/DHPC bicelles (q = 0.8) at a wide range of concentration (from 0.01 to 2.5 mM) for 15 min at 27 °C. The sample buffer was 20 mM HEPES, pH 7.0, with 150 mM NaCl. The FP value of free $CD3\varepsilon_{CD}$ peptide was ~50 mP and it increased gradually in correspondence to the lipid concentration increase, maximally to ~90 mP when the majority of $CD3\varepsilon_{CD}$ bound to the membrane bilayer. **b** After the most of $CD3\varepsilon_{CD}$ (100 nM) was bound to POPG bicelles (0.5 mM) in the same sample buffer as for panel a, Ca^{2+} was titrated into the sample from 0.1 to 20 mM to study the dissociation triggered by Ca^{2+}. $CD3\varepsilon_{CD}$ FP value gradually decreased to ~50 mP in correspondence to the Ca^{2+} concentration increase, indicating that Ca^{2+} specifically disrupted the $CD3\varepsilon_{CD}$ membrane interaction

systematic shifts of amide resonances of all $CD3\varepsilon_{CD}$ residues, including the key ITAM tyrosines, Tyr38 and Tyr49, from membrane-bound state to solution state (Fig. 3.5). The Tyr38 and Tyr49 regions show strong chemical shift perturbation, as well as poly-basic amino acids region, which locate at the N-terminal of $CD3\varepsilon_{CD}$ (Fig. 3.6). $CD3\zeta_{CD}$ displayed similar sensitivity to [Ca^{2+}] increase (Fig. 3.8). As one of the major groups interacting with anionic lipids, the side-chain NHs of most

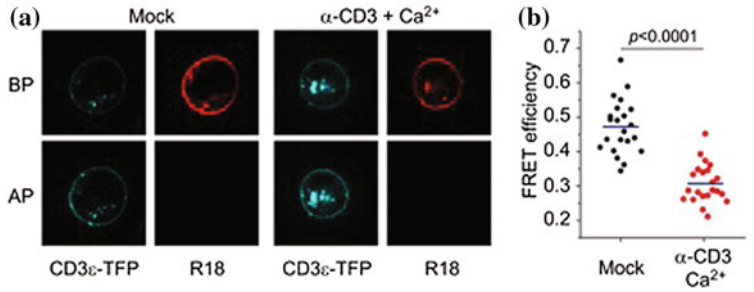

Fig. 3.4 A FRET measurement of the dissociation of $CD3\varepsilon_{CD}$ from the plasma membrane in T cells stimulated by TCR crosslinking. TCR crosslinking was used to stimulate T cells and induce calcium influx. The FRET efficiency between KIR-$CD3\varepsilon_{CD}$-mTFP and the plasma membrane dye R18 reduced significantly upon the α-CD3 treatment. Triggering antibodies (2 μg/ml α-CD3 (UCHT1) and 2 μg/ml α-mouse IgG) were applied to Jurkat cells for 5 min at room temperature before imaging. R18 was then added into the dish and FRET measurements were performed as described previously. The buffer used was the Mg^{2+}-free Ringer's buffer with 1 mM Ca^{2+}. BP represents Before Photobleaching and AP After Photobleaching. The FRET efficiencies were measured for 22 cells per condition. Each dot represents the FRET efficiency from one individual cell

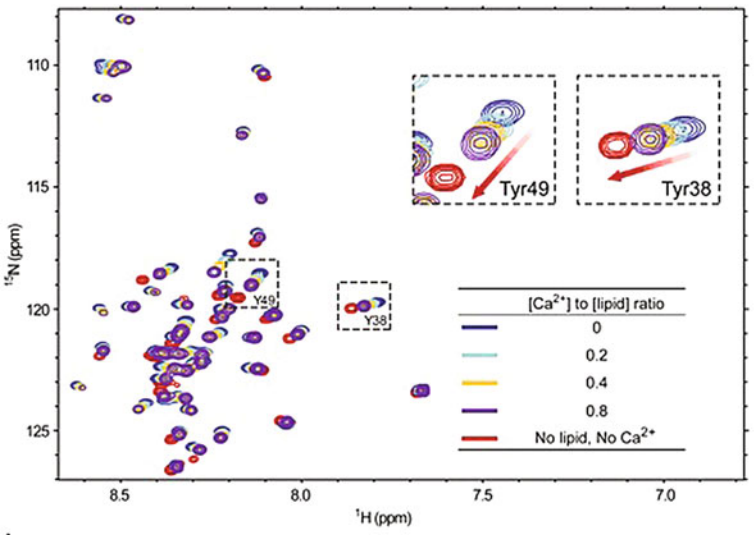

Fig. 3.5 Ca^{2+} induced the solvent exposure of $CD3\varepsilon_{CD}$. Superimposed ^{15}N–^{1}H HSQC spectra of $CD3\varepsilon_{CD}$ with POPG bicelles (*blue*), $CD3\varepsilon_{CD}$ with POPG bicelles and Ca^{2+} with different concentrations (*cyan*, *yellow* and *purple*), and $CD3\varepsilon_{CD}$ with control POPC bicelles (*red*). Membrane-bound $CD3\varepsilon_{CD}$ (*blue*) and solvent-exposed $CD3\varepsilon_{CD}$ (*red*) displayed very different amide resonance spectra. Ca^{2+} was titrated into the $CD3\varepsilon_{CD}$-with-POPG sample at a molar ratio of Ca^{2+}/POPG from 0.2 to 0.8. In response to the increase in the Ca^{2+} concentration, the $CD3\varepsilon_{CD}$ amide resonances exhibited systematic shifts from the membrane-bound state to the solvent-exposed state. The resonance changes of two tyrosine residues, Tyr38 and Tyr49, are enlarged in the inset. HSQC experiments were performed with 0.05 mM ^{15}N-labelled $CD3\varepsilon_{CD}$, 7.5 mM POPG or POPC bicelles (q = 0.8), 10 mM DHPC and 0–6 mM Ca^{2+} in 20 mM Tris-HCl buffer, pH 7.0 (color figure online)

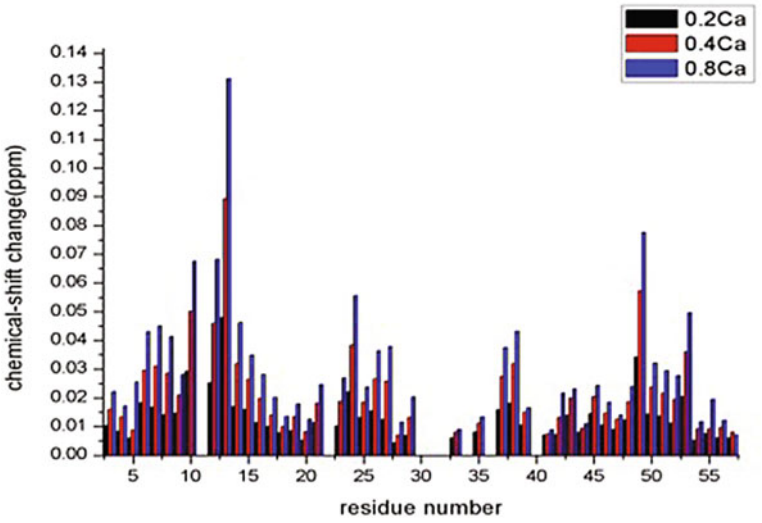

Fig. 3.6 Ca^{2+} induced the chemical shift changes of CD3ε_{CD}. Chemical shift change is calculated based on the assignments of Fig. 3.5 with function $\Delta\delta = [\Delta\delta H_N^2 + (0.1\Delta\delta_N)^2]^{1/2}$, in which $\Delta\delta H_N$ and $\Delta\delta N$ are the chemical shift changes of ^1H_N and ^{15}N respectively

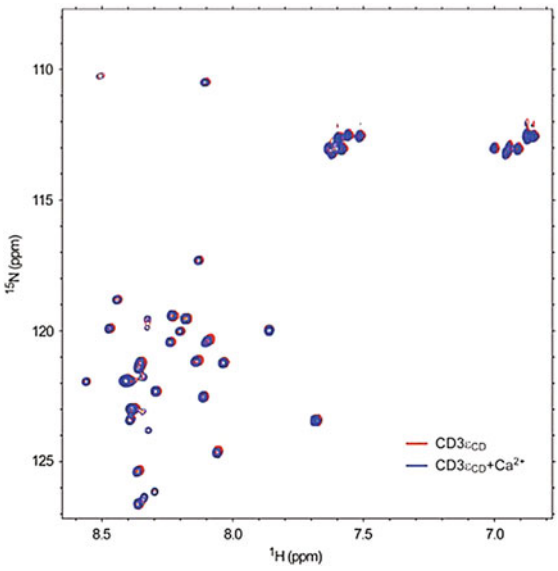

Fig. 3.7 Ca^{2+} did not directly induce conformational change of CD3ε_{CD}. The ^{15}N–^1H HSQC spectra of CD3$\boldsymbol{\varepsilon}_{CD}$ in Tris-HCl buffer without Ca^{2+} (*red*) and with Ca^{2+} (*blue*) were superimposed and no specific chemical shift difference was observed, indicating that Ca^{2+} did not directly induce the conformational change of CD3$\boldsymbol{\varepsilon}_{CD}$. The sample contained 0.05 mM ^{15}N-labelled CD3$\boldsymbol{\varepsilon}_{CD}$ and 12.5 mM Ca^{2+} in 20 mM Tris-HCl buffer, pH 7.0 (color figure online)

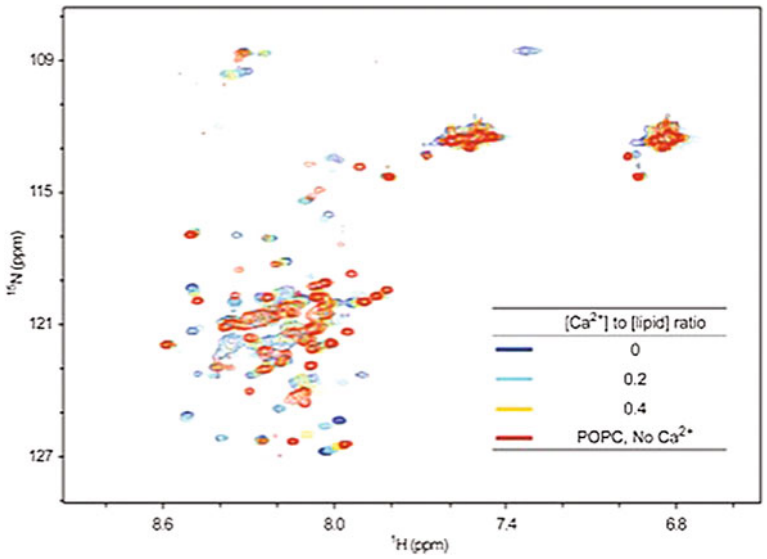

Fig. 3.8 Ca^{2+} induced the solvent exposure of $CD3\zeta_{CD}$. Superimposed ^{15}N–^{1}H HSQC spectra of $CD3\zeta_{CD}$ with POPG bicelles (*blue*), $CD3\zeta_{CD}$ + POPG bicelles + Ca^{2+} with different concentrations (*cyan* and *yellow*), and $CD3\zeta_{CD}$ + control POPC bicelles (*red*). Membrane-bound $CD3\zeta_{CD}$ (*blue*) and solvent-exposed $CD3\zeta_{CD}$ (*red*) displayed very different amide resonance spectra. Ca^{2+} was titrated into the $CD3\zeta_{CD}$ + POPG sample at a molar ratio of Ca^{2+}/POPG from 0.2 to 0.4. In response to Ca^{2+} concentration increase, the $CD3\zeta_{CD}$ amide resonances had systematic shifts from membrane-bound state to solvent-exposed state. This experiment was done with 0.04 mM ^{15}N-labelled $CD3\zeta_{CD}$ and 10 mM POPG or POPC bicelles (q = 0.8) in 20 mM Tris-HCl buffer, pH 7.0 (color figure online)

arginines in $CD3\varepsilon_{CD}$ showed intense peaks in the membrane-bound $CD3\varepsilon_{CD}$ HSQC spectrum. Those peaks were largely missing in the soluble $CD3\varepsilon_{CD}$ spectrum because of the fast proton exchange with the solvent. The addition of Ca^{2+} to the membrane-bound $CD3\varepsilon_{CD}$ sample greatly reduced the signal intensity of the arginine side-chain NHs, again confirming the ability of Ca^{2+} to induce the solvent exposure of $CD3\varepsilon_{CD}$ (Fig. 3.9). This effect was not caused by a Ca^{2+}-induced $CD3\varepsilon_{CD}$ conformational change because adding Ca^{2+} to the $CD3\varepsilon_{CD}$ solution in the absence of bicelles did not result in any specific chemical shift perturbation (Fig. 3.7). Our Circular Dichroism experiment also verified the effect of Ca^{2+} on disrupting the ionic $CD3\varepsilon_{CD}$-membrane interaction (Fig. 3.10). Upon membrane binding, the aromatic rings of tyrosines insert into the hydrophobic core of the lipid bilayer, and substantial Nuclear Overhauser Effect (NOE) signals between the tyrosine aromatic protons and the lipid acyl chain protons were detected by a NOESY experiment (Fig. 3.11). Adding Ca^{2+} substantially weakened the

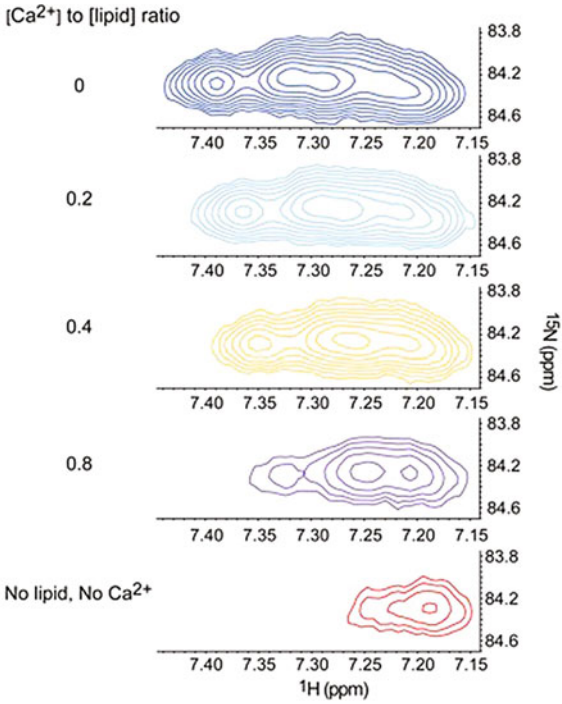

Fig. 3.9 Ca^{2+} induced the solvent exposure of CD3ε_{CD} arginine side-chains. Arginine and lysine residues in CD3ε_{CD} are the major contributors for the CD3ε_{CD}-membrane interaction [1]. When CD3ε_{CD} was not bound to lipid, the guanidino groups of arginine residues underwent rapid proton exchange with water, which led to undetectable guanidino NHs signals in the CD3ε_{CD} + POPC ^{15}N–^{1}H HSQC spectrum. Upon lipid binding, the arginine NHs were protected from water exchange, resulting in the appearance of strong NHs resonances in the CD3ε_{CD} + POPG HSQC spectrum (*blue*). The NHs signals decreased significantly in response to the Ca^{2+} concentration increase, indicating the solvent exposure of the arginine side-chains in CD3ε_{CD}. The sample used for this experiment was the same as for Fig. 3.5 (color figure online)

tyrosine-lipid NOE signals, indicating that the tyrosine side-chains were no longer embedded in the membrane core region. A Tyrosine Fluorescence Emission experiment confirmed the Ca^{2+}-induced solvent exposure of ITAM tyrosines (Fig. 3.12).

We then tested whether Ca^{2+} could facilitate CD3 phosphorylation by both in vitro phosphorylation (IVP) and live T cell stimulation experiments. The IVP data showed that binding to anionic lipids prevented CD3ε_{CD} phosphorylation by Lck but Ca^{2+} could reverse this blockade and rescue CD3ε_{CD} phosphorylation (Fig. 3.13a). Lck activity was not enhanced by Ca^{2+} (Fig. 3.13b). The physiological foreign antigen density on the antigen presenting cell surface is generally very low

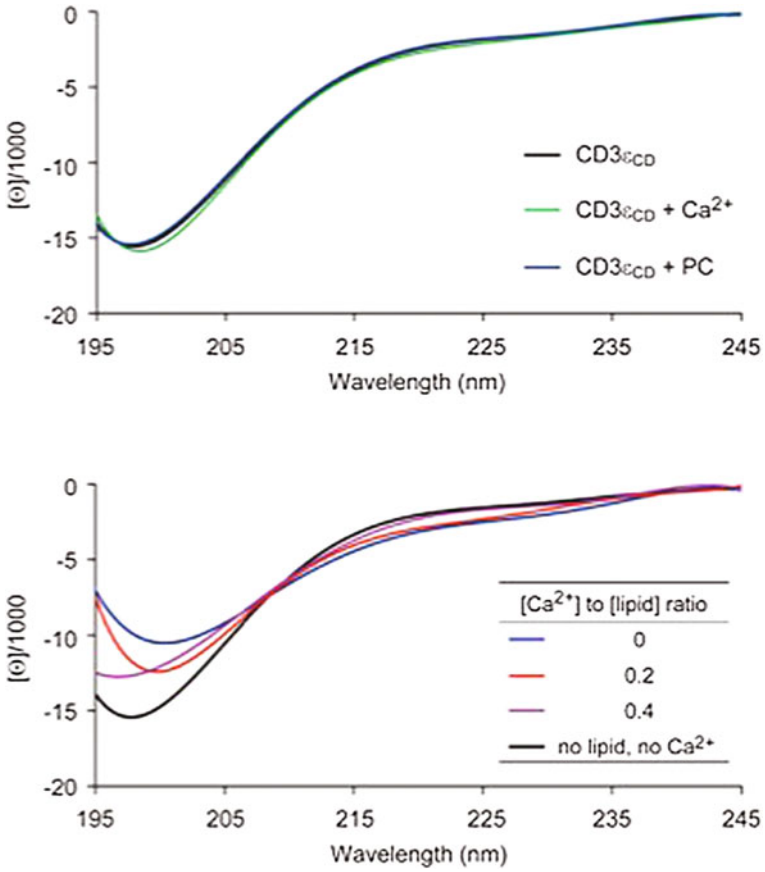

Fig. 3.10 A Far UV Circular-Dichroism experiment measuring the second structure change of $CD3\varepsilon_{CD}$ upon lipid and Ca^{2+} treatments. **a** As measured by a far UV Circular Dichroism (CD) experiment, $CD3\boldsymbol{\varepsilon}_{CD}$ displayed as an unstructured flexible peptide in solution. The addition of Ca^{2+} or zwitterionic lipid POPC did not induce any conformational change of $CD3\boldsymbol{\varepsilon}_{CD}$. **b** The presence of POPS/POPG/POPC mixture bicelles (3:1:6) with q = 0.8 induced partial helical folding of $CD3\boldsymbol{\varepsilon}_{CD}$. Titrating in Ca^{2+} resulted in a gradient change of $CD3\boldsymbol{\varepsilon}_{CD}$ from the partial folded conformation to the unstructured conformation, confirming the effect of Ca^{2+} on disrupting the $CD3\boldsymbol{\varepsilon}_{CD}$-membrane interaction. CD experiments were done with samples containing 10 μM $CD3\boldsymbol{\varepsilon}_{CD}$, 0 or 2 mM mixture bicelles, 10 mM Tris-HCl buffer, pH 7.4. Ca^{2+} was titrated in with at a molar ratio relative to the lipid from 0.2 to 0.4

[17]. To mimic physiological conditions, we activated T cells with α-CD3 antibody at a low concentration. For both Jurkat and mouse primary T cells, CD3 phosphorylation was substantially stronger when 1 mM Ca^{2+} was present in the stimulating buffer (Figs. 3.13 and 3.14a). Chelating intracellular Ca^{2+} with BAPTA significantly reduced CD3 phosphorylation. CJ-1, a Jurkat mutant cell line having

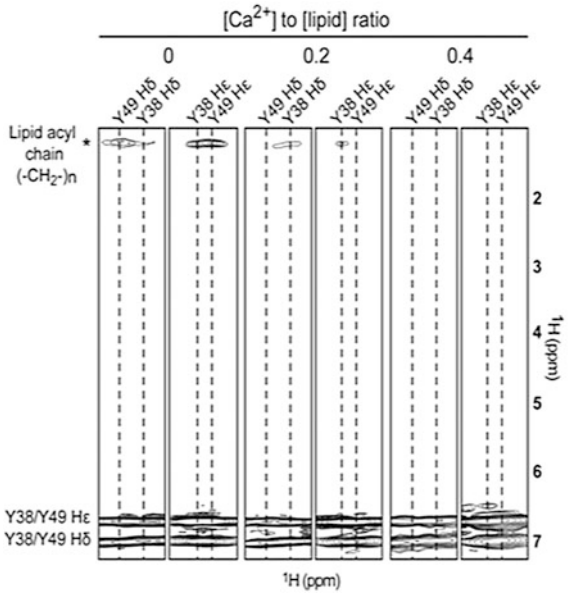

Fig. 3.11 Ca^{2+} induced the solvent exposure of tyrosine residues in $CD3\varepsilon_{CD}$ ITAM. Strips from aromatic NOESY spectra showing NOEs (distance of <5 Å) between the aromatic protons Hε/Hδ of Y38 and Y49 and the methylene protons in the lipid acyl chains. The substantial NOE signals (marked by asterisk) observed in the absence of Ca^{2+} indicated the insertion of tyrosine side-chains into the membrane hydrophobic interior. The addition of Ca^{2+} resulted in the significant impairment of NOE signals, which indicated that tyrosine side-chains were no longer embedded in the membrane core region. NOESY experiments were performed with 0.05 mM ^{15}N-, ^{13}C-labelled $CD3\varepsilon_{CD}$, 7.5 mM POPG bicelles (q = 0.8), 10 mM DHPC and 0–3 mM Ca^{2+} in 20 mM Tris-HCl buffer, pH 7.0. Ca^{2+} was titrated in at a molar ratio relative to POPG of 0.2 to 0.4

only residual expression of CRAC channel [26, 27], had much weaker CD3 phosphorylation after T cell activation when compared with wild-type Jurkat cells (Fig. 3.13d). Moreover, the presence of Ca^{2+} in the stimulating buffer did not cause substantial enhancement of CD3 phosphorylation in CJ-1 cells (Fig. 3.14b). The effect of Ca^{2+} on TCR phosphorylation is not caused by the direct enhancement of Lck activity (Fig. 3.15a). Using a stable Jurkat cell line that overexpresses a constitutively active form of Lck, we found that the effect of Ca^{2+} on TCR phosphorylation was still profound even when active Lck was saturated (Fig. 3.15b, c). To further rule out the potential contributions of Ca^{2+}-dependent signalling pathways in the role of Ca^{2+} in TCR phosphorylation, we replaced Ca^{2+} with Sr^{2+}, a

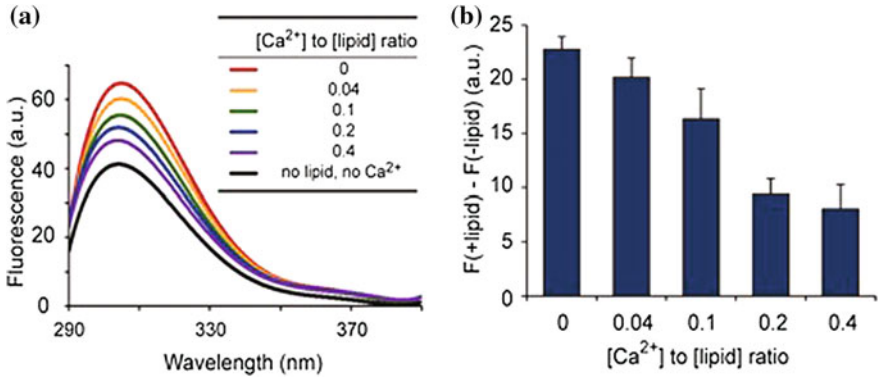

Fig. 3.12 Ca^{2+} induce the tyrosine residue expose to the solvent envirment. **a** Tyrosine Fluorescence Emission (TFE) spectra of $CD3\varepsilon_{CD}$ under different conditions. Mixture bicelles (30% POPS, 10% POPG and 60% POPC) were used to mimic the physiological lipid composition in the inner-leaflet of the plasma membrane. The peak value of the membrane-bound $CD3\varepsilon_{CD}$ TFE spectrum (*red*) was much higher than that of solvent-exposed $CD3\varepsilon_{CD}$ spectrum (*black*). Titrating in Ca^{2+} to the membrane-bound $CD3\varepsilon_{CD}$ sample substantially reduced the peak value (*orange*, *green*, *blue* and *purple*), confirming that Ca^{2+} induced the solvent exposure of tyrosine aromatic rings. **b** The experiments shown in panel a were repeated three times, and the increase in the TFE value at 310 nm upon lipid binding, calculated as F (+lipid)–F (−lipid), was plotted as the mean ± SD. TFE experiments were performed with 6 μM $CD3\varepsilon_{CD}$, 0.1 mM DTT, 0 or 0.5 mM POPS/POPG/POPC mixture bicelles (q = 0.8) and 10 mM Tris-HCl, pH 7.4. Ca^{2+} was titrated in at a molar ratio relative to the total lipid concentration of 0.04–0.4 (color figure online)

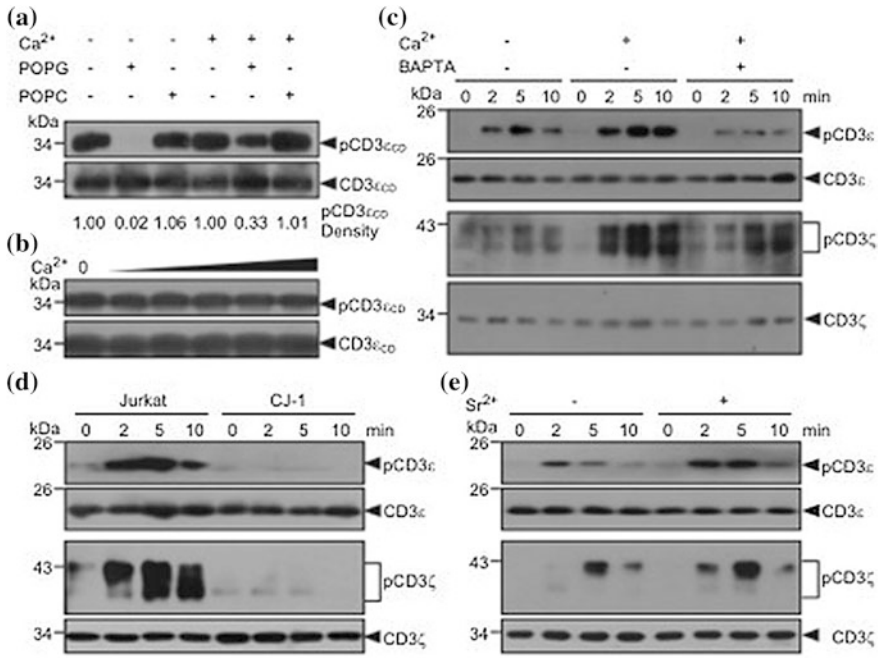

non-physiological divalent cation that can also pass through the CRAC channel [28]. Similar to Ca^{2+}, Sr^{2+} directly disrupted the $CD3\varepsilon_{CD}$-membrane interaction (Fig. 3.16) and facilitated CD3 phosphorylation (Fig. 3.13e).

We next studied the mechanism by which Ca^{2+} undermines the ionic $CD3\varepsilon_{CD}$-lipid interaction. We used ^{31}P NMR spectroscopy to directly probe the change in the chemical environment of the negatively charged lipid phosphorus after Ca^{2+} binding. Lipid nanodiscs were used here instead of bicelles to avoid the signal interference from the detergent molecule [24]. Ca^{2+} binding induced substantial chemical shift change of the phosphorus signal of anionic lipids, but not that of the zwitterionic POPC (Figs. 3.17a, b and 3.18a, b). This perturbation effect can be reversed by the Ca^{2+} chelator EGTA (Fig. 3.18c). Same directional shift of the phosphorus signal was induced by $CD3\varepsilon_{CD}$ binding, implying that both Ca^{2+} and

◂**Fig. 3.13** Ca^{2+} facilitated TCR phosphorylation. **a**, **b** An *in vitro* phosphorylation assay was performed to study $CD3\varepsilon_{CD}$ tyrosine phosphorylation by Lck under different Ca^{2+} concentrations. $CD3\varepsilon_{CD}$ with an N-terminal GST tag was used for the unbiased detection of phosphorylated and unphosphorylated $CD3\varepsilon_{CD}$ peptides by α-GST immunoblotting. The assay was performed using the following buffer condition: 70 mM HEPES, pH 7.0, 5 mM $MgCl_2$, 3 μM Na_3VO_4, 1.25 mM DTT, 150 mM KCl and 0.2 mM ATP. $CD3\varepsilon_{CD}$ was first incubated with lipid in the presence or absence of Ca^{2+} at 37 °C for 30 min. Lck was then added, and the reaction was incubated at 30 °C for 1 h. Tyrosine-phosphorylated and total $CD3\varepsilon_{CD}$ were detected by α-pY100 and α-GST immunoblotting, respectively. **a** The tyrosine residues of $CD3\varepsilon_{CD}$ were efficiently phosphorylated by Lck. The addition of POPG bicelles but not control POPC bicelles prevented $CD3\varepsilon_{CD}$ phosphorylation. Ca^{2+} can reverse this blockade and rescue $CD3\varepsilon_{CD}$ tyrosine phosphorylation. This experiment was performed with 0.5 μM $CD3\varepsilon_{CD}$, 1 mM POPG or POPC bicelles, 2 μg/μl Lck and 0 or 5 mM Ca^{2+}. **b** Ca^{2+} did not directly increase Lck activity for phosphorylating $CD3\varepsilon_{CD}$ tyrosine residues. The Ca^{2+} concentration was raised from 0 to 0.5, 5, 50, 500 and 5000 μM (*left* to *right*). Lck was used at 2 μg/μl for all experimental conditions, and $CD3\varepsilon_{CD}$ was used at 0.5 μM. **c** Jurkat T cells were stimulated by TCR crosslinking (0.2 μg/ml α-CD3 (UCHT1) plus 0.2 μg/ml α-mouse IgG) for the indicated time at 37 °C. The levels of CD3**ε** and ζ phosphorylation were substantially greater in Ca^{2+}-containing triggering buffer (1 mM Ca^{2+}) compared with Ca^{2+}-free buffer. When intracellular Ca^{2+} was chelated with 10 μM BAPTA, the levels of both CD3**ε** and ζ phosphorylations were significantly reduced. CD3ε was immunoprecipitated by UCHT1 and immunoblotted by α-pY100 and α-CD3**ε** (M20) for the detection of phosphorylated and total CD3ε, respectively. CD3ζ phosphorylation was directly detected using cell lysate samples by α-pCD3ζ immunoblotting, and total CD3ζ was detected by 6B10.2 immunoblotting. **d** CRAC channel-deficient Jurkat mutant CJ-1 cells only had weak CD3**ε** and ζ phosphorylation after TCR crosslinking, indicating that Ca^{2+} influx was important for TCR phosphorylation. **e** To rule out the potential contribution of Ca^{2+}-dependent signalling pathways in TCR phosphorylation, nonphysiological Sr^{2+} (0.5 mM) was used instead of Ca^{2+} as the only divalent cation in the triggering buffer. The T cells used for this experiment were a stable Jurkat cell line overexpressing a constitutively active Lck form (Fig. 3.15). Cells were stimulated using the same condition as for panel c. The levels of CD3**ε** and ζ phosphorylation were substantially greater under Sr^{2+}-containing condition compared with Sr^{2+}-free condition, even when Lck activity was already saturated

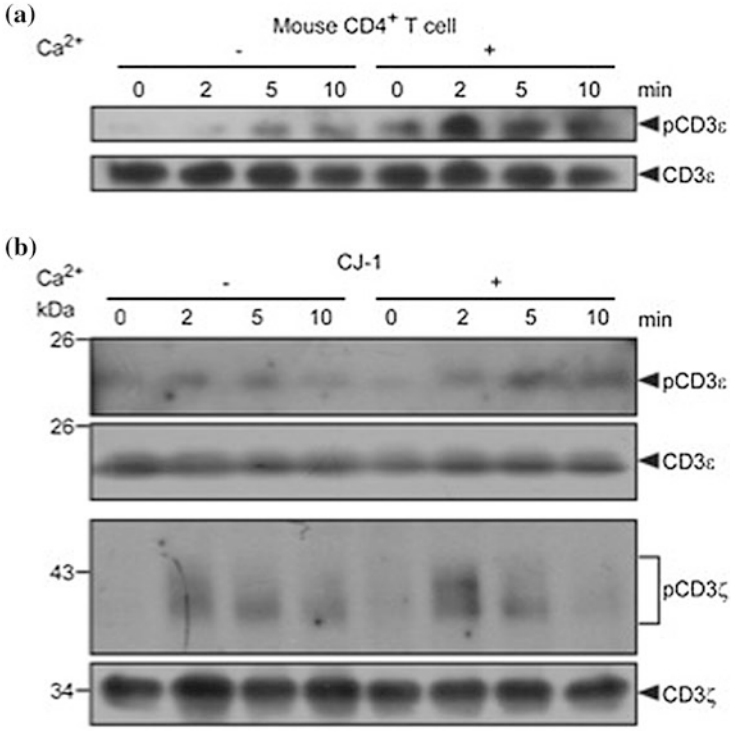

Fig. 3.14 Ca^{2+} facilitated TCR phosphorylation. **a** Mouse primary $CD4^+$ T cells were stimulated by TCR crosslinking (0.5 μg/ml 145-2C11 plus 1 μg/ml α-hamster IgG) for the indicated time at 37 °C. CD3ε was immunoprecipiated and immnoblotted by α-pY100. The membrane was then stripped and re-blotted by α-CD3ε (M20) for the detection of total CD3ε. CD3ε phosphorylation was stronger when 1 mM Ca^{2+} was present in the triggering buffer. **b** CRAC channel-deficient Jurkat mutant CJ-1 cells was stimulated by TCR crosslinking (0.2 μg/ml α-CD3 (UCHT1) plus 0.2 μg/ml α-mouse IgG) for the indicated time at 37 °C. The stimulation buffer was Mg^{2+}-free Ringer's buffer with or without 1 mM Ca^{2+}. The effect of Ca^{2+} on facilitating TCR phosphorylation in CJ-1 cells was only modest. This modest effect should be induced by the low-level Ca^{2+} influx through the residually expressed CRAC channel

basic residues in $CD3\varepsilon_{CD}$ bound to the same lipid phosphate region (Fig. 3.17c). The Ca^{2+}-lipid phosphate binding was further confirmed by a Fourier Transform Infrared experiment (Fig. 3.18d). We then tested the effect of Ca^{2+} at low micromolar level to mimic the physiological Ca^{2+} concentration in activated T cells [14]. An unambiguous perturbation effect on the ^{31}P signal was observed even at l μM Ca^{2+}, indicating that the binding of Ca^{2+} and the lipid phosphate group is

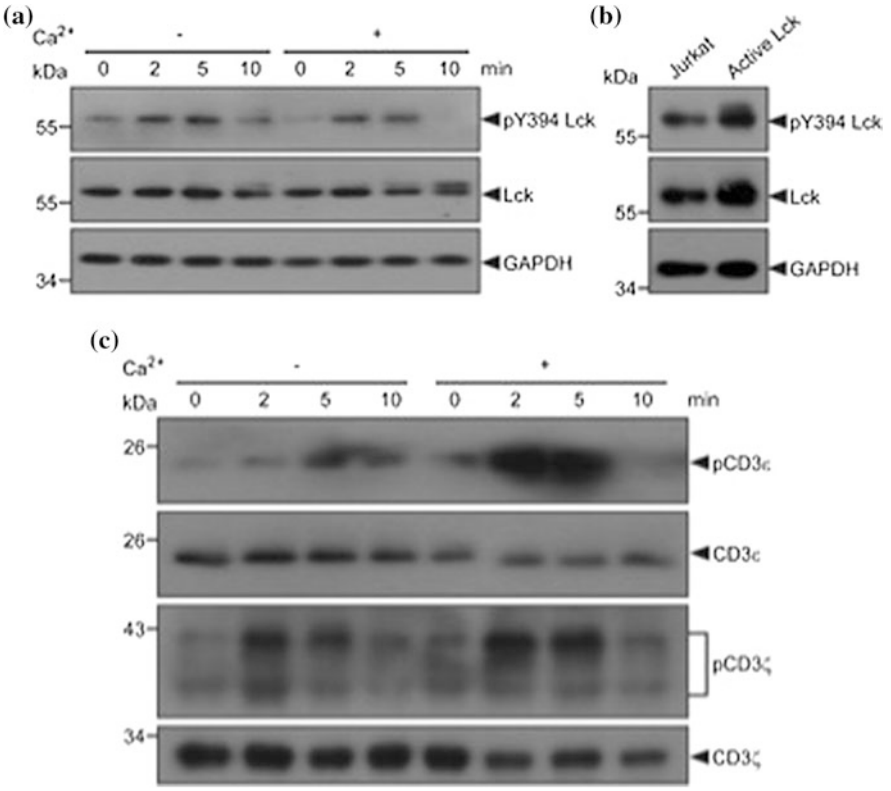

Fig. 3.15 Ca^{2+} facilitated TCR phosphorylation not by increasing Lck activity. TCR is primarily phosphorylated by Lck in T cells [13, 33]. If there would be other Ca^{2+}-dependent signalling pathways in T cells that lead to increased TCR phoshporylation, most likely they should exert this effect by enhancing Lck activity. **a** Jurkat T cells were stimulated with the same condition used for Fig. 3.13b. The amount of active Lck (pY394 Lck) in T cells triggered in Ca^{2+} (1 mM) containing buffer was not more than that in T cells triggered in the absence of Ca^{2+}. **b** A stable Jurkat cell line overexpressing active Lck (mutation of the inhibitory Tyr505 to Phe) was generated. The amount of active Lck (pY394 Lck) in the Lck overexpression cell line is much more than that in Jurkat wild-type cells. **c** The effect of Ca^{2+} on facilitating CD3ε/ζ phosphorylation was profound even when Lck actitivty was saturated. Jurkat T cells were stimulated with the same condition used for Fig. 3.13c

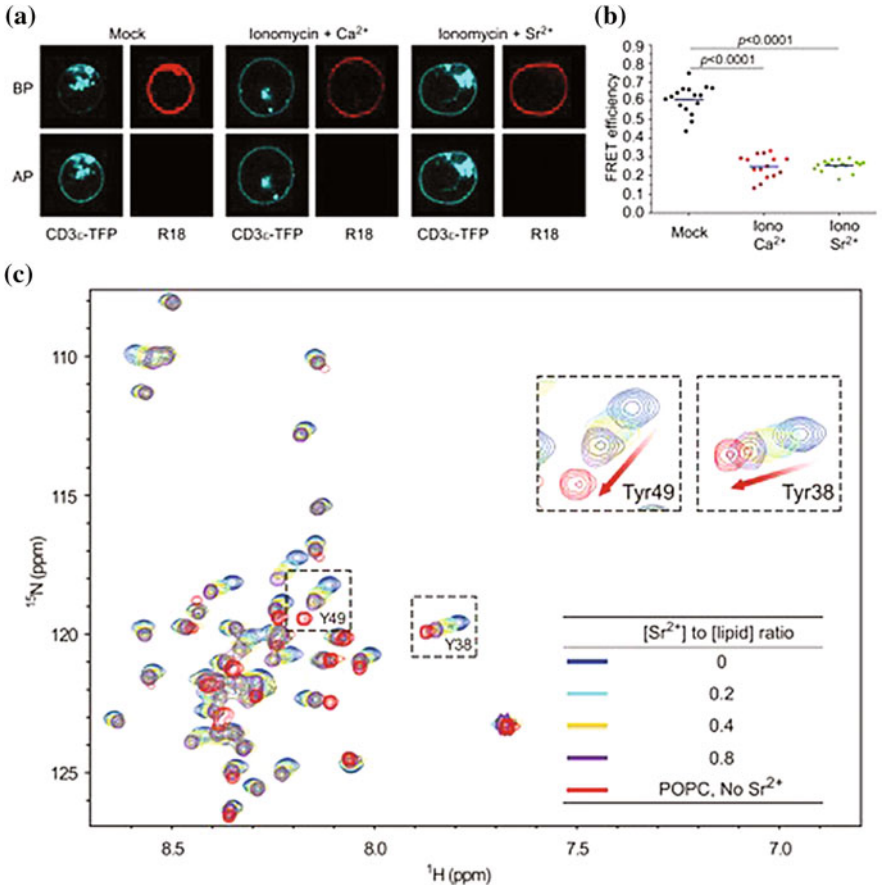

Fig. 3.16 Sr^{2+} induced the dissociation of $CD3\varepsilon_{CD}$ from the membrane. Sr^{2+}, an element from the same group of Ca^{2+} in the periodic table, shares the same charge property as Ca^{2+} and is also permeable through CRAC channel. There is no known physiological function of Sr^{2+} in T cell signalling. **a** Our FRET measurement demonstrated that Sr^{2+} influx induced by the ionomycin treatment caused the dissociation of $CD3\varepsilon_{CD}$ from the plasma membrane, which is similar to the effect caused by Ca^{2+} influx. The FRET experiments were done with either 5 mM Sr^{2+} or 2 mM Ca^{2+} in the Mg^{2+}-free Ringer's buffer and 5 μM ionomycin was applied to induce Sr^{2+} or Ca^{2+} influx in T cells. **b** The FRET efficiencies were measured for more than 15 cells per condition. Each dot represents the FRET efficiency from one individual cell. **c** As measured by a ^{15}N–^{1}H experiment, Sr^{2+} disrupted the $CD3\varepsilon_{CD}$-membrane interaction and induced the solvent exposure of $CD3\varepsilon_{CD}$. HSQC spectra were collected with the samples containing 0.05 mM ^{15}N-labelled $CD3\varepsilon_{CD}$, 7.5 mM POPG or POPC bicelles (q = 0.8),10 mM DHPC and 0 to 6 mM Sr^{2+} in 20 mM Tris-HCl buffer, pH 7.0

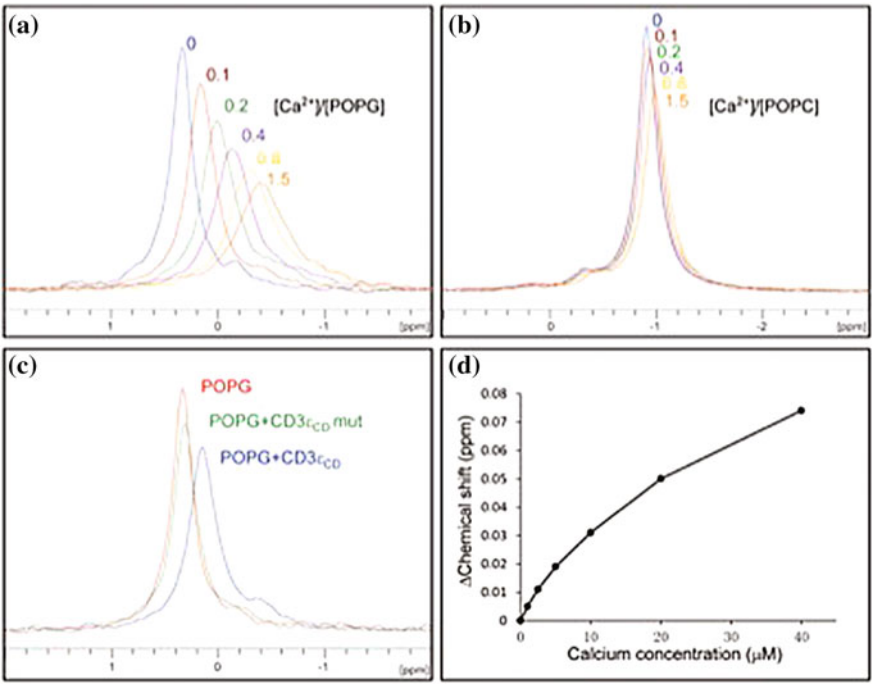

Fig. 3.17 Ca^{2+} bound to the phosphate group of anionic phospholipid at a physiological concentration. One-dimensional ^{31}P NMR experiments were performed to probe the local chemical environment change of the phospholipid phosphate group induced by the binding of Ca^{2+} or $CD3\varepsilon_{CD}$ peptide. A lipid nanodisc system was used to provide a membrane bilayer environment without the interference of detergent molecules. The sample buffer was 20 mM Tris-HCl, pH 7.0, containing 100 mM NaCl. **a**, **b** Ca^{2+} induced a substantial chemical shift change of the phosphorus signal of the anionic POPG (**a**), but not that of the zwitterionic POPC (**b**). **c** The $CD3\varepsilon_{CD}$ peptide induced a shift in the same direction for the POPG phosphorus signal as Ca^{2+} did, implying that both Ca^{2+} and basic residues in $CD3\varepsilon_{CD}$ bound to the same region in the phospholipid headgroup via ionic interactions. Mutation of the first 3 basic residues to Ala in $CD3\varepsilon_{CD}$ ($CD3\varepsilon_{CD}$ mutant) nearly eliminated $CD3\varepsilon_{CD}$'s perturbation effect to the lipid phosphorus signal. **d** The effect of Ca^{2+} in perturbing the ^{31}P signal was tested at physiological Ca^{2+} concentrations. Even 1 μM Ca^{2+} can induce unambiguous chemical shift changes of the POPG phosphorus signal. The POPG concentration used in panel a and c was 4 mM; in panel d the concentration was 0.8 mM. The POPC concentration used in panel b was 5 mM. The $CD3\varepsilon_{CD}$ concentration used in panel c was 0.08 mM

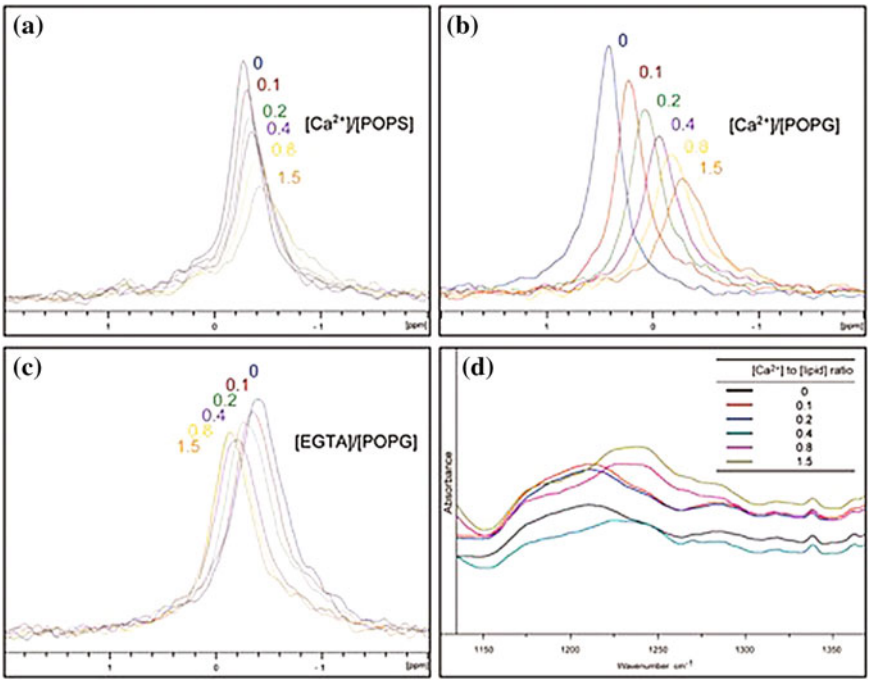

Fig. 3.18 Ca^{2+} reversibly perturbed the phosphorus signal of the anionic phospholipid. **a** As measured by ^{31}P NMR spectroscopy, Ca^{2+} induced the chemical shift change of the phosphorus signal of POPS, to the same direction as it did for POPG. POPS concentration was used at 2.5 mM and Ca^{2+} was titrated in at a molar ratio to POPS from 0.1 to 1.5. **b** The ^{31}P spectrum experiment of Fig. 3.17a was repeated with 150 mM NaCl present in the sample buffer and the perturbation effect of Ca^{2+} was still substantial. **c** The perturbation effect of Ca^{2+} on POPG phosphorus signal was reversed by the addition of the Ca^{2+} chelator EGTA. POPG concentration was used at 4 mM and Ca^{2+} was 6 mM. EGTA was titrated in at a molar ratio to POPG from 0.1 to 1.5. **d** Fourier Transform Infrared (FTIR) spectroscopy was used to confirm Ca^{2+}-lipid phosphate binding. POPG nanodisc samples with various $CaCl_2$ concentrations were overspread on the BaF_2 substrates and air dried at room temperature. FTIR measurements were performed at room temperature on an FTIR spectrometer (BRUKER ALPHA-T) and the software OPUS 6.5 (Bruker Optics GmbH, Ettlingen, Germany) was used to process the data. The sample buffer was 20 mM Tris-HCl, pH 7.0, 100 mM NaCl. With the Ca^{2+}/POPG ratio above 0.4, the PO_2 asymmetric vibration band of POPG, which was centered around 1222 cm^{-1}, shifted towards higher wavenumbers. This shift was caused by a dehydration effect from Ca^{2+} and indicated an ionic interaction between Ca^{2+} and the phosphate group (The FTIR experiment has been shown as Fig. 2.7)

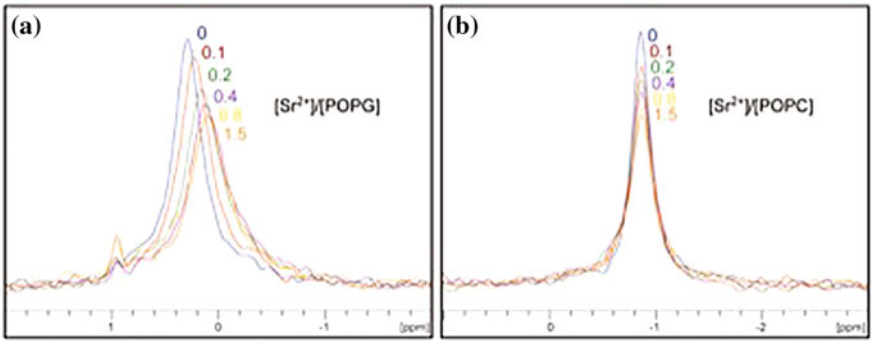

Fig. 3.19 Sr^{2+} perturbed the phosphorus signal of the anionic phospholipid. **a**, **b** Same as Ca^{2+}, Sr^{2+} also caused a substantial perturbation of the phosphorus signal of POPG (**a**) but not that of POPC (**b**). The experiment was done with 4 mM POPG or POPC nanodisc in 20 mM Tris-HCl buffer, pH 7.0

physiologically relevant (Fig. 3.17d). This binding thus explains a mechanism responsible for the role of Ca^{2+} in disrupting the ionic $CD3_{CD}$-membrane interaction and facilitating CD3 phosphorylation. As expected, Sr^{2+} can also specifically perturb the ^{31}P signal of anionic lipids (Fig. 3.19).

This study unveils a new function of Ca^{2+} for feedback regulating initial antigen-stimulated TCR signalling (Fig. 3.20). This feedback loop will not cycle infinitely because the local Ca^{2+} concentration is precisely controlled by the plasma membrane Ca^{2+} ATPase pumps, mitochondria and other ion channels [14, 29]. Moreover, TCRs become internalised and degraded when they move to the central immunological synapse [30]. The Ca^{2+}-mediated signal amplification process helps explain the unique nature of the T cell's hypersensitivity to even a single antigen molecule [18, 19]. Ca^{2+} should also help sustain TCR signalling because the elevation of $[Ca^{2+}]$ persists several hours in synapsed T cells [14, 31]. We believe that the lipid manipulation function of Ca^{2+} could also be applied to understand other biological processes involving protein-lipid interactions [32].

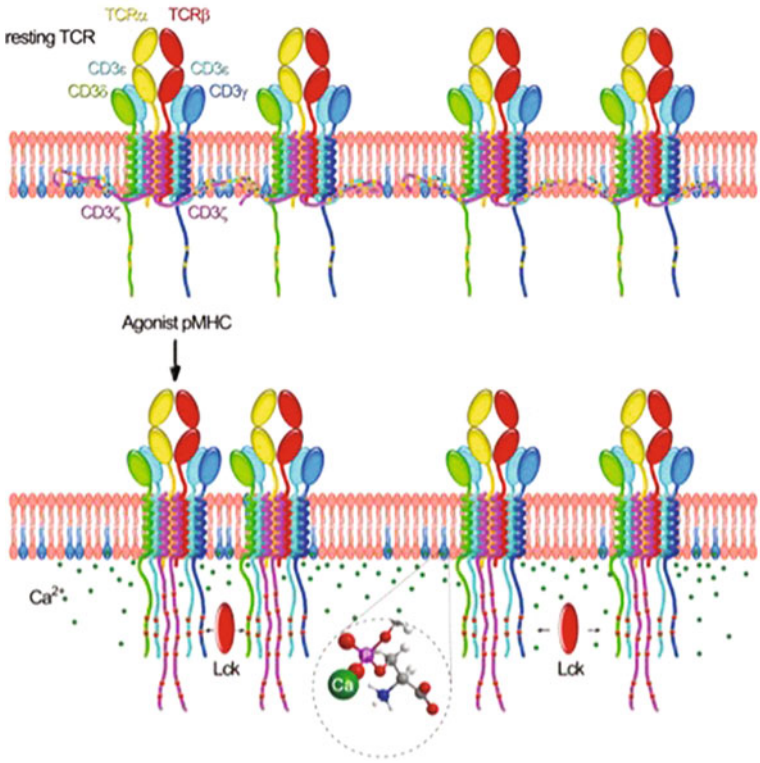

Fig. 3.20 A schematic illustration of the Ca^{2+}-induced TCR signalling amplification model. In the resting state, the positively charged cytoplasmic tails of CD3ε and CD3ζ interact with anionic phospholipids in the inner-leaflet of the plasma membrane and key tyrosine residues are sequestered in the membrane bilayer, which provides a 'safety' control on TCR triggering [1, 10–12]. There is a longstanding debate about the mechanism by which the initial ligand binding on TCR αβ extracellular domain induces the phosphorylation of intracellular ITAM tyrosines. Conformational change, receptor clustering and segregation/redistribution models have been proposed by different groups and each of them is supported by certain level of experimental evidences, implying that the initial TCR triggering should be controlled by a multi-layered mechanism [17, 34, 35]. Determining TCR-CD3 complex structures before and after ligand binding will be required to fully understand this mechanism. However, it is still a big technical challenge to assemble this multi-subunit transmembrane protein complex *in vitro* for structural study. In contrast to the yet controversial initial TCR triggering mechanism, it has been well studied that Ca^{2+} influx starts within a few seconds after the initial TCR triggering [23] and the influx persists several hours in synapsed T cells [32]. Membrane proximal Ca^{2+} ions can then bind to the phosphate group in anionic phospholipids and neutralize their negative charges, which results in the dissociation of CD3ε/ζ cytoplasmic domains from the membrane and increases the accessibility of ITAM for Lck. Ca^{2+} can thus facilitate the phosphorylation of TCR, especially those contacting with low-affinity self antigens or even bystander TCRs, and amplify the initial antigen-stimulated signal to a much greater magnitude. This Ca^{2+}-induced TCR signalling amplification model helps explain the unique nature of T cell's hypersensitivity to even a single antigen [35]. Moreover, the persistent high Ca^{2+} concentration in synapsed T cells can help sustain TCR signalling at a certain level, which is required for full effector potential of T cells [32].

References

1. Xu C et al (2008) Regulation of T cell receptor activation by dynamic membrane binding of the CD3epsilon cytoplasmic tyrosine-based motif. Cell 135(4):702–713
2. Paddock C et al (2011) Residues within a lipid-associated segment of the PECAM-1 cytoplasmic domain are susceptible to inducible, sequential phosphorylation. Blood 117 (22):6012–6023
3. Hansen SB, Tao X, MacKinnon R (2011) Structural basis of PIP2 activation of the classical inward rectifier K + channel Kir2.2. Nat 477(7365):495–498
4. Whorton MR, MacKinnon R (2011) Crystal structure of the mammalian GIRK2 K + channel and gating regulation by G proteins, PIP2, and sodium. Cell 147(1):199–208
5. Kim C et al (2011) Basic amino-acid side chains regulate transmembrane integrin signalling. Nat 481(7380):209–213
6. van den Bogaart G et al (2011) Membrane protein sequestering by ionic protein-lipid interactions. Nat 479(7374):552–555
7. Heo WD et al (2006) PI(3,4,5)P3 and PI(4,5)P2 lipids target proteins with polybasic clusters to the plasma membrane. Sci 314(5804):1458–1461
8. Gerlach H et al (2010) HIV-1 Nef membrane association depends on charge, curvature, composition and sequence. Nat Chem Biol 6(1):46–53
9. Smith-Garvin JE, Koretzky GA, Jordan MS (2009) T cell activation. Annu Rev Immunol 27:591–619
10. Kuhns MS, Davis MM (2008) The safety on the TCR trigger. Cell 135(4):594–596
11. DeFord-Watts LM et al (2011) The CD3 zeta subunit contains a phosphoinositide-binding motif that is required for the stable accumulation of TCR-CD3 complex at the immunological synapse. J Immunol 186(12):6839–6847
12. Aivazian D, Stern LJ (2000) Phosphorylation of T cell receptor zeta is regulated by a lipid dependent folding transition. Nat Struct Biol 7(11):1023–1026
13. Palacios EH, Weiss A (2004) Function of the Src-family kinases, Lck and Fyn, in T-cell development and activation. Oncog 23(48):7990–8000
14. Hogan PG, Lewis RS, Rao A (2010) Molecular basis of calcium signaling in lymphocytes: STIM and ORAI. Annu Rev Immunol 28:491–533
15. Weiss A, Littman DR (1994) Signal transduction by lymphocyte antigen receptors. Cell 76 (2):263–274
16. Ma G et al (2015) Inside-out Ca(2+) signalling prompted by STIM1 conformational switch. Nat Commun 6:7826
17. van der Merwe PA, Dushek O (2011) Mechanisms for T cell receptor triggering. Nat Rev Immunol 11(1):47–55
18. Irvine DJ et al (2002) Direct observation of ligand recognition by T cells. Nat 419(6909): 845–849
19. Purbhoo MA et al (2004) T cell killing does not require the formation of a stable mature immunological synapse. Nat Immunol 5(5):524–530
20. Sigalov AB et al (2006) Lipid-binding activity of intrinsically unstructured cytoplasmic domains of multichain immune recognition receptor signaling subunits. Biochem 45 (51):15731–15739
21. Leventis PA, Grinstein S (2010) The distribution and function of phosphatidylserine in cellular membranes. Annu Rev Biophys 39:407–427
22. Nika K et al (2010) Constitutively active Lck kinase in T cells drives antigen receptor signal transduction. Immun 32(6):766–777
23. Huse M et al (2007) Spatial and temporal dynamics of T cell receptor signaling with a photoactivatable agonist. Immun 27(1):76–88
24. Denisov IG et al (2004) Directed self-assembly of monodisperse phospholipid bilayer Nanodiscs with controlled size. J Am Chem Soc 126(11):3477–3487

25. Delaglio F et al (1995) NMRPipe: a multidimensional spectral processing system based on UNIX pipes. J Biomol NMR 6(3):277–293
26. Fanger CM et al (1995) Characterization of T cell mutants with defects in capacitative calcium entry: genetic evidence for the physiological roles of CRAC channels. J Cell Biol 131 (3):655–667
27. Park CY, Shcheglovitov A, Dolmetsch R (2010) The CRAC channel activator STIM1 binds and inhibits L-type voltage-gated calcium channels. Sci 330(6000):101–105
28. Yeromin AV et al (2006) Molecular identification of the CRAC channel by altered ion selectivity in a mutant of Orai. Nat 443(7108):226–229
29. Quintana A et al (2011) Calcium microdomains at the immunological synapse: how ORAI channels, mitochondria and calcium pumps generate local calcium signals for efficient T-cell activation. EMBO J 30(19):3895–3912
30. Varma R et al (2006) T cell receptor-proximal signals are sustained in peripheral microclusters and terminated in the central supramolecular activation cluster. Immun 25(1):117–127
31. Huppa JB et al (2003) Continuous T cell receptor signaling required for synapse maintenance and full effector potential. Nat Immunol 4(8):749–755
32. Zilly FE et al (2011) Ca2+ induces clustering of membrane proteins in the plasma membrane via electrostatic interactions. EMBO J 30(7):1209–1220
33. van Oers NS, Killeen N, Weiss A (1996) Lck regulates the tyrosine phosphorylation of the T cell receptor subunits and ZAP-70 in murine thymocytes. J Exp Med 183(3):1053–1062
34. Kuhns MS, Davis MM, Garcia KC (2006) Deconstructing the form and function of the TCR/CD3 complex. Immun 24(2):133–139
35. Davis MM et al (2007) T cells as a self-referential, sensory organ. Annu Rev Immunol 25:681–695

Chapter 4
Study on the Structure of Dengue Virus NS2B–NS3p in Complex with Aprotinin

Abstract Dengue virus, a member of Flaviviridae, is one of the most prevalent Mosquito-borne viruses in tropical and subtropical regions of the world. It causes a range of clinical diseases, such as dengue fever, dengue hemorrhagic fever (DHF) and dengue shock syndrome (DSS) [1]. Lack of approved vaccine or effective antiviral therapy for these diseases puts millions of lives at risk. Like other flaviviruses, the genome of dengue virus contains a positive single-stranded 11-kilobases RNA, which encodes three structural proteins (capsid protein C, membrane protein M, and envelope protein E) and seven non-structural proteins (NS1, NS2A, NS2B, NS3, NS4A, NS4B, and NS5) [2]. The N-terminus of NS3 (NS3p) functions as a serine protease, whose catalytic activity requires NS2B. A combination of NS2B–NS3p and the host proteases, cleaves the viral polyprotein into individual mature proteins. Therefore it is essential for viral replication [3]. Aprotinin, a classic inhibitor for trypsin and related proteolytic enzymes, was reported to inhibit the activity of NS2B–NS3p protease at submicromolar concentration [4]. In this chapter, the backbone 1H, ^{15}N, ^{13}C resonance assignments of the N terminal fragment of NS2B (4.8 kDa) and NS3p (18.5 kDa) in complex with aprotinin (6.5 kDa) is reported, which provides a requisite step for determining the solution structure of the complex. It is also important for screening and developing new antiviral drugs by structure-based designing strategies.

4.1 Experiment Methods

4.1.1 Clone, Expression and Purification of NS2B–NS3p

An NS2B–NS3p gene, comprising the 47-amino acids co-factor domain of NS2B connected to NS3p via a GGGGSGGGG flexible linker, was constructed and then cloned into the protein expression vector pET15b(Novagen). The recombinant plasmid was transformed into *E. coli* BL21 (DE3) strain (Invitrogen) for protein

© Springer-Verlag GmbH Germany 2018

Y. Bi, *Study of the Calcium Regulation Mechanism of TCR Activation Using Nanodisc and NMR Technologies*, Springer Theses,
DOI 10.1007/978-3-662-54618-5_4

expression. The *E. coli* cells were cultured overnight in 5 mL of Luria–Bertani (LB) broth medium containing 100 μg/mL of Ampicillin at 37 °C. The cells were centrifuged and transferred into $^{2}H/^{13}C/^{15}N$-labeled M9 medium. The protein expression was induced by adding isopropyl-b-D-thiogalactoside (IPTG) at a final concentration of 0.5 mM when OD_{600} reached 0.8. The cells were cultured at 20 °C for 36 h and then harvested by centrifugation. The protein was purified by Ni-Sepharose affinity chromatography and the His tag was removed by thrombin digestion overnight at 4 °C. Subsequently, the anion-exchange chromatography (Mono Q) and gel filtration (Superdex-75) by an AKTA FPLC system (Amersham Biosciences) were taken for further purification. The unlabeled aprotinin was purchased from Sigma.

4.1.2 NMR Sample Preparation

The NMR sample of NS2B–NS3p/aprotinin complex was prepared in a buffer containing 20 mM Na_2HPO_4/NaH_2PO_4, 100 mM NaCl in 90% H_2O/10% D_2O (pH 7.0). The protein concentration was about 0.65 mM. Aprotinin was added to the triple-labeled NS2B–NS3p solution at the molar ratio of 2:1. The original NS2B–NS3p/aprotinin complex degraded over time, and a protein complex (30 kDa) containing the N terminal fragment of NS2B (4.8 kDa), NS3p (18.5 kDa) and aprotinin (6.5 kDa) was identified. The sample was incubated at 30 °C for 4 days and further purified with size exclusion chromatography to obtain the stable complex.

4.1.3 NMR Spectra Collection and Data Processing

The NMR spectra were acquired at 30 °C on Bruker Avance 850 MHz (with a cryoprobe), equipped with four RF channels and a triple-resonance probe with pulsed field gradients. The TROSY [5] versions of the three-dimensional (3D) HNCA, HNCACB, HN(CO)CA, HNCO, HN(CA)CO experiments were carried out for the backbone assignments [6, 7]. The ^{1}H chemical shifts were referenced to internal 2,2-dimethyl-2-silapentanesulfonic acid (DSS), and ^{13}C and ^{15}N chemical shifts were referenced indirectly [8]. All spectra were processed using the software package NMR-Pipe [9] and analyzed by the program Sparky (Goddard and Kneller, 2006, SPARKY3, University of California, San Francisco, CA).

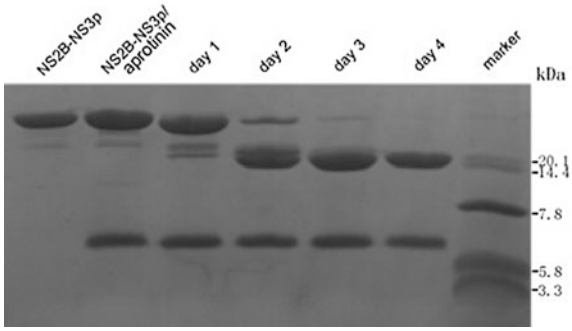

Fig. 4.1 The time course of NS2B–NS3p/aprotinin complex degradation. The NS2B–NS3p/aprotinin complex degradation was shown by the 16% Tricine SDS-PAGE. The first two lanes are the control samples. The left four lanes are the samples incubated with one to four days, which shows that NS2B–NS3p/aprotinin complex becomes stable after four days degradation

4.2 Experiment Results

A series of 2D ^{1}H–^{15}N HSQC spectra show that NS2B–NS3p/aprotinin complex experiences degradation, but becomes stable after 4 days, which is consistent with the SDS-PAGE experiment result (Fig. 4.1). Size exclusion chromatography (Fig. 4.2) and mass spectrum data identified a stable protein complex (30 kDa) containing the N terminal fragment of NS2B (1–45, 4.8 kDa), NS3p (77–247, 18.5 kDa) and aprotinin (6.5 kDa). The preserved residues from NS2B–NS3p/aprotinin complex show the almost identical resonances to those of the full

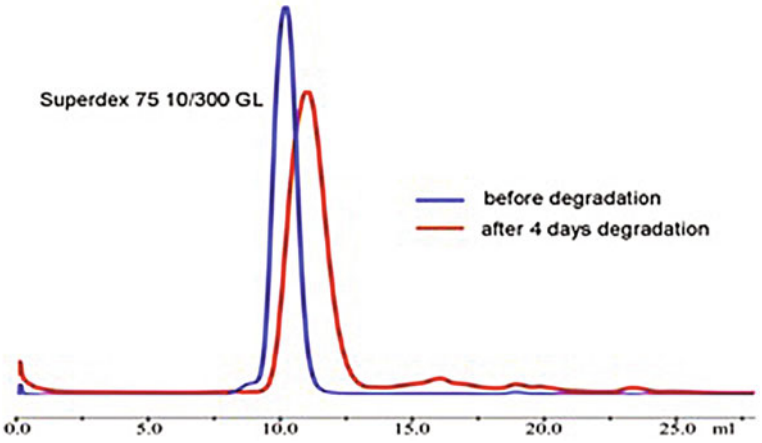

Fig. 4.2 Size exclusion chromatography of NS2B–NS3p/aprotinin complex. Size exclusion chromatography shows an obvious shift after four days degradation

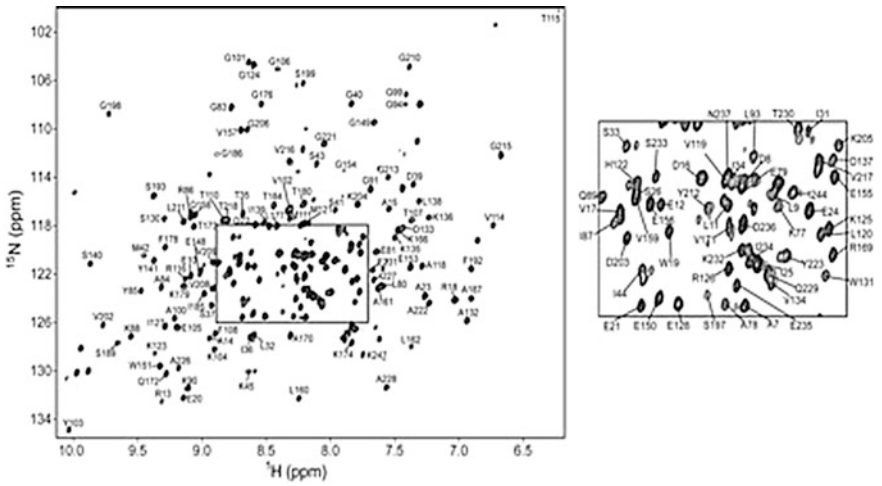

Fig. 4.3 The 2D TROSY HSQC spectrum of dengue virus NS2B–NS3p in complex with aprotinin (*left* panel) and an expanded portion (*right* panel) of the most congested region. The spectrum was collected on a Bruker Avance 850 MHz spectrometer (with a cryoprobe) at 30 °C. The assignments are annotated with the one-letter amino acid code and the sequence number

length complex before degradation. The 2D TROSY ^{1}H–^{15}N HSQC spectrum of NS2B–NS3p/aprotinin complex is shown in Fig. 4.3. Except for 8 proline residues, we observed 187 resonances out of the remaining 208 NS2B–NS3p residues (1–45, 77–247). The triple resonance NMR experiments led to an assignment of 91% (170 residues) of the observed signals. Among them, CO, Cα and Cb chemical shifts have been determined for all residues except for K77, E148 and F245, which have Cα and Cβ but not CO assignments. Furthermore, CO, Cα and Cβ chemical shifts have been determined for 3 of the 8 prolines. For the remaining amino acids with unassigned and/or missing NH resonances, CO, Cα and Cβ chemical shifts were determined for E6, E38, Q97, H113, K152, G165, G183, D191, T196, S220 and D243, and only Cα and Cβ chemical shifts were assigned for I92, P129 and L147, by correlating them with the NH groups of the respective amino acids in the N+1 position. In summary, we were able to assign 88, 88, and 83% of all Cα, Cβ and CO chemical shifts, respectively. The absent resonances are mainly from residues within the flexible loops. The computer program TALOS [10] shows that the structure of complex is mainly composed of β-strands, as shown in Fig. 4.4. The assigned backbone ^{1}H, ^{15}N and ^{13}C chemical shifts of NS2B–NS3p/aprotinin complex have been deposited in the BioMagResBank (http://www.bmrb.wisc.edu/) under the accession number 18266.

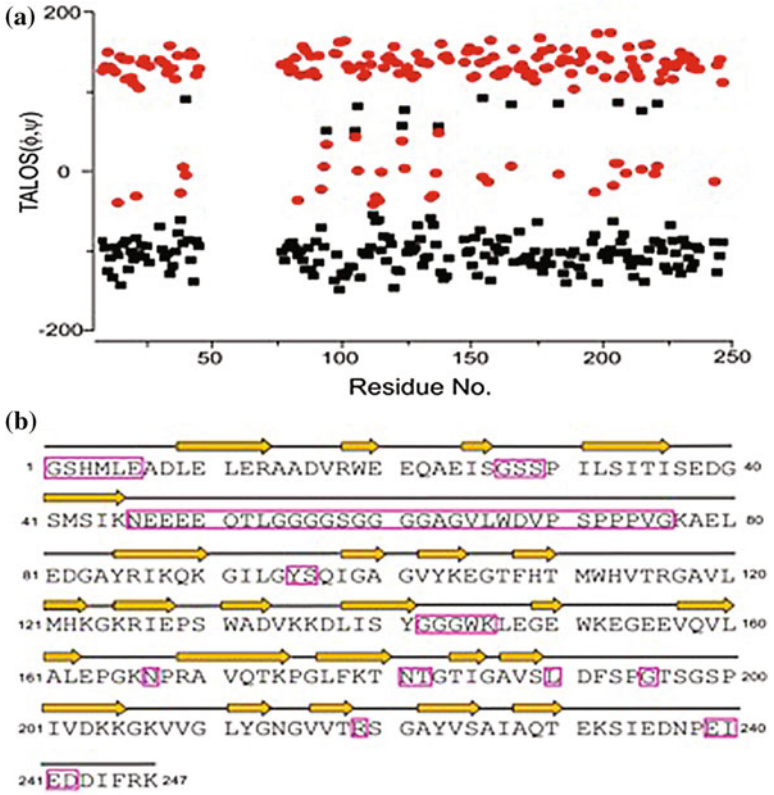

Fig. 4.4 TALOS plot of dengue virus NS2B–NS3p in complex with aprotinin. **a** Backbone dihedral angles (phi, psi) were calculated using TALOS [10]. Phi (u) and psi (w) angles are shown in *black* and *red*, respectively. **b** Predicted secondary structure elements are indicated using arrows for β-strands. The stable NS2B–NS3p/aprotinin complex contains an N terminal fragment of NS2B (1–45, 4.8 kDa), NS3p (77–247, 18.5 kDa) and aprotinin (6.5 kDa). The residues are not included in TALOS prediction are labeled in boxes (color figure online)

References

1. Jacobs MG, Young PR (1998) Dengue: a continuing challenge for molecular biology. Curr Opin Infect Dis 11(3):319–324
2. Chambers TJ et al (1990) Flavivirus genome organization, expression, and replication. Annu Rev Microbiol 44:649–688
3. Falgout B et al (1991) Both nonstructural proteins NS2B and NS3 are required for the proteolytic processing of dengue virus nonstructural proteins. J Virol 65(5):2467–2475
4. Leung D et al (2001) Activity of recombinant dengue 2 virus NS3 protease in the presence of a truncated NS2B co-factor, small peptide substrates, and inhibitors. J Biol Chem 276 (49):45762–45771

5. Pervushin K et al (1997) Attenuated T2 relaxation by mutual cancellation of dipole-dipole coupling and chemical shift anisotropy indicates an avenue to NMR structures of very large biological macromolecules in solution. Proc Natl Acad Sci U S A 94(23):12366–12371
6. Salzmann M et al (1998) TROSY in triple-resonance experiments: new perspectives for sequential NMR assignment of large proteins. Proc Natl Acad Sci U S A 95(23):13585–13590
7. Eletsky A, Kienhofer A, Pervushin K (2001) TROSY NMR with partially deuterated proteins. J Biomol NMR 20(2):177–180
8. Markley JL et al (1998) Recommendations for the presentation of NMR structures of proteins and nucleic acids–IUPAC-IUBMB-IUPAB Inter-Union Task Group on the standardization of data bases of protein and nucleic acid structures determined by NMR spectroscopy. Eur J Biochem 256(1):1–15
9. Delaglio F et al (1995) NMRPipe: a multidimensional spectral processing system based on UNIX pipes. J Biomol NMR 6(3):277–293
10. Cornilescu G, Delaglio F, Bax A (1999) Protein backbone angle restraints from searching a database for chemical shift and sequence homology. J Biomol NMR 13(3):289–302

Conclusion and Future Work

Conclusion

Membrane binding protein is an importance protein, accounting for a significant proportion of the total amount protein in vivo. It associates and dissociates to the phospholipid component of the membrane dynamically and therefore can participate in cell signaling regulation. Previous studies show that electrostatic forces and the hydrophobic effect mainly contribute to interactions between the phospholipid and membrane binding protein. Unfortunately, little has been done to study the regulatory mechanisms among them and how this relates to transmembrane cell signal transduction. This thesis discusses these topics, using the calcium modulated T cell receptor(TCR) activity as a model system.

(1) Ca^{2+} regulates T-Cell receptor activation by modulating the charge property of lipids.In resting T cells, the CD3ε cytoplasmic domains ($CD3\varepsilon_{CD}$) bind at the cytoplasmic face of the plasma membrane, and their ITAM tyrosines are inserted into the hydrophobic core of the plasma membrane to prevent phosphorylation. Immediately after the initial TCR triggering, Ca^{2+} locally influxes into T cells and co-localizes with the TCR. The divalent cation Ca^{2+} can directly alter the local electrostatic environment and interfere with the ionic $CD3\varepsilon_{CD}$-membrane interaction to effect the dissociation of the ITAM from the membrane. The solvent-exposed ITAM tyrosines would then be accessible for phosphorylation by Lck, resulting in downstream signal transduction that increases calcium infux. Ca^{2+} thus has a positive feedback effect on amplifying and sustaining CD3 phosphorylation, which in turn amplifies the initial antigen-stimulated signal to a greater magnitude. This may explain the unique nature of the hypersensitivity of T cells to a single antigen molecule. The regulatory mechanism by ionic protein-lipid interaction exists not only in TCR and other immune receptors, but also occurs in other cell signaling pathways [1, 2].

(2) The molecular mechanism of the lipid molecule-ion interaction is further studied. Electrostatic forces and coordinate bonds may contribute to the interactions between ions and phosphates of the hydrophilic headgroups of the phospholipid molecules. The interaction pattern and binding affinity varies

© Springer-Verlag GmbH Germany 2018

Y. Bi, *Study of the Calcium Regulation Mechanism of TCR Activation Using Nanodisc and NMR Technologies*, Springer Theses,
DOI 10.1007/978-3-662-54618-5

with the type of ions and phospholipid. The ions could also affect the phase behavior of the phospholipid and may further influence the conformation and function of the embedded membrane proteins.

(3) The newly designed membrane mimic Nanodisc is introduced in this thesis. Compared to other systems, such as micelles and bicelles, Nanodisc is the closest to recapitulating the native membrane environment because it is completely devoid of detergent. This thesis also optimized the Nanodisc assembly. The small Nanodisc and mixed lipid component, as well as using Urea and DHPC instead of cholate, demonstrate how the Nanodisc application can be broadened to include membrane protein study by solution NMR.

(4) The preliminary structure study of NS2B-NS3p/aprotinin complex from type 2 Dengue virus is also covered by this thesis. Using the computer program TALOS and the backbone chemical shift assignments, the structure of complex is shown to be mainly composed of β-strands.

Future Work

(1) This thesis reveals how calcium can amplify the activation TCR by changing the local electrostatic environment. However, there may be other factors that could also contribute to the calcium-mediated regulation of TCR activation. The scientists have found evidence suggesting that the high concentration calcium could activate the lipid flippases on the plasma membrane, which transport PS from the inner leaflet to the outer leaflet and thus reduce the negative charge of the inner leaflet of lipid bilayer [3, 4]. This may also cause CD3ε_{CD} to dissociate from the membrane. However, compared to our model this seems kinetically unfavorable. Additionally, TCR will aggregate after recognizing antigen, which may cause steric hindrance and ITAM competing with negatively charged phospholipids. The presence of certain ions could also reduce the fluidity of the phospholipid and further influence the conformation and function of the embedded protein. We will focus on how these factors cooperate to orchestrate the activation of TCR.

(2) The initiating events of TCR activation are also unknown. How the first antigen activates the TCR is an important and interesting question and we would like to pursue this further.

(3) The long distance constraint is useful in NMR studies of protein-lipid interactions because it supplies information on the changes in protein conformation. In this work, we introduced three paramagnetic spin labels into the study of CD3ε_{CD}-phospholipid interaction to reveal the membrane-embedded situation of residues. 16-DOXYL-stearic acid (16-DSA) and 5-DOXYL-stearic acid (5-DSA) are the spin labels that insert into the hydrophobic region of lipid bilayer, while 1,4,7,10-tetraazacyclododecane-1,4,7,10-tetraacetic acid (DOTA) is a lanthanide chelator that is unable to access the hydrophobic region. Figure A.1 shows that the residues near no. 50 are deeply embedded into the

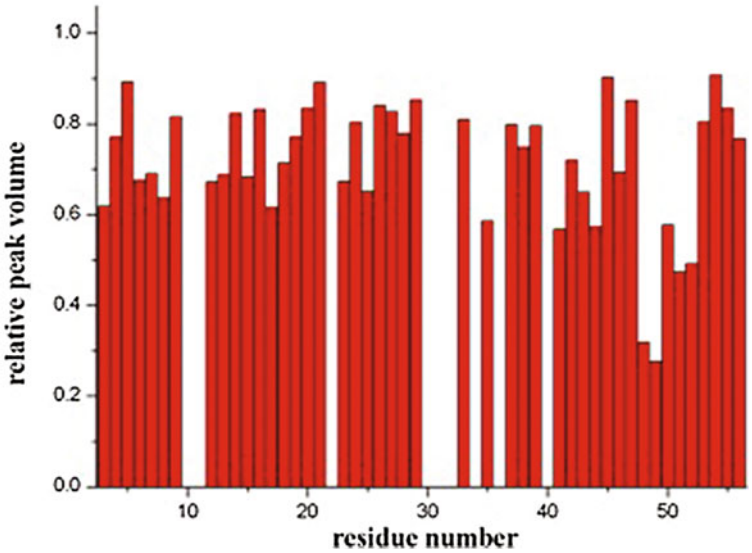

Fig. A.1 16-DSA affect the signal intensity of CD3ε_{CD} membrane binding state. The ratio of CD3ε_{CD} signal intensity before and after 16-DSA addition. 16-DSA could insert into the lipid bilayer deeply and cause a drop in the signal intensity of membrane-embedded residues. The uncalculated residues are due to prolines or uncertainty calculating the signal intensity

lipid bilayer, which is consistent with previous work [5]. This technique should be employed in other studies to detect the membrane-protein interaction because it is a rapid means of studying the membrane embedded situation of a protein at the residue level. We would like to combine information from all three spin labels to study the early dynamic process of CD3ε_{CD} dissociation from the membrane.

References

1. Wang Y et al (2014) Regulation of EGFR nanocluster formation by ionic protein-lipid interaction. Cell Res 24(8):959–976
2. Chen X et al (2015) Acidic phospholipids govern the enhanced activation of IgG-B cell receptor. Nat Commun 6:8552
3. Fischer K et al (2006) Antigen recognition induces phosphatidylserine exposure on the cell surface of human CD8+ T cells. Blood 108(13):4094–4101
4. Zwaal RF, Comfurius P, Bevers EM (2005) Surface exposure of phosphatidylserine in pathological cells. Cell Mol Life Sci 62(9):971–988
5. Xu C et al (2008) Regulation of T cell receptor activation by dynamic membrane binding of the CD3epsilon cytoplasmic tyrosine-based motif. Cell 135(4):702–713